



MASTER THESIS

Quantification of the impact of adjusted ozone climatology on a warmer than present climate simulated by AWI-ESM-2.1-LR

UNIVERSITY OF BREMEN
POSTGRADUATE PROGRAMME ENVIRONMENTAL PHYSICS

ALFRED WEGENER INSTITUTE – HELMHOLTZ CENTRE FOR POLAR AND MARINE
RESEARCH

Author :
Arpita Bose

First Examiner:
Prof. Dr. Gerrit Lohmann

Anagraphic data
November 3, 1993

Second Examiner:
Prof. Dr. Mihalis Vrekoussis

Matriculation Number :
3175903

Supervisors:
Dr. Christian Stepanek
Dr. Monica Ionita-Scholz

January 3, 2022

Declaration of copyright

Hereby I declare that my Master's Thesis was written without external support and that I did not use any other sources and auxiliary means than those quoted. All statements which are literally or analogously taken from other publications have been identified as quotations.

Declaration with regard to publishing theses

I agree that for research purposes third parties can look into my thesis stored in the University archive.

Bremen, January, 2022

Arpita Bose



Acknowledgements

Foremost, I would like to express my sincere gratitude to my principal supervisor Prof. Dr. Gerrit Lohmann for giving me the opportunity to accomplish this master thesis at the Alfred Wegener Institute in Bremerhaven and for his time and guidance throughout my master thesis process. My sheer interest to work in the field of climate modelling developed from the course on Climate System II taught by Prof. Lohmann.

I extend my heartfelt thanks to my tutor Dr. Christian Stepanek for his constant support and encouragement in joining the discussions and the enormous knowledge shared with me. He came up with this brilliant idea of the project. I am sincerely grateful to him for his guidance throughout the journey, which made it possible to what I can present today.

Special thanks to Prof. Dr. Mihalis Vrekoussis for accepting to review my thesis.

A big thank you to Peer Nowack for providing the ozone datasets and making it possible to accomplish my work.

Finally, I would like to thank my family and friends for always cheering me up and trusting in my abilities. The last three years would not have been fun without their constant support and motivation.

Abstract

The existence of ozone as a greenhouse gas in the Earth's climate system has a great impact on the radiative transfer in the atmosphere, affecting among others, the global climate. Various climate modelling studies have highlighted the importance of ozone as a key driver of climate change. However, the climate models at the research group, Paleoclimate Dynamics at The Alfred Wegener Institute (AWI) lacked the interactive chemistry scheme for calculating ozone changes due to the enormous computational expenses. In this respect, this thesis addresses the vital question of the accuracy of specific climate patterns in the atmosphere-ocean coupled model AWI-ESM-2.1-LR, in comparison to the behaviour of a real climate state where ozone is fully forcing and reacting to climate changes. Quantification of the adjusted ozone in response to $4xCO_2$ is crucial, taking into account how modified ozone impacts the climate. In this study, the average values of surface temperature, total precipitation, vertically integrated water vapour, geopotential height at 500 hPa, 250 hPa, 100 hPa levels, and sea ice concentration together with the model metrics like climate sensitivity and polar amplification has been investigated under the aegis of Pre-Industrial (PI), $4xCO_2$, and $4xCO_2_{O_3}$ simulations. These simulations have been performed by AWI-ESM-2.1-LR, a state-of-the-art climate model that will be used as a workhorse for simulating various climate states, from much warmer to present, to much colder than present climate states. Noteworthy is the intense Arctic warming during boreal winter in the $4xCO_2$ simulation. This pronounced warming can be manifested by the strong increase in vertically integrated water vapour in the Northern Hemisphere (NH) high latitudes. However, the modified ozone forcing on the surface temperature response to $4xCO_2$ produces a cooling pattern. Furthermore, an enhanced precipitation pattern of 1069.72 mm/year is observed in the tropical mid-latitude region covering parts of South Asia due to a robust land-sea pressure and temperature contrast. The presence of the modified ozone forcing in the $4xCO_2_{O_3}$ simulation decreases the precipitation to 1056.15 mm/year and causes drying in certain parts of Indonesia, Indian Ocean and Pacific Ocean. Quadrupled carbon dioxide concentration in the $4xCO_2$ simulation inevitably produces the canonical temperature response driving tropospheric warming due to the steepening of the moist adiabatic lapse rate and stratospheric cooling which enhances the infrared cooling to space by decreasing the upward thermal radiation. Climate Sensitivity (CS), as depicted from the Gregory plot is analysed here as the global surface air temperature change due to a quadrupled carbon dioxide concentration with PI as a reference climate state in the atmosphere and is computed to be $3.43^\circ C$, whereas a minor reduction of CS ($3.34^\circ C$) is noted due to the response of the modified ozone forcing. Defining the Arctic Amplification Index (AAI) from (60-90°N) and (30-60°N), the polar amplification factor is measured as 1.82 with $4xCO_2$ and PI and 1.79 with $4xCO_2_{O_3}$ and PI. Overall, the final goal of this

thesis is to study the prospective climate impacts of adjusting ozone towards a background climate state. This has been executed by digging deep into the broad pool of data obtained from PI, 4xCO₂ simulation together with the third simulation with modified ozone forcing, 4xCO₂_O₃, where AWI-ESM-2.1-LR is forced with ozone and computed for 4xCO₂ climate state, by the HadGEM3 model.



Contents

1	Introduction	8
2	Scientific Background and Motivation	10
3	Data and Methods	13
3.1	AWI-ESM-2.1-LR setup	13
3.2	The Atmospheric Model ECHAM6	15
3.3	The Finite Volume Sea-Ice Ocean Model FESOM2	15
3.4	The Jena Scheme for Biosphere-Atmosphere coupling in Hamburg JSBACH	16
3.5	The Climate Data Operator CDO	17
3.6	Experimental Design	17
3.7	T-Test analysis	18
3.8	Pre-industrial control simulation (PI)	19
3.9	4xCO ₂ simulation (4xCO ₂)	20
3.10	4xCO ₂ with modified ozone simulation (4xCO ₂ _O ₃)	20
3.11	Methodology	21
3.12	The imposed ozone forcing	22
4	Results	23
4.1	Surface Temperature	23
4.2	Zonal mean surface temperature	26
4.3	Vertical Temperature Structure	30
4.4	Precipitation	31
4.5	Vertically Integrated Water Vapor	34
4.6	Climate Sensitivity (CS)	36
4.7	Polar Amplification	37
4.8	Sea ice concentration	38

4.9	Geopotential height at 500 hPa, 250 hPa and 100 hPa levels.....	43
4.10	Zonal mean geopotential height	51
5	Discussion	53
5.1	Impact of modified ozone on simulated large-scale global geographic Patterns.....	53
5.2	Impact of ozone forcing on climate sensitivity and polar amplification	56
6	Conclusion and Outlook	58
	Acronyms	60
	Bibliography	62
	Appendix	69

Introduction

Atmospheric Ozone is a trace gas and a primary greenhouse gas which plays an important role in the radiative transfer of the Earth system by influencing the Earth's energy budget and subsequently the climate. Ozone is an asymmetric inorganic molecule, and due to this distinct property, it plays a dual role in the atmosphere. Stratospheric ozone enabled with its optical properties is capable of absorbing shortwave or longwave radiation, but also cools down the atmosphere through the emission of longwave radiation (Rae et al., 2019). Hence, the primary impact of stratospheric ozone is that, it substantially affects the climate by means of a positive feedback loop signifying the presence of more ozone in the air which results in more heat retention (Rae et al., 2019). Nonetheless, tropospheric ozone also absorbs in the infrared, visible, and UV spectral region (Lacis et al., 1990) and represents of about 10% of the total amount of atmospheric ozone. It is considered as the near-term climate forcer due to its relatively short lifetime of about 23 days (Gaudel et al., 2018). However, it is quite evident that ozone's distribution in the atmosphere is subject to change (Nowack et al., 2018).

Ozone also plays a key role in the global radiative transfer and successively implicates various feedback effects on the Earth system by modulating temperature, dynamics, and the biosphere (Lacis et al., 1990, Thompson and Solomon 2002, Son et al., 2008, Williamson et al., 2014).

Furthermore, the representation of interactive ozone chemistry in the climate models is a key step in studying the impact of ozone on climate metrics like climate sensitivity (CS), polar amplification, and changes in global average temperature (Chiodo et al., 2017). Regardless of the extensive research studies that deal with the representation of ozone towards the analysis of the various climate implications, the impact of ozone on these climate metrics like CS and polar amplification is still missing with the atmosphere-ocean coupled model AWI-ESM-2.1-LR.

The key issue why ozone is not interactive in the in-house atmosphere-ocean coupled model, AWI-ESM-2.1-LR, despite the diverse research studies, is the high computational cost and the limited computational power associated with calculating ozone changes that involves running the model for

a long time as potentially done in the paleoclimate simulations. Therefore, scientists choose to replicate Earth's climate realistically. For paleoclimate simulations, a model has to typically run for 1000 years as shown in Table 1 of [Stepanek et al. \(2020\)](#) with the COSMOS model. Nonetheless, [Nowack et al. \(2018\)](#) show that the atmosphere-ocean coupled configuration of the Hadley Centre Global Environment Model version 3 (HadGEM3-AO) with interactive ozone chemistry, each simulation run was for 200 years for the purpose of controlling the computational expenses.

Motivated by this, there arose a need to study how much the quantification of the type and magnitude of effects the modern ozone concentration has on the simulation results with AWI-ESM-2.1-LR in comparison to a simulation with fixed ozone which fits the mean climate state. AWI-ESM-2.1-LR is a major future tool for relatively high-resolution paleoclimate simulation at times when atmospheric constituents were very much different from today. It has the atmospheric model ECHAM6 where interactive ozone is absent and the ocean model FESOM 2.0 ([Scholz et al., 2019](#)).

This thesis is structured as follows. In chapter 2, a background study with reference to some previous publications is provided. In this context, the motivation for investigating the impact of atmospheric ozone with the atmosphere-ocean climate model AWI-ESM-2.1-LR in a warmer climate state compared to the present climate state is illustrated. Chapter 3 gives a detailed description on the data and methods in the AWI-ESM-2.1-LR with a brief description of each of the sub models and the simulations. Chapter 4 illustrates the results of the anomalies for the surface temperature, total precipitation, vertically integrated water vapour, sea ice concentration and geopotential height at 500 hPa, 250 hPa, 100 hPa levels along with the analysis of climate metrics such as CS and polar amplification. Chapter 5 discusses the main results obtained from this study. Chapter 6 concludes and provides an outlook of this study.

Scientific Background and Motivation

This chapter commences with a scientific background that emphasizes a concise description from previous publications that have dealt with interactively computed ozone on various climate models. It vividly stands in context with previous scientific research studies which confirm, that the representation of interactively computed ozone is a key step in understanding the various ways it affects the climate modelling results. Subsequently, it also announces the contribution of interactively computed ozone as a striking measure in climate modelling results with special evidence to global CS estimate. However, in this thesis research study, using the atmosphere-ocean coupled model, AWI-ESM-2.1-LR, ozone fields are prescribed from the HadGEM3 model used by [Nowack et al. \(2018, 2015\)](#). Hence, the main aim is to use the interactive ability of the atmosphere-ocean coupled Hadley Centre Global Environment Model version 3 (HadGEM3) from [Nowack et al. \(2018\)](#) to generate an ozone field that is in agreement with 4xCO₂ forcing and implement the same climate forcing in AWI-ESM-2.1-LR in a non-interactive way without the representation of the ozone-climate feedbacks in the executed simulations. Similar effects reproduced by ozone as reflected in the following research studies have been established depending on the presence of quantified ozone and absence of ozone-climate feedbacks in AWI-ESM-2.1-LR.

The primary focus is the publication by [Nowack et al. \(2018\)](#) which describes the potential climate impacts concerning ozone changes in the upper troposphere and lower stratosphere, where the ozone was allowed to react to the CO₂ forcing in the lower part of the atmosphere. Elsewhere in the atmosphere, the ozone was held fixed and forbidden to adapt in the middle-upper stratosphere. This study is based on four simulations of the atmosphere-ocean coupled Hadley Centre Global Environment Model version 3 (HadGEM3) for CMIP5. The model setup is enabled with prescribed pre-industrial control ozone together with 4xCO₂ climate state to test the feedback in-between the stratospheric ozone and CS. This analysis is allied to their previous publication [Nowack et al. \(2015\)](#) where it has been observed that the ozone feedback leads to ~20% increased global warming with the HadGEM2-ES model, a significant rise in the regional surface temperature changes, a

reduction in the climate sensitivity due to the changes in the tropical upper tropospheric and lower stratospheric ozone, and the contribution from the stratospheric water vapour feedback and tropospheric cirrus cloud changes. The characteristic difference between the HadGEM3 model with its predecessor version, HadGEM2-ES is that the latter is a low top model, without the stratospheric representation (Collins et al., 2011), but it included a sophisticated tropospheric chemistry scheme. Furthermore, it was also evaluated that the stratospheric water vapour (SWV) increases similarly as in HadGEM2-ES in the corresponding CMIP5 simulations. This effectively helps in tracking the progress of climate modelling.

Marsh et al. (2016) tested the impact of ozone on the Community Earth System Model-Whole Atmosphere Community Climate Model (CESM1-WACCM) to assess the importance of chemistry feedbacks and the determination of equilibrium climate sensitivity (ECS). By performing two $4\times\text{CO}_2$ experiments including one with interactive chemistry scheme (WACCM) and the other, designated as SC-WACCM, where the chemical constituents were held fixed at pre-industrial levels other than CO_2 . The difference in ECS and the feedback was found to be 0.01 K and as $0.01 \text{ Wm}^{-2} \text{ K}^{-1}$ respectively. SC-WACCM specifies the ozone concentration whereas the model resolution, vertical grid, other physical parameterization, and the active components including land, ocean, and sea ice were kept identical as in WACCM. The global mean CO_2 concentration was held fixed at 285 ppm and SC-WACCM used ozone fields from the WACCM preindustrial control simulation. It was effectively concluded from their study, that the larger CO_2 values affect the ozone distribution showing a strong increase in the upper stratosphere and decrease in the lower stratosphere. The methodology from Gregory et al. (2004) was used to determine the magnitude of the chemistry feedback effect on the radiative forcing (RF), ECS, and the net feedback was calculated to be approximately in the order of 1%. Their study concludes that exclusion of chemistry feedbacks in the CESM model does not lead to any pivotal error source for the analysis of global climate sensitivity metrics.

Chiodo and Polvani, (2019) quantify the climate impacts due to the changes induced by the stratospheric ozone in agreement with a $4\times\text{CO}_2$ climate state and assess the subsequent effects of the ozone layer in the climate state. Proceeding to the experiments, they used the SC-WACCM model enabled with the stratosphere-resolving version of the National Center for Atmospheric Research (NCAR) Community Earth System Model (CESM), version 1.2.0. Three experiments were performed each over a span of 100 years with pre-industrial control forcing of the year 1850. The ozone forcing in the simulation runs was obtained from the WACCM, the coupled general circulation model (CM3) from the Geophysical Fluid Dynamics Laboratory (GFDL), and the coupled model for Solar-Climate-Ozone-Links (SOCOL). The advantage of implementing the ozone forcing was to identify the impact of ozone that results from the quadrupled carbon dioxide

concentrations on the climate system. In the simulation with ozone forcing, there is an increase of ozone concentration in the upper stratosphere in the range of (1-10) hPa and a consequent decrease in the lower tropospheric ozone concentration due to an intensified tropical up-welling (Shepherd, 2008). The reason behind the increase in the stratospheric ozone concentration was due to the radiative cooling induced by the increase in the carbon dioxide concentrations, which ultimately affects the reaction rates of the Chapman cycle (Haigh and Pyle 1982; Jonsson et al., 2004). Chiodo and Polvani, 2019 studied CS, to identify the impact of ozone caused due to 4xCO₂. Surprisingly, it was found that the temperature increase after 100 years of the simulated run with modified ozone was identical to the temperature increase with pre-industrial ozone in all the seasons. Henceforth, it was effectively concluded from their findings that the induced ozone forcing in agreement with a 4xCO₂ climate state does not have an impact on CS on the model SC-WACCM inspite of the consistency between the small global mean of the adjusted radiative flux (R_{adj}) induced by ozone in response to 4xCO₂.

Furthermore, Chiodo and Polvani 2019, confirm the validity of the “semi-offline” approach as outlined by Nowack et al. (2015, 2018), by prescribing ozone as a forcing in the model without interactive chemistry. This was successfully executed by comparing the 4xCO₂ integration from SC-WACCM with the WACCM integration with interactive ozone as documented in Chiodo and Polvani (2017). The results obtained from the SC-WACCM integrations with 4xCO₂ and PI ozone (W4x and W4xO₃) were identical to that of the 4xCO₂ integration from WACCM concerning global-mean temperature, as shown in Marsh et al. (2016).

In this context, the main motivation of my thesis lies in studying and understanding the impact of modified ozone forcing in the atmosphere-ocean coupled model AWI-ESM-2.1-LR by implementing a climate-state adapted ozone forcing derived from the HadGEM3 model used by Nowack et al. (2018).

Data & Methods

This chapter initiates with the description of the atmosphere-ocean coupled model, AWI-ESM-2.1-LR setup based on the model description by [Sidorenko et al. \(2019\)](#). Furthermore, a general overview of the sub-models, ECHAM6 and, FESOM2.0 that generates monthly climate outputs are described in sections [3.2](#), [3.3](#) respectively. A description of the Climate Data Operator (CDO) and the motivation for using it for this thesis is provided in section [3.5](#). An experimental design with an elaborate description of the three respective simulations, that generate the monthly mean model output, is described in sections, [3.6](#), [3.8](#), [3.9](#), and [3.10](#). Additionally, a short outlook on the methodology towards reformatting the ozone fields for the atmospheric model, ECHAM6 obtained from [Nowack et al. \(2018\)](#) and then successfully implementing the following in the atmosphere-ocean coupled model, AWI-ESM-2.1-LR is presented in section [3.11](#). A concise description of t-test analysis and the purpose of using it in this thesis is given in [3.7](#). A description of the ozone forcing imposed on AWI-ESM-2.1-LR winds up this chapter.

3.1 AWI-ESM-2.1-LR setup

The AWI Earth system model (AWI-ESM-2.1-LR) is an extended version of the AWI Climate Model (AWI-CM; [Sidorenko et al., 2015](#)) employed for earth system modelling. The AWI-ESM-2.1-LR setup (Fig. [1](#)) mainly comprises of the spectral atmospheric component ECHAM6 based on the T63 grid (1.88 x 1.88°) with 47 vertical layers ([Stevens et al., 2013](#)), the finite element sea ice-ocean model (FESOM2.0) employing the core II mesh (~127,000 surface nodes) ([Danilov et al., 2017](#), [Sidorenko et al., 2019](#)) and the land surface model JSBACH that computes land surface processes and interactive vegetation dynamics ([Raddatz et al., 2007](#), [Brovkin et al., 2009](#), [Reick et al., 2013](#)). The coupling between atmosphere, land, and ocean components is carried out by the OASIS3-MCT coupler ([Valcke, 2013](#)). It exchanges 12 fluxes in total, including momentum, heat and freshwater fluxes, that are passed on between atmosphere and ocean ([Sidorenko et al., 2019](#)).

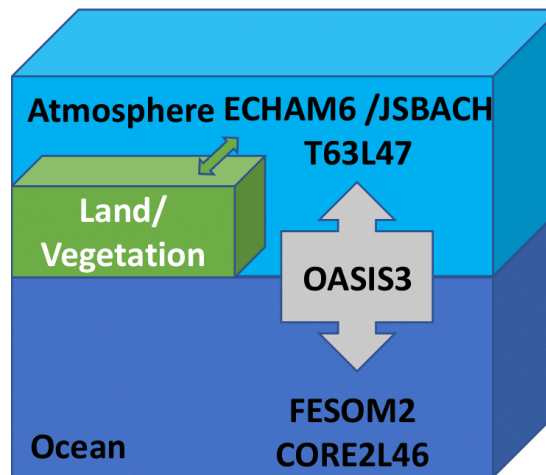


Figure 1: Schematic view of AWI-ESM-2.1-LR

Figure 2 displays the mesh representation of ECHAM6 (left), where the corresponding grid is at T63 horizontal resolution, and FESOM CORE II (right) showing modern land-sea configuration. The dark green areas of the T63 grid indicate land, whereas the grid resolution of FESOM in km is shown through colour-coding and is high in critical regions. JSBACH uses the same lateral resolution as the atmospheric component ECHAM6 and receives most of the boundary conditions from it.

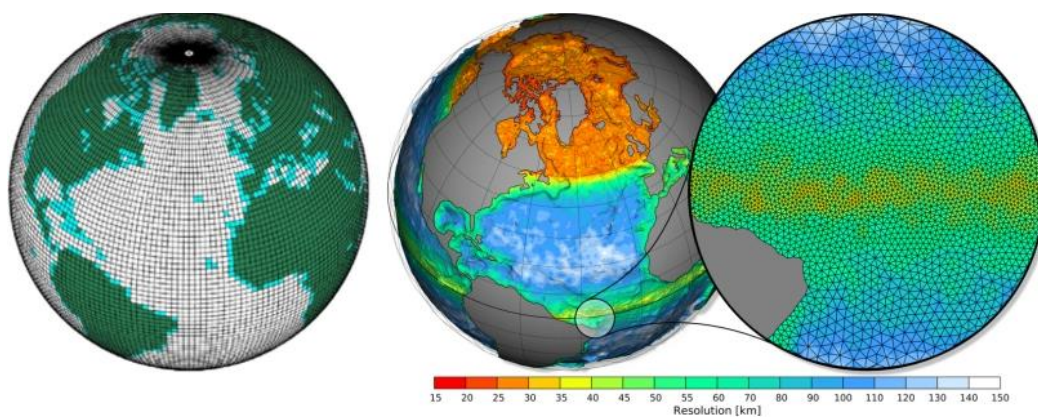


Figure 2: ECHAM6 T63 (left) - FESOM2.0 mesh representation. Dark green areas of T63 grid represent land fraction exceeding 50% and light green areas represent land fraction between 0 and 50%. Grid resolution for FESOM is illustrated through colour coding (in km) (Sidorenko et al., 2015).

3.2 The Atmospheric Model ECHAM6

ECHAM, an atmospheric general circulation model that has been developed by the Max Planck Institute for Meteorology (MPI-M) in Hamburg, Germany (Stevens et al., 2013). ECHAM is an adaptation from the earlier version of the global numerical weather prediction model developed at the European Centre (EC) for Medium-Range Weather Forecasts (ECMWF) (Roeckner et al., 1989) and since then it has been continually developed at the Max Planck Institute for Meteorology. ECHAM6 is the newest and final sixth generation version of ECHAM which was mainly developed for serving the purpose to support the institute's contribution to the fifth and sixth phase of the coupled model inter-comparison project (CMIP) (Stevens et al., 2013). ECHAM6 primarily focuses on the coupling between diabatic processes such as convection, diffusion, turbulence and gravity waves (Schultz et al., 2018) correlated with small-scale fluid dynamics and large-scale circulations, whereas the minor change with regard to ECHAM5 includes the treatment of deep convection (Stevens et al., 2013). Stevens et al. (2013) outline some underlying changes and advantages of ECHAM6 compared to ECHAM5. The major changes implemented in ECHAM6 include the shortwave radiative transfer, the development of the new surface albedo description, new aerosol climatology and the progressing efforts to add complexity to the representation of the land surface by comprehensively including dynamic vegetation. ECHAM6 uses the ozone fields explicitly used in the radiation computation. It is not interactive and is prescribed according to the CMIP6 ozone dataset (Keeble et al., 2021). In the 4xCO₂_O₃ simulation, the ozone fields accessed by the model will be modified based on the ozone datasets obtained from the HadGEM3 model as referred in Nowack et al. (2018, 2015).

3.3 The Finite Volume Sea Ice-Ocean Model FESOM2

FESOM, the first mature global multi-resolution and hydrostatic ocean circulation model, developed at the Alfred Wegener Institute, Helmholtz Centre for Polar and Marine Research (AWI) is designed to simulate the large-scale ocean (Wang et al., 2014) and is known for solving primitive dynamical equations in the Boussinesq, hydrostatic, and traditional approximations of sea ice and ocean by addressing the momentum, continuity equations, and geostrophic balance (Danilov et al., 2017; Scholz et al., 2019). In the AWI-ESM-2.1 LR setup, used in this study, FESOM2.0 has been used. FESOM 2.0 is based on finite-volume discretisation (Danilov et al., 2017). The distinct advantage of using FESOM2.0 is that it uses a faster dynamical core, increasing throughput by 3 times compared to its predecessor version, ensuring good scalability characteristics, and high numerical efficiency by a factor of 3-5 (Koldunov et al., 2019).

3.4 The Jena Scheme for Biosphere-Atmosphere Coupling in Hamburg JSBACH

JSBACH, the land surface component of the Earth system model, includes interactive dynamic vegetation, and is developed by the Max Planck Institute (MPI-M) in Hamburg, Germany (Raddatz et al., 2007; Reick et al., 2013). It simulates fluxes of energy, water, momentum, and CO₂ between land and atmosphere (Brovkin et al., 2009). JSBACH is equipped with different plant functional types (PFT) that enable it to easily differentiate amongst the various natural flora species like trees, shrubs, and grasses (Brovkin et al., 2009).

In the AWI-ESM-2.1-LR setup used in this research, vegetation changes are particularly important and relevant for the 4xCO₂ simulation since the vegetation cover is free to change from a state referring to PI to that of the 4xCO₂ simulation and allowing simulations to correctly represent the strong differences in various climate parameters such as surface albedo.

Based on the work by Stepanek et al. (2020), it has been shown with the COSMOS model, together with ECHAM5 as an atmospheric component, that there is significant variation in the vegetation distribution from the mid-Pliocene to the modern state. The E560 simulation that was performed is based on the modern geography. The simulation E560 demonstrates the impact of CO₂ on climate, in contrast to a superposition of geographic and CO₂ changes in other simulations as listed in Table 1 of Stepanek et al. (2020). So, E560 isolates the impact of CO₂ on climate, which is similar to the 4xCO₂ simulation in this research albeit with a different model configuration and at a different amplitude of CO₂ change. It has been explicitly observed in Fig. 25 of Stepanek et al. (2020), that due to changes in CO₂ concentration, the climate changes, which has an impact on vegetation, as different plant species are adapted to different climates. The NH high latitudes experience a vegetation shift, that then leads to a change in surface albedo (as trees are darker than grass), which then leads to a further change in climate due to the albedo-temperature feedback. Furthermore, in the context of the aforesaid publication, my thesis deals with a CO₂ concentration that has been abruptly quadrupled. Hence, a stronger climate anomaly is expected in the 4xCO₂ simulation in this research study due to the influence of the large carbon dioxide concentration. Therefore, it is of particular relevance that vegetation dynamics and feedbacks are dynamically resolved in my 4xCO₂ simulation. Hence, the consideration of dynamic vegetation is an important tool in this study, because without the vegetation state that is in agreement with 4xCO₂ there is no other choice to simulate vegetation.

3.5 The Climate Data Operator (CDO)

[Schulzweida et al. \(2006\)](#) have provided in their publication a precise explanation of the Climate data operator (CDO). CDO is enabled with a collection of about 700 command line operators, which eases the processing of climate and numerical weather prediction model data along with the simple statistical and subsampling tools and spatial interpolation.

In the light of the aforesaid publication, CDO serves as an essential tool in this project in the following way:

1. CDO is programmed in a way, which efficiently processes large amounts of NetCDF climatological datasets by various operators.
2. CDO has the ability to interpolate 3D data to specific levels. The interpolation tools have been effectively used twice in this thesis to interpolate the atmospheric data along with the ozone values. Firstly, to interpolate ozone to specific pressure levels to the atmospheric component of the model, ECHAM6 and then finally to interpolate the model output from model levels to specific pressure levels for analysis.

In this thesis research work, the 4 dimensional ozone data with a time component on different levels was provided by [Nowack et al. \(2018\)](#). Henceforth, the interpolation of a hybrid atmosphere to a regular pressure grid by means of CDO was of particular importance.

3. It supports the ECHAM T63 grid and, with the help of the code table provided by ECHAM6, the meaning of any output variable is well understood.

3.6 Experimental Design

In this section, an overview of the three categorised simulations, namely the pre-industrial control simulation (PI), the simulation with an abrupt quadrupling of carbon dioxide (4xCO₂), and 4xCO₂ with modified ozone (4xCO₂_O₃) are briefly introduced. The PI and 4xCO₂ simulations are standard core experiments performed in climate modelling intercomparison projects ([Eyring et al., 2016](#), [Kravitz et al., 2013](#), [Taylor et al., 2012](#)). The three aforesaid simulations have been performed under different setups by the coupled models of AWI-ESM-2.1-LR and have been integrated for a total length of approximately up to 800 years. Table 1 provides an overview on the simulation specific details including the variables necessary for the radiation calculation and the greenhouse gas concentrations, while Table 2 lists the model-specific details along with the associated radctl namelist values, types, and a brief explanation with the reference to the ECHAM6 user manual. The external orbital forcing from the year 1850 is kept constant in all of the experiments. The

greenhouse gas concentration and volume mixing ratio of CH₄=808.25 ppb and N₂O=273.02 ppb has been kept identical in all the three simulations.

Table 1: An overview on the model setup of the simulations employed in this thesis

Experiment Name	CO ₂ Forcing	Prescribed Ozone Dataset	Approx run (analysis) time in years
PI	284.32 ppm	Pre industrial ozone from CMIP6	800
4xCO ₂	1137 ppm	Pre industrial ozone from CMIP6	800
4xCO ₂ _O3	1137 ppm	Modified ozone concentration taken from Nowack et al.(2018)	800

Table 2: Model –specific details with radctl namelist values, types and brief explanation

Namelist radctl			
Name	Type	Value	Explanation
ich4	double prec	3	Volume mixing ratio of methane in the troposphere indicating a decay above the tropospheric layers while using the radiation computation
io3	double prec	4	Climatological ozone volume mixing ratio used for radiation calculation in the NetCDF format provided by the IPCC. [Remark – In the abrupt-4xCO ₂ _O ₃ simulation, the io3 data set accessed by the model has been modified.]
in2o	double prec	3	Uniform volume mixing ratio of N ₂ O used in the troposphere with a decay above the tropospheric layers while radiation computation
iaero	integer	3	Aerosol climatology compilation by S. Kinne (Kinne et al., 2013)
isolrad	integer	6	CMIP6 pre-industrial solar constant documented in source code

3.7 T-Test analysis

The t-test is the most widely used statistical hypothesis testing tool ([Kim, 2015](#)). The most commonly used t-test is the two-sample t-test commonly known as the Student's t-test or the independent samples t-test. It is used as a statistical method used to assess whether the mean value of the data from an independent sample differs significantly under different conditions ([Yang-chun et al., 2017](#)).

The formula for t-test as described in [Fernandez, \(2020\)](#) is

$$t = \frac{\text{difference between means}}{\text{standard error of difference}} = \frac{X_1 - X_2}{\sqrt{\frac{s_1^2}{n_1} + \frac{s_2^2}{n_2}}}$$

where X_1 and X_2 are the mean values of the two independent datasets or samples, s_1 and s_2 are the standard deviations of the respective samples, n_1 and n_2 indicates the respective sample sizes.

In this thesis research, the Student's t-test is applied to vividly identify the insignificant difference for the surface temperature and precipitation anomalies for (4xCO₂-PI) and (4xCO₂_O₃-4xCO₂). It is used as a significance testing method to check the internal variability or noise of the simulated climate state. The principal purpose is to check whether the change created by the modified ozone forcing in the 4xCO₂_O₃ simulation generates a climate anomaly that exceeds the internal variability in the 4xCO₂ simulation. Figs. 6(a-e) demonstrate more hatches, whereas in Figs. 5(a-e) there are no insignificance hatchings. This indicates that the climates in the 4xCO₂ and PI simulations are completely different from each other and there is no “climatic overlap” due to internal variability. It is well attributed to the fact that the change due to quadrupling of carbon dioxide creates a much stronger climate anomaly than the additional change in ozone.

3.8 Pre-industrial control simulation (PI)

Eyring et al. (2016) outlined that the PI simulation is a part of the CMIP6 experimental design and serves as a reference baseline for the further experiments that branches off. It beneficially helps in studying the unforced variability of the climate system. The underlying importance of this simulation is to better understand climate variability without human influences (Bellenger et al., 2013). The atmosphere-ocean coupled PI run employed in this thesis study comprises the unaltered pre-industrial climate conditions with a fixed orbital forcing from the year 1850. The estimated total length of the run is envisioned to be 1000 years and three simulations ran for upto 800 years. From the perspective of the equilibrium at the surface and the availability of the computer time, it is most likely that the simulation should at least run for 500 years considering the spin-up period into account, although it is quite evident that 500 years are not sufficient to reach a perfect equilibrium state especially when the carbon dioxide concentration is increased in the further experiments (Eyring et al., 2016). The prescribed value of the CO₂ concentration is 284.32 ppm (Meinshausen et al., 2017). The prescribed ozone dataset is represented here as 4 dimensional, with 66 pressure levels, geographical latitude-longitude grid (2.5° x 1.9°) (Maycock et al., 2018), and time and is obtained from the PI ozone fields from CMIP6. It comprises monthly mean ozone mixing ratios on 66 pressure levels between 1000-0.0001 hPa (Maycock et al., 2018). Greenhouse gas concentration of CH₄ and N₂O referred from Meinshausen et al. (2017) are listed in Table 1. A precise description

of the forcings that stem from the CMIP6 experiments including atmospheric trace gas concentrations is also taken from [Meinshausen et al. \(2017\)](#) and presented in Table 2, along with the value of the solar constant and aerosol loading. The value of the solar constant is the shortwave radiation defined at the TOA per square meter on the earth's sphere and is summed up over 14 shortwave spectral bands for the pre-industrial CMIP6 simulation, averaged over the years from 1870-1873 and is about 1360.744 W/m^2 (documented in the source code file `mo_radiation.f90`) or approximately 1361 W/m^2 ([Wild, 2020](#)).

3.9 4xCO₂ simulation (4xCO₂)

The simulation with 4xCO₂ has been initialised from the PI setup with the only difference that the CO₂ concentration (1137 ppm) that has been abruptly quadrupled and held fixed with respect to the pre-industrial volume mixing ratio. [Eyring et al. \(2016\)](#) outline that by changing the CO₂ concentration and keeping all other forcings similar to that in the pre-industrial control, the climatic consequences caused due to the increase in the CO₂ concentrations like the radiative forcing characteristics and estimation of CS can be ably understood. Studying CS ([Ceppi and Gregory 2017](#), [Knutti et al., 2017](#)) and the response of globally warming climate to increased carbon dioxide concentration is the main centre of focus of this simulation ([Nowack et al., 2018](#)). This simulation also provides a deep insight into the changes of the climate dynamics in a scenario equipped with high carbon dioxide concentration.

At the start of the equilibrium simulations of PI and 4xCO₂ ([Eyring et al., 2016](#)), the model components are being instantly exposed to the full set of the boundary conditions and model forcing. [Eyring et al. \(2016\)](#) suggest that the minimum length of the simulation should be at least 150 years, but the model was ensured to run at least for 500 years in order to attain the quasi-equilibrium climate state.

3.10 4xCO₂ with modified ozone simulation (4xCO₂_O₃)

This simulation serves as an important benchmark in analysing the impact of adjusted ozone in the atmosphere-ocean coupled model AWI-ESM-2.1-LR. It has been facilitated to gather evidence on the climate implications in response to modified ozone in a climate state with quadrupled carbon dioxide concentration. The modified ozone field is obtained from the atmosphere-ocean coupled HadGEM3 model used by [Nowack et al. \(2018\)](#). It is taken into consideration that, in this thesis research using the atmosphere-ocean coupled model, AWI-ESM-2.1-LR, ozone is only adjusted in agreement with a warmer climate state and is not computed interactively. Hence, this simulation captures the most significant impact due to the ozone change on climate and neglects the higher

order impact which is the ozone-climate feedback. The comprehensive elaboration on the method of obtaining the ozone data fields from HadGEM3 followed by the anomaly method and then interpolating it to the model grid is scripted in the methodology section 3.11.

3.11 Methodology

This section gives an overview on the methodology towards the adjustment of ozone following the anomaly approach. In the $4xCO_2-O_3$ simulation, AWI-ESM-2.1-LR is forced with ozone computed for a climate state with $4xCO_2$. Intending to successfully accomplish this, the following two files were obtained from [Nowack et al. \(2018\)](#).

- `ozone_4xCO2_clim_on_plevs_ECHAM6_ymonmean` (derived from a simulation with $4xCO_2$ and interactive ozone)
- `ozone_piControl_clim_on_plevs_ECHAM6_ymonmean` (derived with PI CO_2 and interactive ozone)

Moving forward with the procedure, a fractional anomaly was computed between the ozone fields of the $4xCO_2$ simulation enabled with interactive ozone and the PI simulation from [Nowack et al. \(2018\)](#), and then the result was added to the ozone forcing of the PI simulation by AWI-ESM-2.1-LR. The fractional anomaly was computed as a percentage change (Fig. 1) which then is applied to the ozone forcing employed in the ECHAM6 simulation which facilitates that, only changes in ozone due to enhanced carbon dioxide are considered in AWI-ESM-2.1-LR, whereas differences in the reference states between the work by [Nowack et al. \(2015, 2018\)](#) and the ECHAM6 ozone files in AWI-ESM-2.1-LR are ignored. Hence, in order to overcome the potential biases in the simulated climate, that could be introduced by offsets between the observational ozone dataset in AWI-ESM-2.1-LR on one side and the simulated ozone dataset in HadGEM3 on the other side, a fractional anomaly approach was beneficial.

Fig. 3a, shows the fractional anomalies of the [Nowack et al. \(2018\)](#) dataset ($4xCO_2$ w.r.t PI) and Fig. 3b shows the fractional anomalies of the ECHAM6 dataset ($4xCO_2$ w.r.t PI).

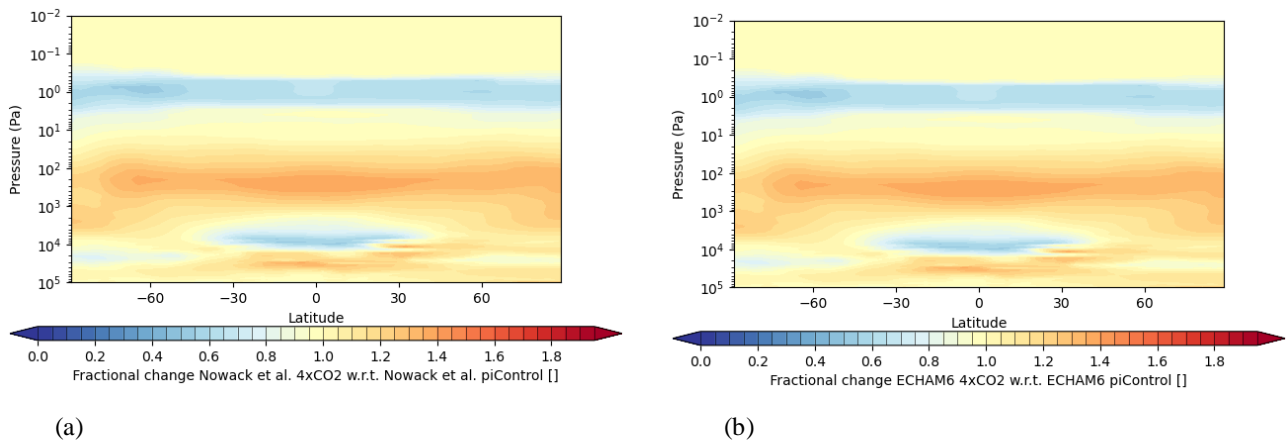


Figure 3: Fractional change Nowack et al. (4xCO₂ w.r.t. PI) (a) and Fractional change ECHAM6 (4xCO₂ w.r.t. PI) (b).

3.12 The imposed ozone forcing

The annual mean ozone response anomaly with respect to 4xCO₂_O₃-4xCO₂ is shown in Fig. 4. The climate ozone forcing is implemented into the atmosphere-ocean coupled model AWI-ESM-2.1-LR from a climate-state adapted ozone-chemistry model HadGEM3 as described by Nowack et al. (2018). The pattern of the ozone forcing depicts an increase of ozone in the upper stratosphere (10²-10³ Pa) in the low latitudes and a subsequent decrease of ozone in the tropical lower stratosphere (TLS) (10³-10⁴ Pa). The increase of ozone in the upper-stratospheric region is interrelated to the radiative cooling induced due to the high carbon dioxide concentrations which further decreases the reaction rate coefficient of the Chapman reaction (Haigh and Pyle 1982, Jonsson et al., 2004).

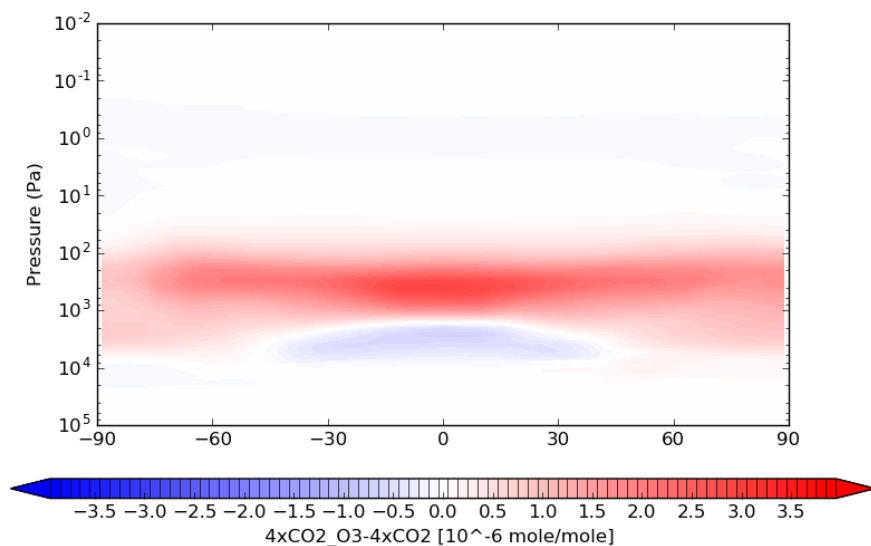


Figure 4: The computed ozone anomaly between 4xCO₂_O₃ and 4xCO₂ simulations. Units of pressure are in Pa and unit of ozone concentration is mole/mole.

Results

In this section, the results from the PI, 4xCO₂ and the 4xCO₂_O₃ simulation are presented for a time period of last 100 years of the model simulation, except the Gregory plot (Fig. 14) where the analysis is done for 500 years. The results for surface temperature and, precipitation are obtained via the anomaly approach (4xCO₂-PI) and (4xCO₂_O₃-4xCO₂) for annual mean, boreal spring, summer, autumn and winter respectively defined as March-April-May (MAM), June-July-August (JJA), September-October-November (SON) and December-January-February (DJF). The necessary calculations are explicitly done by CDO. The variable of surface temperature (temp2) used in this thesis research, is defined as the temperature at 2 metre above the surface. The total precipitation is obtained from the sum of convective and large-scale precipitation (aprl+aprc). Water vapour is an important greenhouse gas that modifies the Earth's radiative balance and the zonal mean of the vertically integrated water vapour is presented here through the extraction of the variable qvi. Furthermore, an estimate of CS based on the method by Gregory et al. (2004) is presented in Fig. 14. This CS analysis shows the climatic impact that a quadrupling of carbon dioxide has on the global average temperature and the “speed” with which the climate system adapts to a new equilibrium state. Section 4.8 sheds light on the effect of modified ozone forcing to the sea ice concentration (a_ice). Lastly, in order to illustrate the response of polar vortex to the modified ozone forcing in AWI-ESM-2.1-LR, results of geopotential height anomalies of (4xCO₂_O₃-PI) and (4xCO₂_O₃-4xCO₂) and absolute values of PI, 4xCO₂ and 4xCO₂_O₃ simulations are presented in Figs. 19-24 and Figs. A.1-A.9. The variable geopoth is used in the analysis of geopotential height at 100 hPa, 250 hPa and 500 hPa levels.

4.1 Surface Temperature

The simulated 2 metre surface temperature patterns of seasonal anomalies in MAM, JJA, SON, DJF and annual mean are illustrated a based on the anomaly approach analysis (4xCO₂ -PI; Figs. 5 (a-e)) and (4xCO₂_O₃-4xCO₂; Figs. 6 (a-e)). The annual mean temperature during abrupt-4xCO₂

displays a large-scale warming in the NH high latitudes (up to 29°C) in comparison to the Southern Hemisphere (SH). A warmer winter (nearly 15°C) is observed in the SH near the Weddell Sea and the Ronne-Filchner ice shelf near Antarctica (Fig. 5b) notably between 60°S to 65°S. Noteworthy are the hotspots of warming observed in all the seasons except boreal summer across regions of Arctic Ocean, Greenland Sea, Barents Sea, and Kara Sea due to the response of the strong radiative forcing from a quadrupling of CO₂. The comparison of 4xCO₂ to PI indicates the reduction of the seasonal cycle in Arctic as warming in spring, autumn and winter is stronger than in summer. The cause of this large-scale warming in the NH high latitudes is related to the vertically integrated water vapour in the NH high latitudes. Water vapour is an important greenhouse gas that amplifies the greenhouse effect and instigates Arctic warming. However, consistent year-round warming is prominent in Africa, South America, North America, Australia and parts of Asia. Seasonal anomalies of surface temperature with respect to 4xCO₂ and PI (Figs. 5(a-e)) is almost significant everywhere.

In general warming is predominant over landmasses, since land heats up stronger because of reduced heat capacity in comparison to the ocean. This results in a robust land-sea contrast with the only exception in the Arctic Ocean. The annual mean temperature anomaly for 4xCO₂ and PI differs from 7°C to around 2°C.

Contrary to the analysis in Figs. 5(a-e), the presence of the modified ozone forcing consistent with quadrupled carbon dioxide concentration in the 4xCO₂_O₃ simulation induces a cooling in the NH high latitudes, with the dominant effect observed in MAM and DJF than in SON and JJA. Consequently, the modified ozone decreases the impact of carbon dioxide on the seasonal cycle of Arctic, leading to a stronger seasonality if only carbon dioxide was modified. The modified ozone forcing induces a cooling in between -1°C to -3°C in the tropical lower stratosphere and warming elsewhere in the stratosphere as evident from Figs. 10a and 10b.

In general, a cooling is observed all over the year in the 4xCO₂_O₃ simulation. Strikingly, the modified ozone is the key influencer in increasing the anomalies that exceeds upto 0.8°C in parts of North America, parts of western Antarctica and parts of Australia. Hence, changes of surface air temperature due to modified ozone forcing to 4xCO₂ act as a strong mitigating factor to increased levels of carbon dioxide.

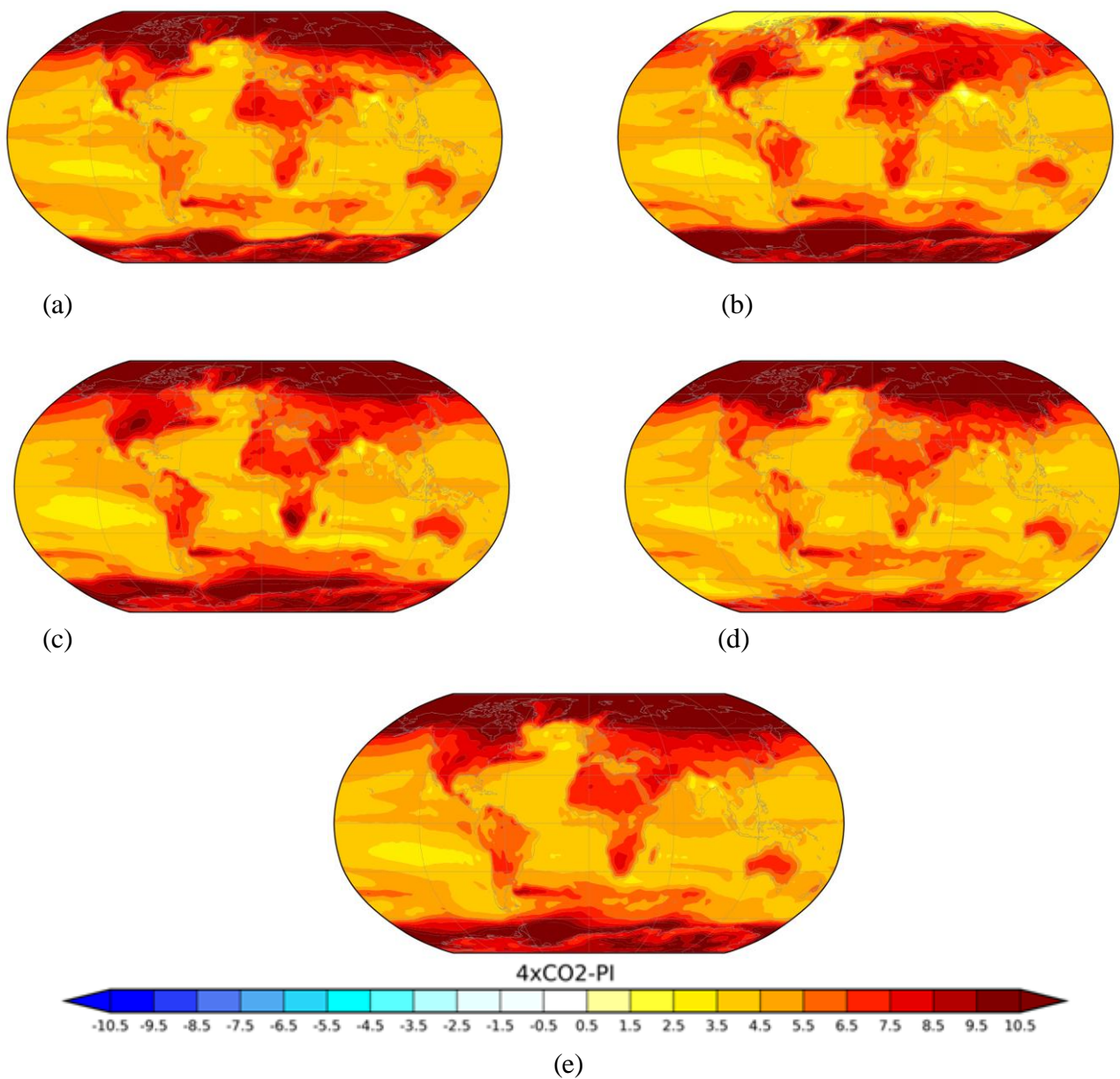


Figure 5: Surface temperature anomaly of 4xCO₂-PI for MAM (a), JJA (b), SON (c), DJF (d) and Annual (e). There are no insignificant anomalies here based on a t-test with 95% confidence interval. The unit is °C.

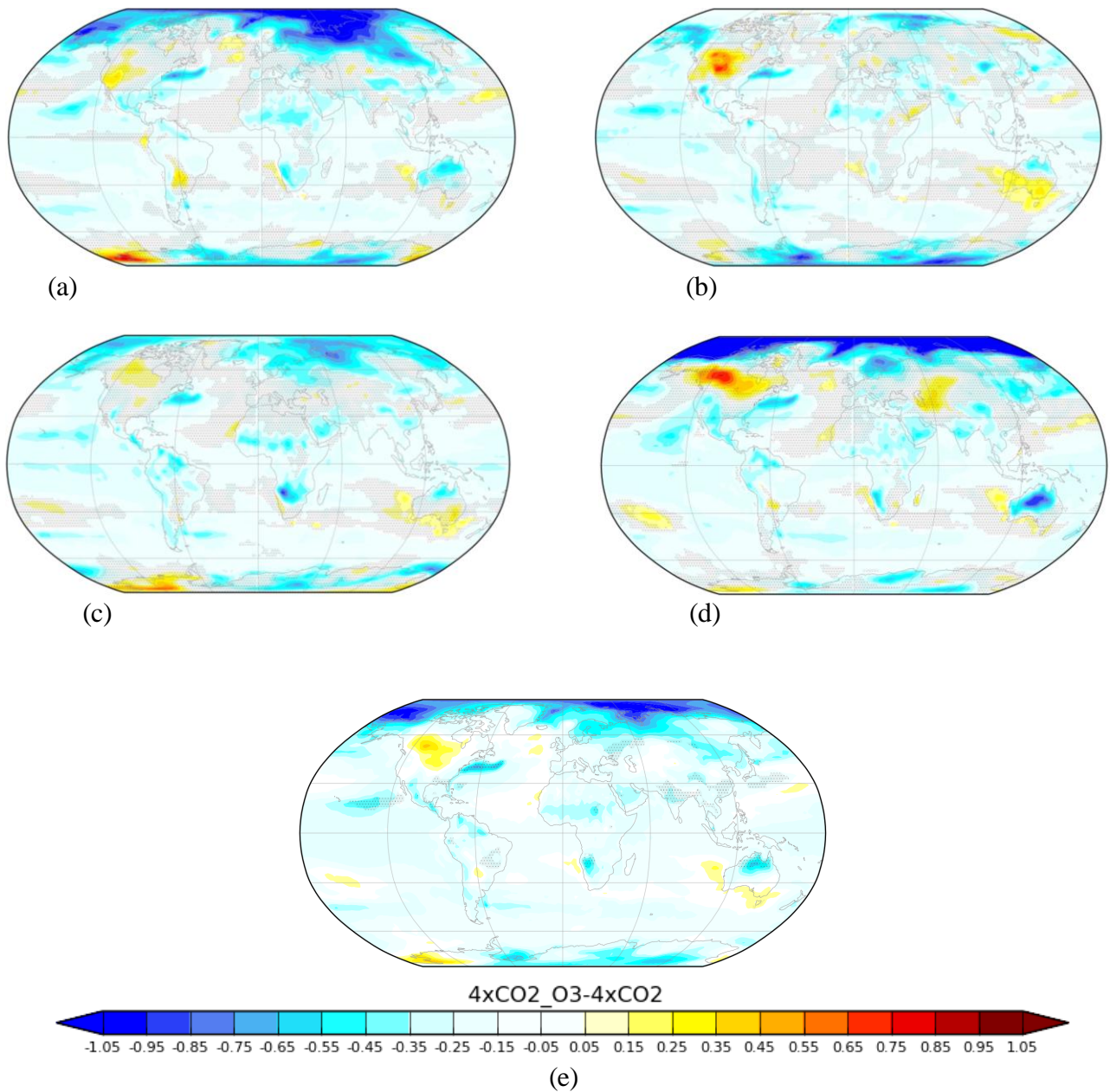


Figure 6: Surface temperature anomaly of $4xCO_2_{O_3} - 4xCO_2$ for MAM (a), JJA (b), SON (c), DJF (d) and Annual (e). The hatched areas indicate the regions with insignificant anomalies based on a t-test with 95% confidence interval. The unit is °C.

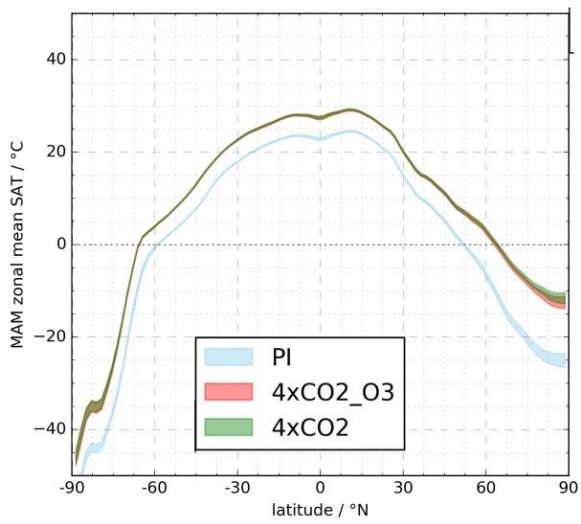
4.2 Zonal mean surface temperature

The zonal mean temperature and the meridional temperature gradient for the PI (blue), $4xCO_2$ (green) and $4xCO_2_{O_3}$ (red) simulations of MAM, JJA, SON, DJF and the annual mean are shown in Figs. 7(a-e). The shadings in Figs. 8(a-e) indicate the standard deviation over time. The wider the shading, the more variable is the zonal temperature over the averaging period for the respective seasonal and annual time average. The zonal mean surface temperature shown here is the 2-metre temperature as a function of latitude. A comparison of the zonal mean surface temperature patterns in

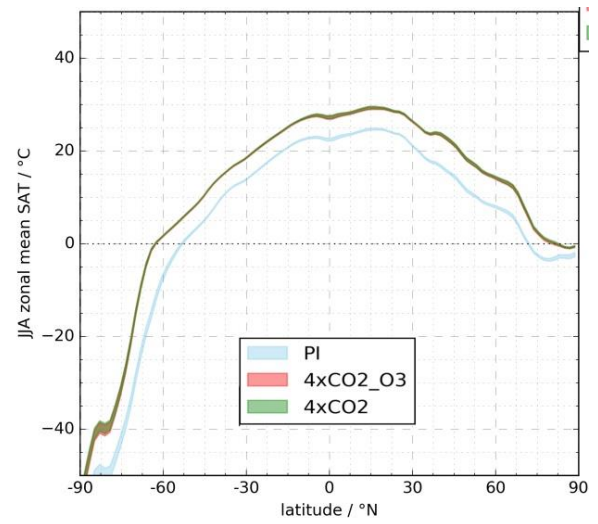
between $4xCO_2$ and $4xCO_2_{-}O_3$ simulations with PI illustrate a large change in temperature in the high latitude and a lower change of temperature in the low latitudes. Warming is observed in the tropics throughout the year. Towards north of $50^\circ N$, significant warming is observed in the $4xCO_2$ simulation resulting mainly from the enhanced carbon dioxide concentration. Whereas, due to the presence of the modified ozone forcing in the $4xCO_2_{-}O_3$ simulation, there is a minor reduction of temperature causing a cooling in the NH high latitude. This cooling of about $-0.2^\circ C$ in the NH high latitudes is effectively visible in spring and winter (Figs. 7a, 7e). Fig. 7e, shows that the annual zonal mean surface temperature in the PI simulation reach $15^\circ C$ in the tropics (in between $30^\circ S$ and $30^\circ N$) and $\sim 23^\circ C$ at the poles (beyond $70^\circ N$).

Figs. 8(a-e), clearly shows an asymmetric distribution of the zonal mean surface air temperatures around the equator. The presence of the modified ozone forcing mostly has a cooling effect across all latitudes with some variability of surface temperature observed in the positive range (Figs. 8(a-e)). Annually, at very high latitudes in the North, the average is cooling with minor warming observed. Fig. 8e shows that the NH is cooler than the SH by $-0.6^\circ C$. Strong seasonal variations are observed in DJF ranging from about $-3^\circ C$ in the NH to about $-0.3^\circ C$ in the SH in JJA. The inter-hemispheric surface temperature difference vanishes in MAM. Nonetheless, a small difference of $-1.5^\circ C$ is observed in SON.

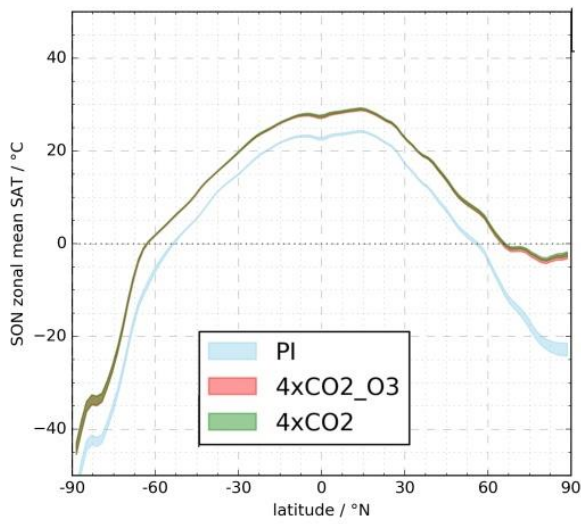
Figs. 8(a-e), confirms that the interannual variability due to the modified ozone forcing is the largest in the SH in all the seasons except in winter, where the interannual variability spread is mostly focussed in the NH. Fig. 8c depicts that the autumn zonal mean surface temperature varies from $1.8^\circ C$ to $-1.8^\circ C$ in the SH polar region and from $-1.2^\circ C$ to $0.4^\circ C$ in the NH polar regions. Hence, between the warmest autumn in the SH and the warmest autumn in the NH, there's a slight difference of $1.4^\circ C$ of warming. Nonetheless, appreciable is the interannual variability due to the adjusted ozone ultimately resulting in a temperature of $1.8^\circ C$ in the SH compared to $0.4^\circ C$ in the NH.



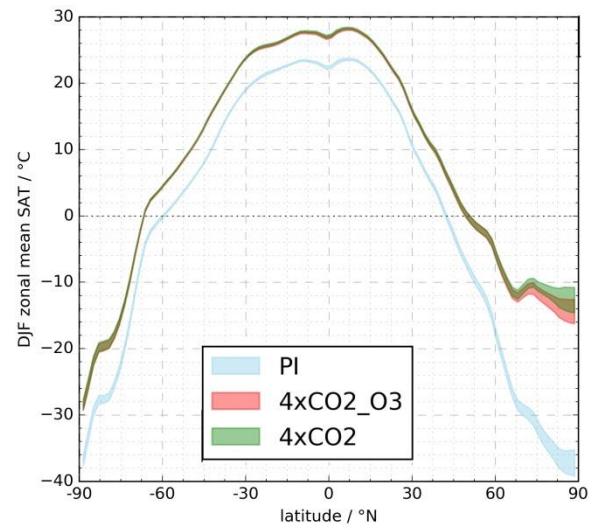
(a)



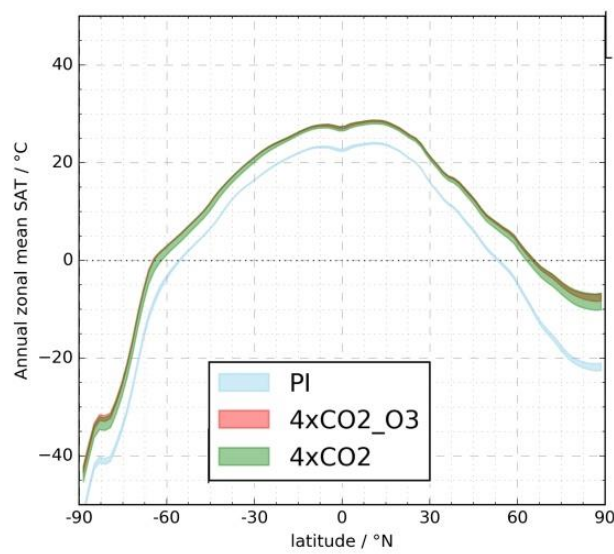
(b)



(c)

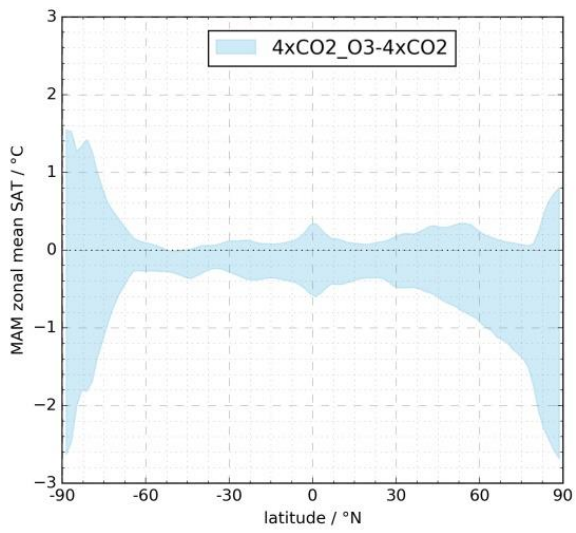


(d)

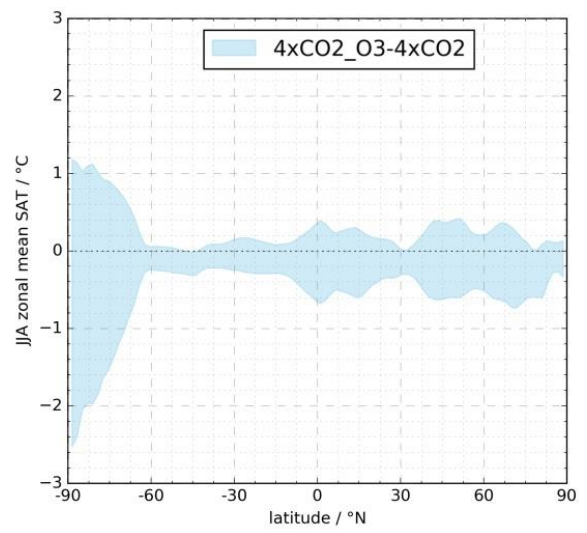


(e)

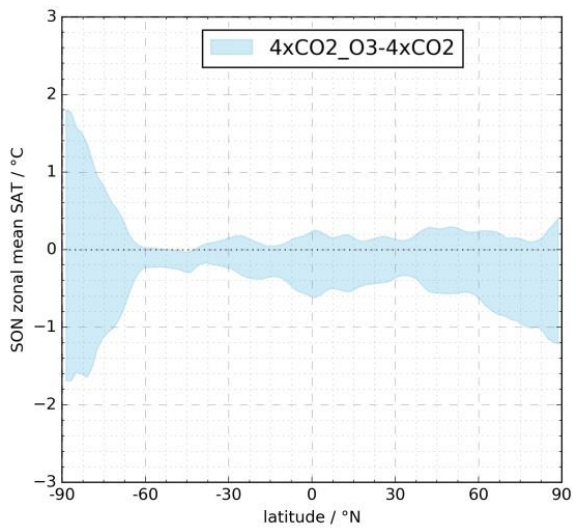
Figure 7: Meridional range of zonal mean surface air temperature (SAT) of PI, 4xCO₂ and 4xCO₂_O₃ simulations for MAM (a), JJA (b), SON (c), DJF (d) and Annualmean (e).



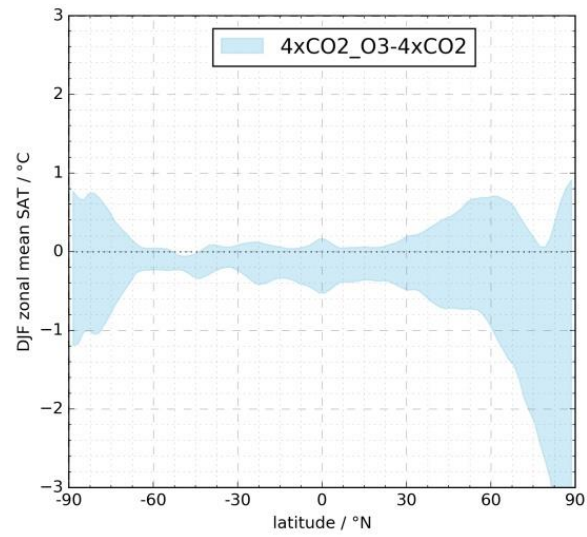
(a)



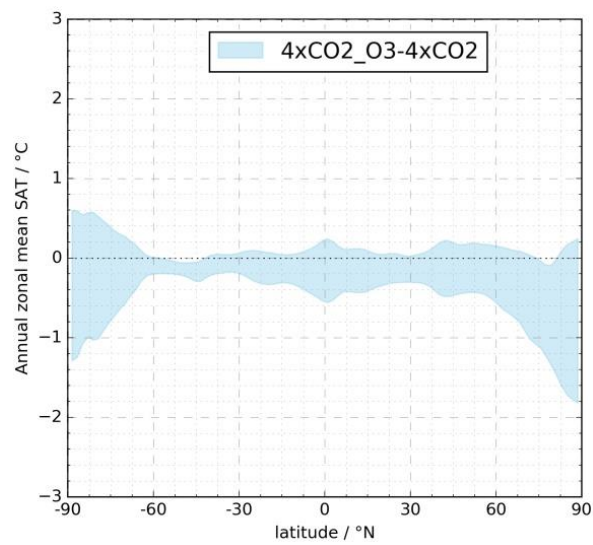
(b)



(c)



(d)



(e)

Figure 8: Meridional range of zonal mean surface air temperature (SAT) anomaly of PI, 4xCO₂ and 4xCO₂_O₃ simulations for MAM (a), JJA (b), SON (c), DJF (d) and Annual mean (e).

4.3 Vertical Temperature Structure

In this sub-section, the results for the vertical mean temperature are shown. The motivation to examine the zonal mean temperature response across the atmosphere column is twofold;

1. Changes in the tropical surface air temperature changes are broadly analogous with the changes in the tropical belt (Adam et al., 2014) as the quadrupled carbon dioxide leads to a significant expansion of the tropical belt as measured by the Hadley cell edge latitudes in the Northern and Southern Hemisphere (Frierson et al., 2007).
2. From the observation of a zonal mean temperature response, information about the model's sensitivity to a $4xCO_2$ forcing is obtained (Davis et al., 2016). Fig. 9 exhibits a canonical pattern of zonal mean temperature response to $4xCO_2$ with fixed ozone at pre-industrial level. It is observed that the quadrupled carbon dioxide concentration propels an amplified warming in the tropical upper troposphere and stratospheric cooling which increases with height (Manabe and Wetherald, 1967). In the tropics, the upper tropospheric warming is observed due to the moist adiabat that communicates with the surface warming to the TOA (Held et al., 1993). Stratospheric cooling is identified due to the quadrupled carbon dioxide concentration which enhances the infrared cooling to space (Davis et al., 2016) and decreases the upward thermal radiation (Goessling et al., 2016). Consistently, the quadrupled carbon dioxide concentration portrays a canonical temperature response with tropospheric warming and stratospheric cooling.

Unlike the robust vertical temperature structure response in the $4xCO_2$ simulation, Figs. 10a and 10b depicts that the modified ozone forcing in the $4xCO_2_{-}O_3$ simulation induces cooling between $0.55^{\circ}C$ to $1^{\circ}C$ (50-250 hPa) in the tropical lower stratosphere (TLS) and warming of about $2.91^{\circ}C$ (10-30 hPa) in the stratosphere. The ozone induced TLS cooling is coherent with the decrease of ozone in that region (Fig. 4). In the $4xCO_2_{-}O_3$, due to the induced ozone forcing there is a significant pattern of temperature change observed in the stratosphere (30-80 hPa) in between tropics and high latitudes, while there is a monotonic increase in the temperature with respect to height due to $4xCO_2$ with little variation across high latitudes.

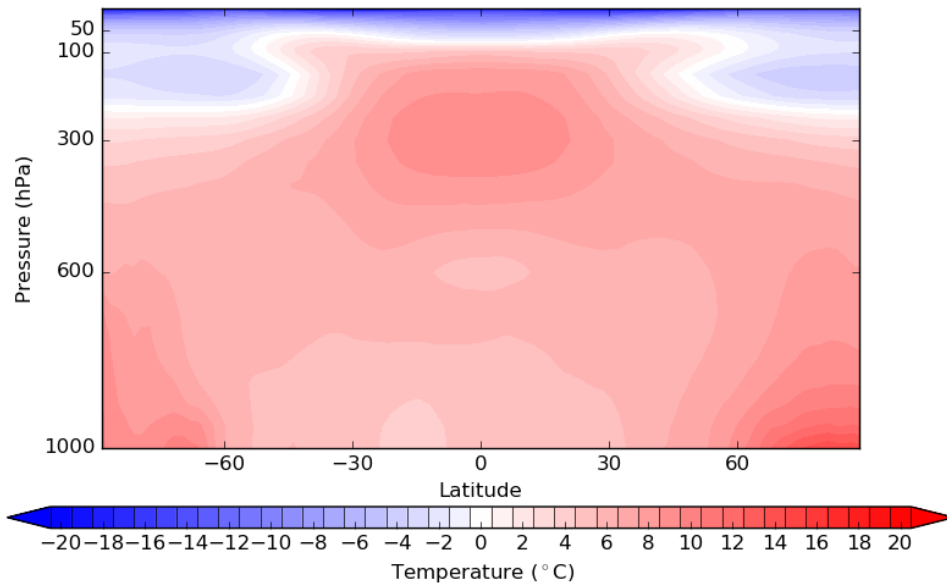


Figure 9: The difference in the zonal-mean temperature response between the $4xCO_2$ and PI experiment. The unit of temperature unit is $^{\circ}C$ and the unit of pressure is hPa.

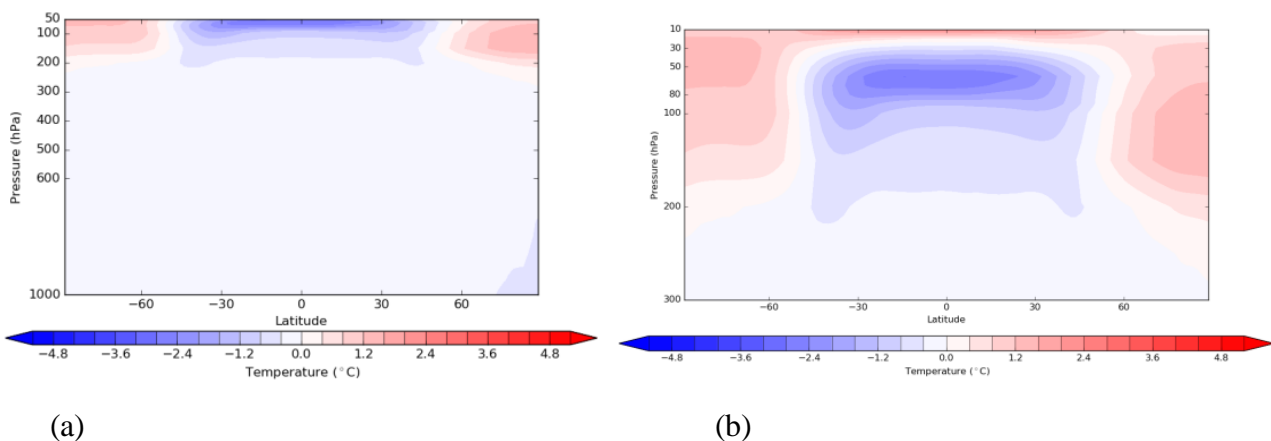


Figure 10: The difference in the zonal-mean temperature response between the $4xCO_2_{O_3}$ and $4xCO_2$ experiment showing pressure levels ranging from 50-1000 hPa (a) and 10-300 hPa (b). The unit of temperature unit is $^{\circ}C$ and the unit of pressure is hPa.

4.4 Precipitation

The total annual precipitation shows predominant and strengthened spatial monsoon patterns in the tropical mid-latitude region as a result of quadrupling carbon dioxide (Fig. 11e). Strengthened summer monsoon covering parts of South Asia, Southeast Asia including Indonesia, Northwest Pacific, and Northeast Pacific are more dominant during $4xCO_2$ than compared to PI. The intensification of the monsoon over these regions is caused due to a contrast between the temperature difference, leading to land-sea pressure gradients which inhibits the strong moist onshore inflow towards the land, resulting in large shifts of rainfall. Additionally, much reduced

precipitation patterns in and around the Caribbean Sea are perceived throughout the year. Globally, precipitation associated with the Intertropical Convergence Zone (ITCZ) is much stronger in $4xCO_2$ compared to PI. In boreal summer, the northward shift of the ITCZ contributes to increased rainfall towards the north of equator, and consequently reduced rainfall over south of the equator. Furthermore, a comparison of total precipitation shows stronger winter monsoon over Bay of Bengal, Sri Lanka, Indonesia, Northwest of Australia, and, Amazon and a more feeble precipitation over Western Pacific Ocean and western Indian Ocean (Figs. 11(a-e)). In response of $4xCO_2$ alone, a drying over the subtropical Atlantic and $30^\circ S$ is observed. The global average precipitation changes from 976.15 mm/year in the PI simulation to 1069.72 mm/year in $4xCO_2$ simulation.

Figs. 12(a-e) clearly indicate that the precipitation anomaly in between the $4xCO_2_{O_3}$ and $4xCO_2$ simulations is insignificant in most of the regions. In DJF the strongest precipitation is observed in the tropics and the subtropics.

Particularly, the land regions experience stronger precipitation in $4xCO_2_{O_3}$ in comparison to $4xCO_2$. However, most of the negative anomalies are visible in the tropical, subtropical and polar regions in both the NH and SH. The ozone adjustments in the $4xCO_2_{O_3}$ lead to a predominant drying over the west of Indonesia, Southern part of Indian ocean, the Southern pacific Ocean, the Northern portion of the North Atlantic, and parts of Scandinavia, and wetting over central and southern Europe. During boreal summer in JJA, extreme rainfall is visible in South Asia, the Western part of Indian Ocean and the Pacific Ocean. The global average precipitation in $4xCO_2_{O_3}$ is 1056.15 mm/year, indicating that there are small differences in precipitation between PI (976.15 mm/year) and $4xCO_2$ (1069.72 mm/year).

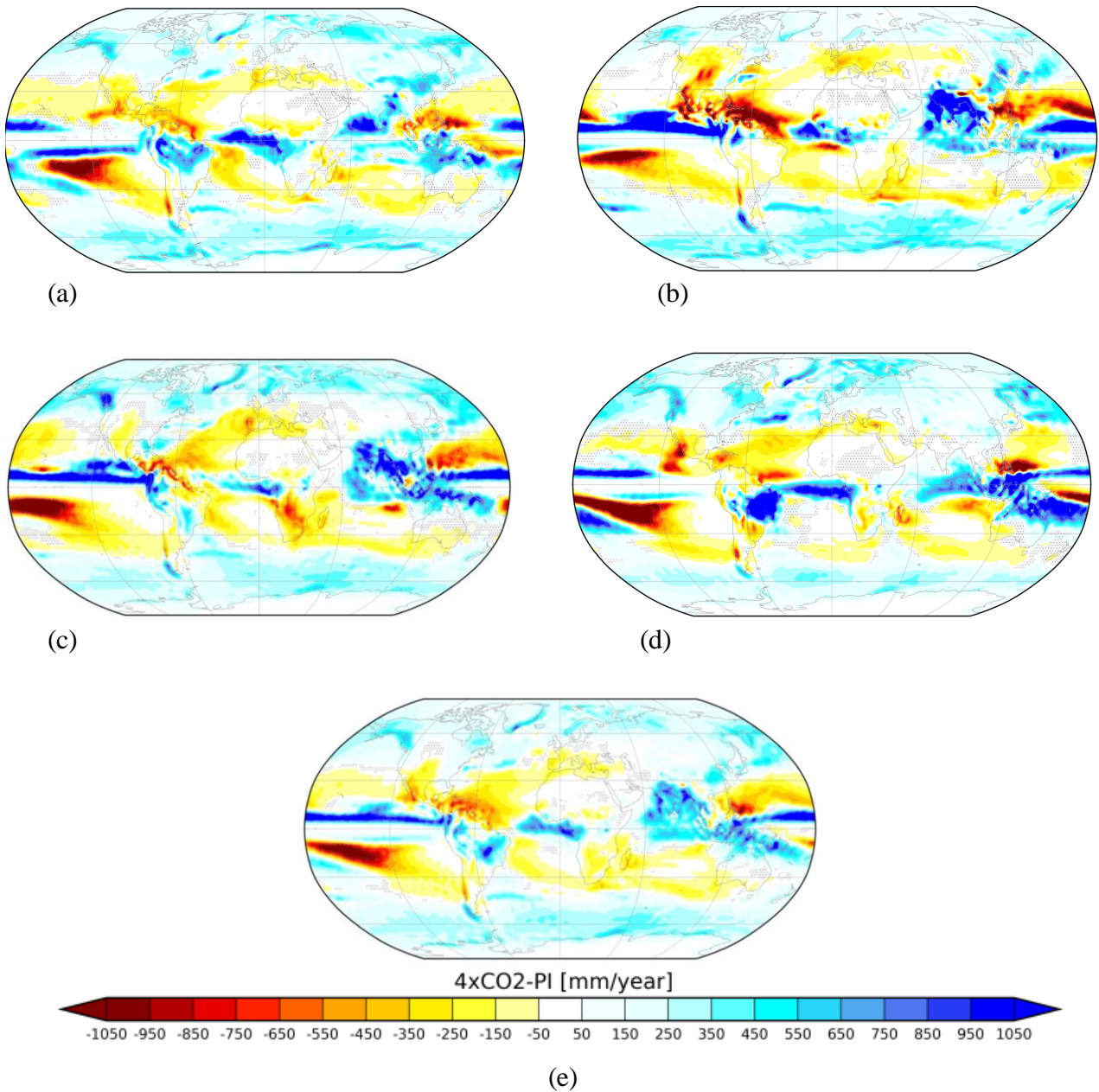


Figure 11: Precipitation anomaly of 4xCO₂-PI simulations for MAM (a), JJA (b), SON (c), DJF (d) and Annual mean (e). The hatched areas indicate regions with insignificant anomalies based on a 95% confidence interval. The unit is mm/year.

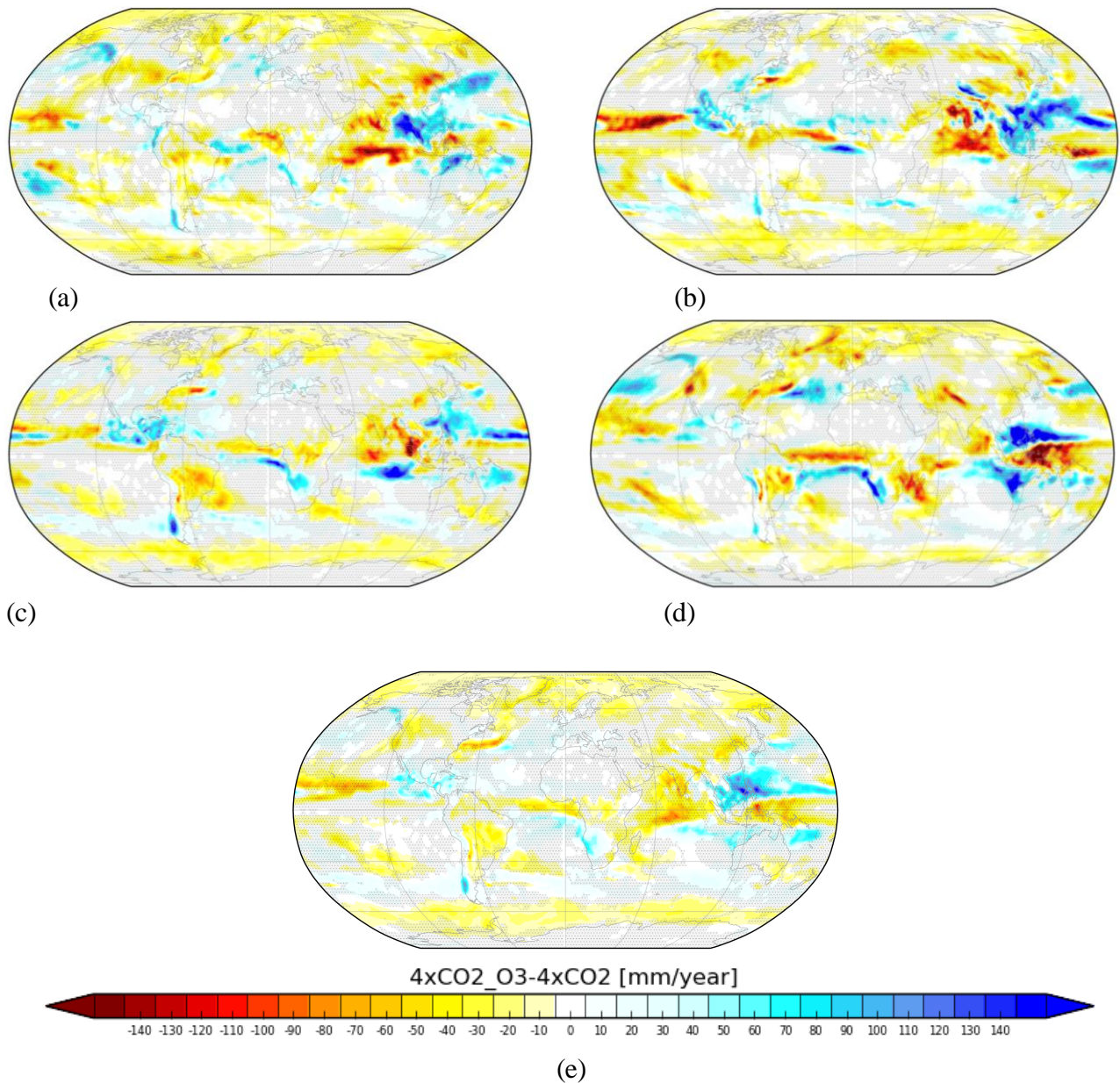


Figure 12: Precipitation anomaly of 4xCO₂_O₃-4xCO₂ simulations for MAM (a), JJA (b), SON (c), DJF (d) and Annual mean (e). The hatched areas indicate regions with insignificant anomalies based on a 95% confidence interval. The unit is mm/year.

4.5 Vertically Integrated Water Vapour

Water Vapour is an effective greenhouse gas which contributes to warming in the atmosphere by absorbing thermal infrared radiation and radiating it back to the Earth's surface. In the 4xCO₂ simulation, an enhanced greenhouse gas effect is observed due to the amplified warming instigated by the quadrupled carbon dioxide concentration. Eventually, this warmer climate with 4xCO₂ concentration can store more water vapour according to Clausius-Claperyon equation which leads to a larger water vapour content resulting in an increase of temperature and a positive water vapour feedback. Overall, in the 4xCO₂ and 4xCO₂_O₃ simulation the integrated water vapour content is increasing and there are some asymmetries. The largest relative differences of the water vapour

content are substantially visible at the low latitude, whereas, there is a near doubling of water vapour content in high latitudes. Fig. 13a shows a strong increase in vertically integrated water vapour in NH high latitudes, compared to the SH high latitudes. Since water vapour is a primary greenhouse gas, the strong increase in water vapour in the atmosphere will certainly also provide a contribution to the warming being particularly pronounced in the NH high latitude (Fig. 5d). From figs. 13a and 13b it is observed that the modified ozone concentration in the 4xCO₂_O₃ simulation have a minor impact on the water vapour mostly focused in the tropics.

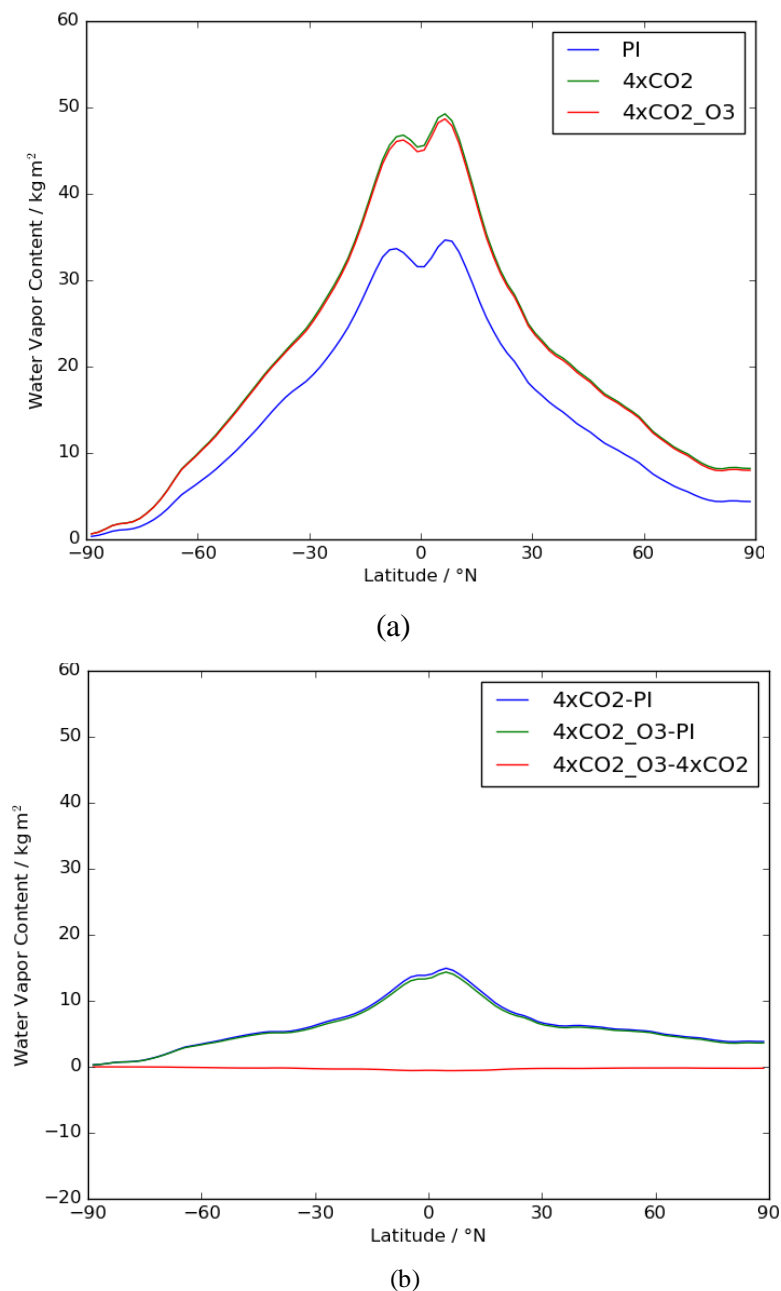


Figure 13: Zonal mean vertically integrated water vapour compared to the 4xCO₂ (green) and PI (blue), 4xCO₂_O₃ (red) (a). Zonal mean vertically integrated water vapour anomalies 4xCO₂-PI (blue), 4xCO₂_O₃-PI (green) and 4xCO₂_O₃-4xCO₂ (red) (b).

4.6 Climate Sensitivity

Climate sensitivity (CS) is a fundamental and quantitative measure of the susceptibility of Earth's climate by the global-mean surface air temperature change due to a doubled carbon dioxide concentration in the atmosphere from pre-industrial period (Danek et al., 2020). It is considered as an important measure to quantify the impact of predicted anthropogenic climate change. This is beneficial in diagnosing the global climate feedback and the impact of radiative global mean due to the quadrupling of carbon dioxide concentration on climate.

Based on the method by Gregory et al. (2004), the CS analysed here, is based on a linear relationship by estimating the intersection of the linear trend between global averages of TOA radiative imbalance (W/m^2) and ΔSAT ($4\times\text{CO}_2$ -PI) with the abscissa. CS is estimated to be 3.43°C per doubling CO_2 with modern ozone and 3.34°C per doubling CO_2 with the modified ozone forcing (Fig.14).

The two different regressions - one with the $4\times\text{CO}_2_O_3$ simulation and the other with $4\times\text{CO}_2$ simulation for 100-500 years of data sample depict a noticeable change in the relationship between annual mean TOA radiative imbalance and SAT temperature change.

From Fig. 14 it is visible that the CS with respect to the modified ozone forcing in the $4\times\text{CO}_2_O_3$ simulation is lower as compared to the $4\times\text{CO}_2$ simulation. The slope of the curve instead of expected to be reduced with increasing SAT anomaly, seems to be much steeper, for which it is assumed that AWI-ESM-2.1-LR has more efficiency in mixing the additional heat down into the deep ocean, leading to a quicker equilibration and to a convergence that can rarely be observed in other models.

Fig. 14 shows that the modified ozone forcing in the $4\times\text{CO}_2_O_3$ simulation has a minor impact on the climate sensitivity consistently in response to the $4\times\text{CO}_2$ simulation. Figs. 6a and 6d also show that the impact of modified ozone on surface temperature in boreal spring and winter is not evenly spread across the globe. It is biased towards the NH high latitudes. Nevertheless, CS is a globally integrated climate signal which correlates with the results in Figs. 6a and 6d showing that the NH bears the strongest cooling which reduces the CS to 3.34°C and polar amplification to 1.79 as visible from Fig. 6e.

Nonetheless, there are some caveats to this CS analysis: firstly, the estimate of the linear regression based on the relationship between the TOA radiative imbalance and ΔSAT is based on 500 years of model output data and until then full equilibration of the climate state has not been reached. Secondly, AWI-ESM-2.1-LR lacks the ozone-climate feedback whereas other models as described in Dietmüller et al. (2014), Muthers et al. (2014), Nowack et al. (2015), and Marsh et al. (2016) includes the interactive chemistry scheme and the ozone-climate feedback. It has also been shown

in the aforementioned publications that the model dependencies in the ozone feedback are due to the differences in their respective models and not due to the modified ozone forcing in the simulations.

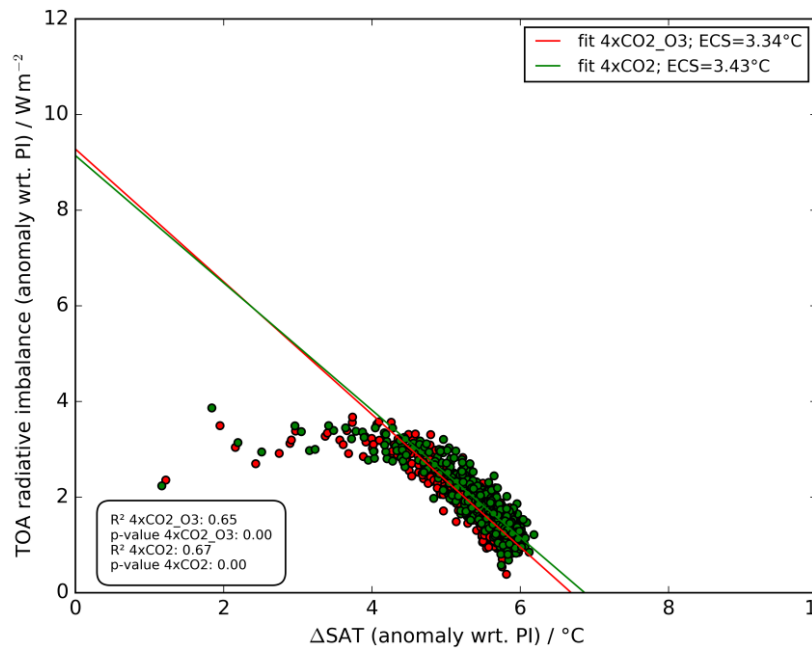


Figure 14: Gregory plot: regression of top of the atmosphere (TOA) radiative imbalance (sum of incoming shortwave and incoming and outgoing longwave radiation at top of atmosphere) versus change of global average surface air temperature (SAT) for (4xCO₂-PI) (green) and for (4xCO₂-O₃-PI) (red) based on annual means.

4.7 Polar Amplification

Arrhenius's argument regarding the change of carbon dioxide concentration that leads to an amplified global average warming signal especially in the polar latitudes appears to be the first formal acknowledgement of polar amplification (Arrhenius, 1896). Polar amplification arises from various radiative forcing patterns (Huang et al., 2017), and diverse feedback mechanisms at high and low latitudes (Taylor et al., 2013, Pithan and Mauritsen, 2014).

Nonetheless, in spite of many controversies regarding the potential contributor of Arctic amplification, the most well established is the sea-ice-albedo feedback at high latitudes (Manabe and Stouffer, 1994; Hall, 2004), but the other associated feedbacks are the temperature, water vapour, clouds, and lapse-rate (Pithan and Mauritsen, 2014). The increase in the vertically integrated water vapour content in the NH high latitudes indicates a positive contribution of water vapour feedback towards polar amplification (Fig. 13a).

However, alongside several hypothesised consequences of Arctic amplification, the predominant goal in this thesis is to quantify the polar amplification in response to the radiative forcing imposed due to quadrupled carbon dioxide concentration along with the modified ozone field in the atmosphere-ocean coupled model, AWI-ESM-2.1-LR.

Here, polar amplification is examined from the PI, 4xCO₂ and 4xCO₂_O₃ simulations through a quantitative comparison of temperature changes with latitude. This is implicitly calculated from the annual SAT anomalies (4xCO₂-PI) and (4xCO₂_O₃-PI) over (60-90°N) and (30-60°N). The absolute values of the SAT of the three aforesaid simulations and the polar amplification factor are presented in Table 3.

Based on the simulations, it is observed that the modified ozone fields weaken the polar amplification. Contrary to the 4xCO₂ simulation which creates a strong global warming that is subject to an intense polar amplification, there is a robust weakening of the polar amplification that predominantly occurs due to the cooling in the NH high latitudes initiated from the imposed modification of ozone forcing as portrayed in Fig. 6e.

Table 3: Values of surface air temperature in (Kelvin) and polar amplification factor as a ratio over (60-90°N) and (30-60°N)

Experiment Name	SAT (global) (K)	SAT (60-90°N) (K)	SAT (30-60°N) (K)
PI	284.39	259.72	280.00
4xCO ₂	290.26	271.66	286.53
Polar Amplification : 1.82			
4xCO ₂ _O ₃	290.10	271.22	286.39
Polar Amplification : 1.79			

From Table 3 it is evidently visible that the difference in between the surface air temperatures computed is rather small, whereas Fig. 6e shows that these small exceptions of the temperature anomalies are statistically significant.

4.8 Sea ice concentration

Sea ice serves as a major component of the climate system which is very sensitive to the model formulation (Sidorenko et al., 2015). The last 100 years of averaged data of March (maximum sea ice concentration) and September (minimum sea ice concentration) maps of sea ice concentration are shown in Figs. 15 and 16 respectively.

Higher sea ice concentration is observed in the PI from the Arctic Ocean in the north to Weddell Sea in the SH as compared to the $4xCO_2$ and $4xCO_2_O_3$ simulation. However, there is a decline in the sea ice concentration in the $4xCO_2$ and $4xCO_2_O_3$ simulation as observed in Figs. (15b, 15c) and Figs. (16a, 16c).

One of the main contributors to this sea ice decline in Figs. 15b, 15d, 16a, and 16c is due to the increase of the surface temperature caused by the quadrupling of carbon dioxide and the impact of the modified ozone forcing in the $4xCO_2$ and $4xCO_2_O_3$ simulations. Fig. 13a shows that the water vapour feedback plays a crucial role in the arctic amplification. Since, water vapour is an effective greenhouse gas, it plays a prominent role in an amplified surface warming and as a contributor to the sea ice melt.

In response to the quadrupled carbon dioxide, sea ice concentration is reduced in the SH both in March and September. In March, the decline of sea ice concentration is observed in the high southern latitudes most prominently in the Weddell Sea and Ross Sea. On the contrary in the winter months, that is in September, reduction of sea ice is observed all over Antarctica extending further to the north, reaching $55^\circ S$ in the Atlantic sector.

The sea ice concentration anomalies in the NH show a predominance of negative anomalies along the Beaufort and Chukchi Sea extending up to the north-eastern Canadian sector eastward to the Greenland Sea and along the Siberian Coast. While, positive anomalies are shown in Figs. 17c, 17d and 18d with existence of sea ice in the central Arctic covering Beaufort Sea, Chukchi Sea, Laptev Sea and Kara Sea. The areas with largest anomalies in Figs. 17a, 17b, 18a, 18b and 18c including Beaufort Sea, Chukchi Sea, East Siberian Sea, Laptev Sea, Kara Sea, and Greenland Sea are generally ice free. In Fig. 16a, the remaining sea ice cover is mostly below 10% coverage leading to a nearly ice-free Arctic Ocean in summer. Whereas, in winter there is a sea ice coverage of upto 20% (Fig. 15a).

The anomaly between $4xCO_2_O_3$ and $4xCO_2$ shows positive anomalies in the SH both in March and September prevailing over the Southern Ocean. Positive anomalies are visible in the western Pacific Ocean, Amundsen Sea, and Ross Sea (Figs. 17d, 18d). Nevertheless, negative sea ice concentration anomalies are observed in the northern Weddell Sea and the Western coast of the Antarctic Peninsula. The sea ice concentration as seen in Fig. 16c is slightly increased due to the cooling effect of ozone as compared to the $4xCO_2$ simulation, where there is no sea ice left in the summer (Fig. 16a). A sea ice coverage of about 20% is noticed towards northern end of Greenland due to the presence of ozone (Fig. 16c).

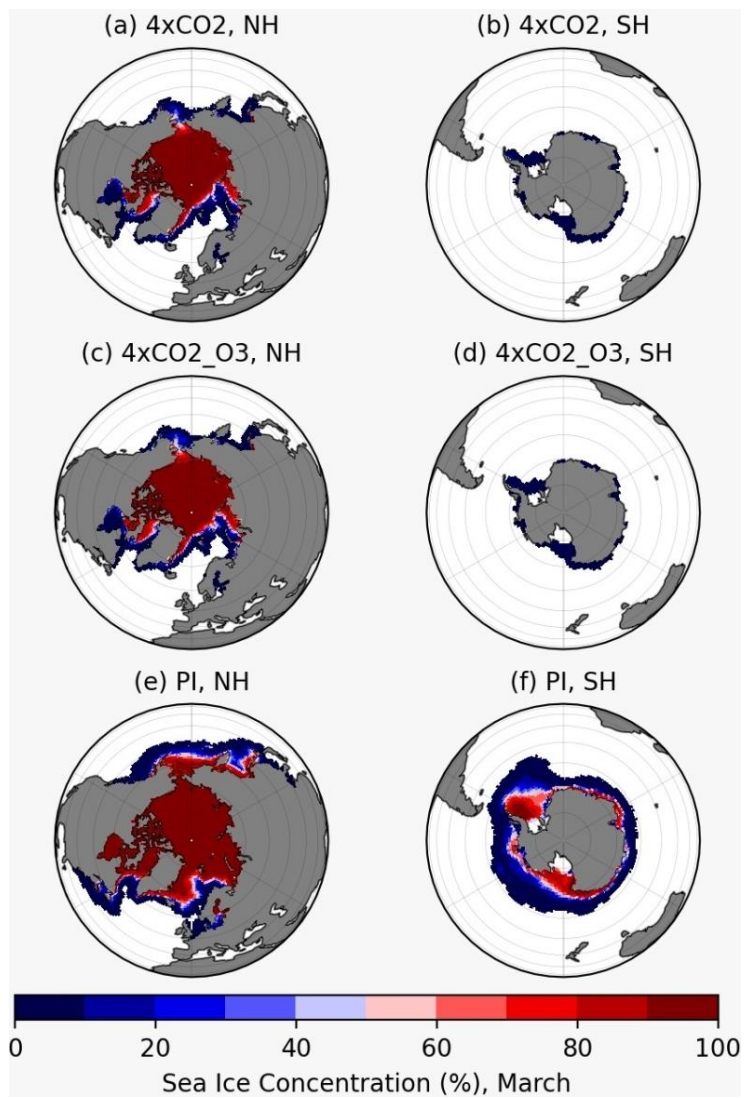


Figure 15: Simulated sea ice concentration of 4xCO₂, 4xCO₂_O₃ and PI simulations with their respective land sea mask in March: winter in NH (a,c,e) and summer in SH (b,d,f). Units are in percentage (%).

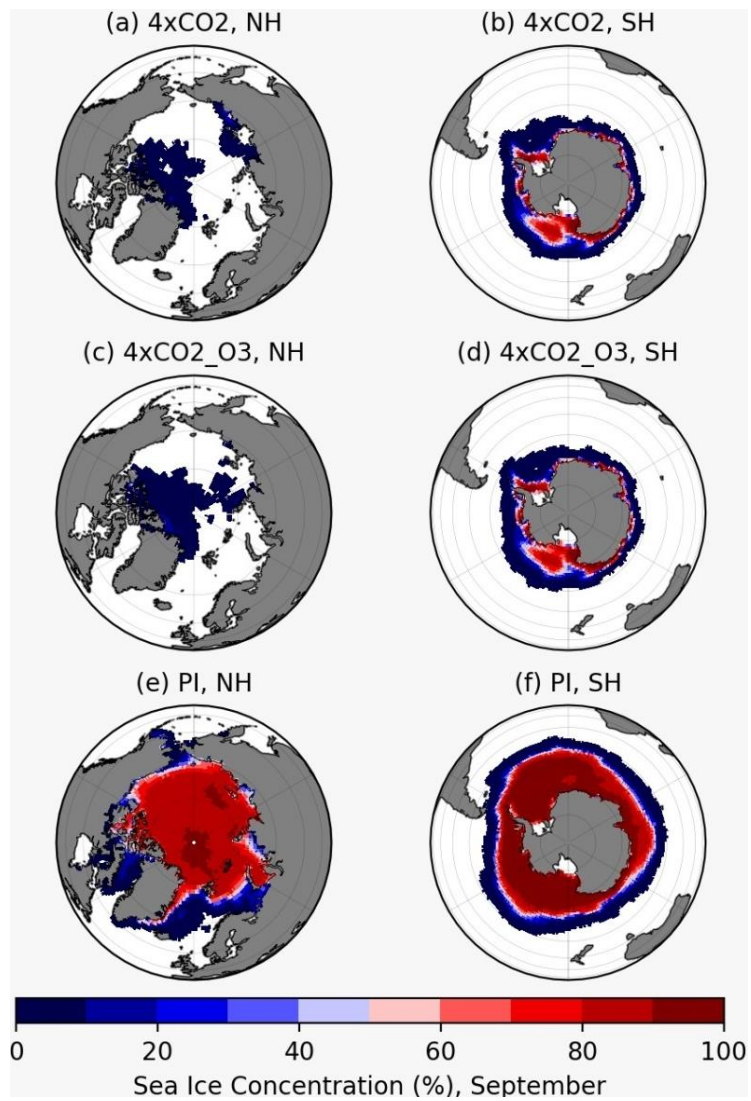


Figure 16: Simulated sea ice concentration of 4xCO₂, 4xCO₂_O₃ and PI simulations with their respective land sea mask in September: summer in NH (a,c,e) and winter in SH (b,d,f). Units are in percentage (%).

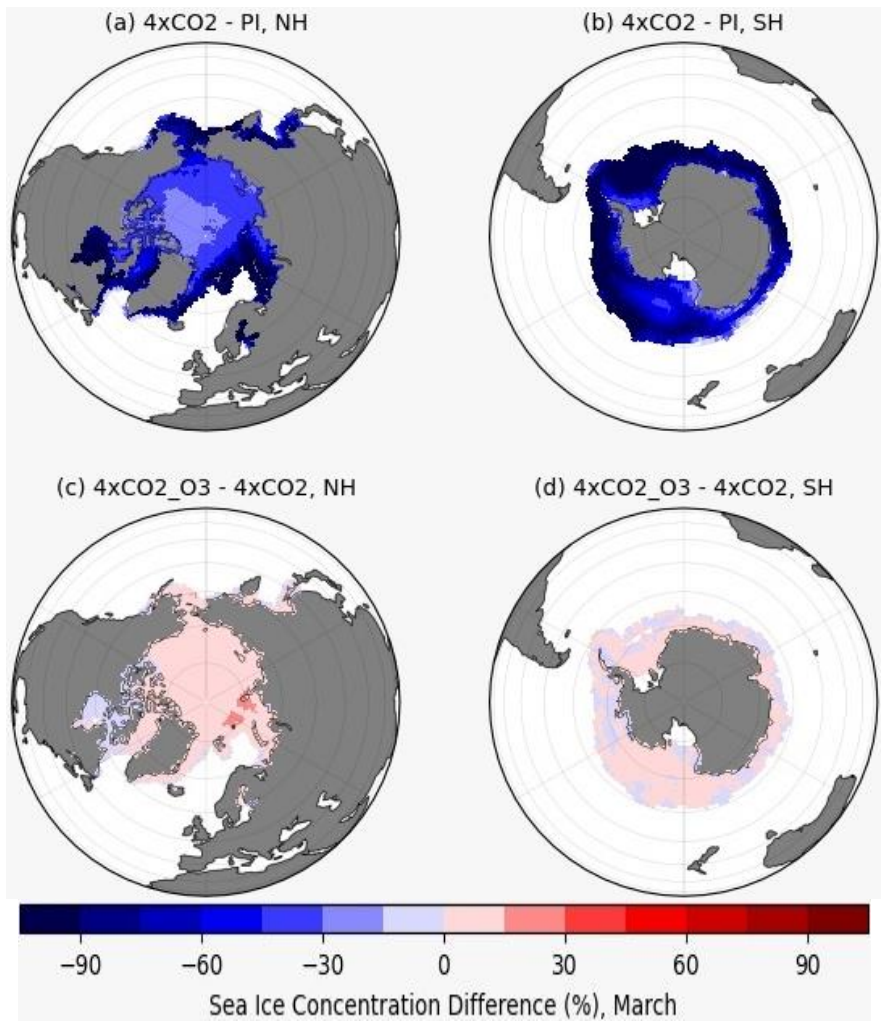


Figure 17: Simulated sea ice concentration of 4xCO₂-PI and 4xCO₂_O₃-4xCO₂ simulations with their respective land sea mask in March: winter in NH (a,c) and summer in SH (b,d). Units are in percentage (%).

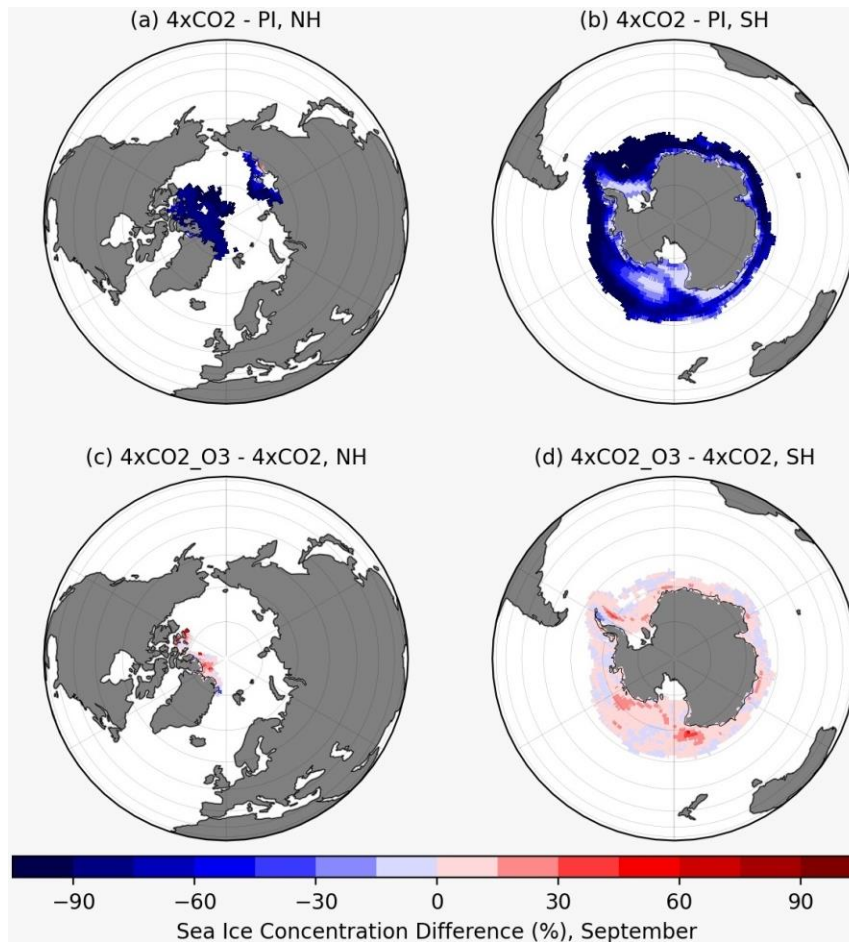


Figure 18: Simulated sea ice concentration of $4xCO_2$ -PI and $4xCO_2_{O_3}$ - $4xCO_2$ simulations with their respective land sea mask in September: summer in NH (a,c) and winter in SH (b,d). Units are in percentage (%).

4.9 Geopotential Height at 500 hPa, 250 hPa and 100 hPa levels

The linkage of the polar vortex to the ozone depletion has generated considerable interest and research into the formation and breakup of the polar vortex. Theoretically, it has been shown that a weakening of the polar vortex can be triggered also by an increase in the ozone layer, but no clear evidences have been found regarding the physical mechanisms behind this theory. In this respect, one of my aim in this thesis was to investigate the response of the polar vortex to the prescribed ozone fields in AWI- ESM- 2.1- LR, based on the 800 years of simulation datas. The influence of prescribed ozone fields on the variability of the polar vortex was tested by looking at geopotential height in the atmosphere between 500 hPa, 250 hPa and 100 hPa levels.

In order to analyse the response of the large-scale atmospheric circulation to ozone forcing, in this sub-section the geopotential height at 500 hPa, 250 hPa and 100 hPa levels of annual mean and seasonal anomalies in MAM, JJA, SON and DJF are illustrated, based on the anomaly analysis

$4xCO_2_O_3-4xCO_2$ and $4xCO_2_O_3-PI$. The 100 hPa geopotential height is used to illustrate the evolution of the polar vortex (Overland et al., 2020). This analysis is useful in the context of this thesis since the changes in the strength of the polar vortex influences significantly the frequency and magnitude of extreme weather events over the mid-latitudes. Fig. A.2a shows a large scale warming signal in the NH than compared to PI. In the $4xCO_2_O_3$ simulation, there is a bit of cooling observed in the NH high latitude close to Northern Siberia and towards Russian islands (Fig. A.3a). It is noticed that the impact of modified ozone is much lower than carbon dioxide, but it certainly does not overrule it.

Fig. 19a shows strong geopotential height positive anomalies over Siberia, but negative anomalies over Canada and the North Atlantic due to the imposed ozone forcing with respect to quadrupled carbon dioxide concentration in the $4xCO_2_O_3$ simulation. This could be an indication of a weak polar vortex. The altering positive and negative geopotential height anomalies are an indication of chains of Rossby waves (Figs. 21(a-e), 22(a-e), 23(a-e), 24(a-e)). In the 250 hPa geopotential height anomaly (Fig. 21a), a wave-like structure with negative anomalies in North Atlantic, northern Europe, and East Asia, and two centres of positive anomalies over the North Atlantic around $60^\circ N$ and central Eurasia is predominantly visible. This is mainly due to the shift in the mode of Rossby waves. Polar vortex is an essential component in driving the large scale circulation and Figs. 23(a-e) clearly has an impact on the polar vortex. It has an influence on the atmospheric circulation at the mid-latitudes in between $\pm 30^\circ-70^\circ$.

Negative geopotential height anomalies ($4xCO_2_O_3-4xCO_2$; Figs. 23(a-e)) are observed across Bering Sea and Labrador Sea while positive geopotential height anomalies are perceptible over the Central North Pacific Ocean and Southern Ocean. This indicates that the induced ozone forcing together with quadrupling of CO_2 in the $4xCO_2_O_3$ simulation weakens the polar vortex and as a result, the atmospheric circulation and the jet stream weakens. This weakening of the polar vortex is consistent with the findings of Xie et al. (2016) confirming that the weakening of polar vortex leads to a positive North Pacific Oscillation pattern with a subsequent increase in the Arctic stratospheric ozone. Mostly, the positive geopotential height anomalies ($4xCO_2_O_3-4xCO_2$; Fig. 23(a-e)) and ($4xCO_2_O_3-PI$; Fig. 24(a-e)) are observed in the polar regions due to the extreme climate warming signal caused by $4xCO_2$ and the modified ozone, that effectively indicates a weak polar vortex (Zhang et al., 2019).

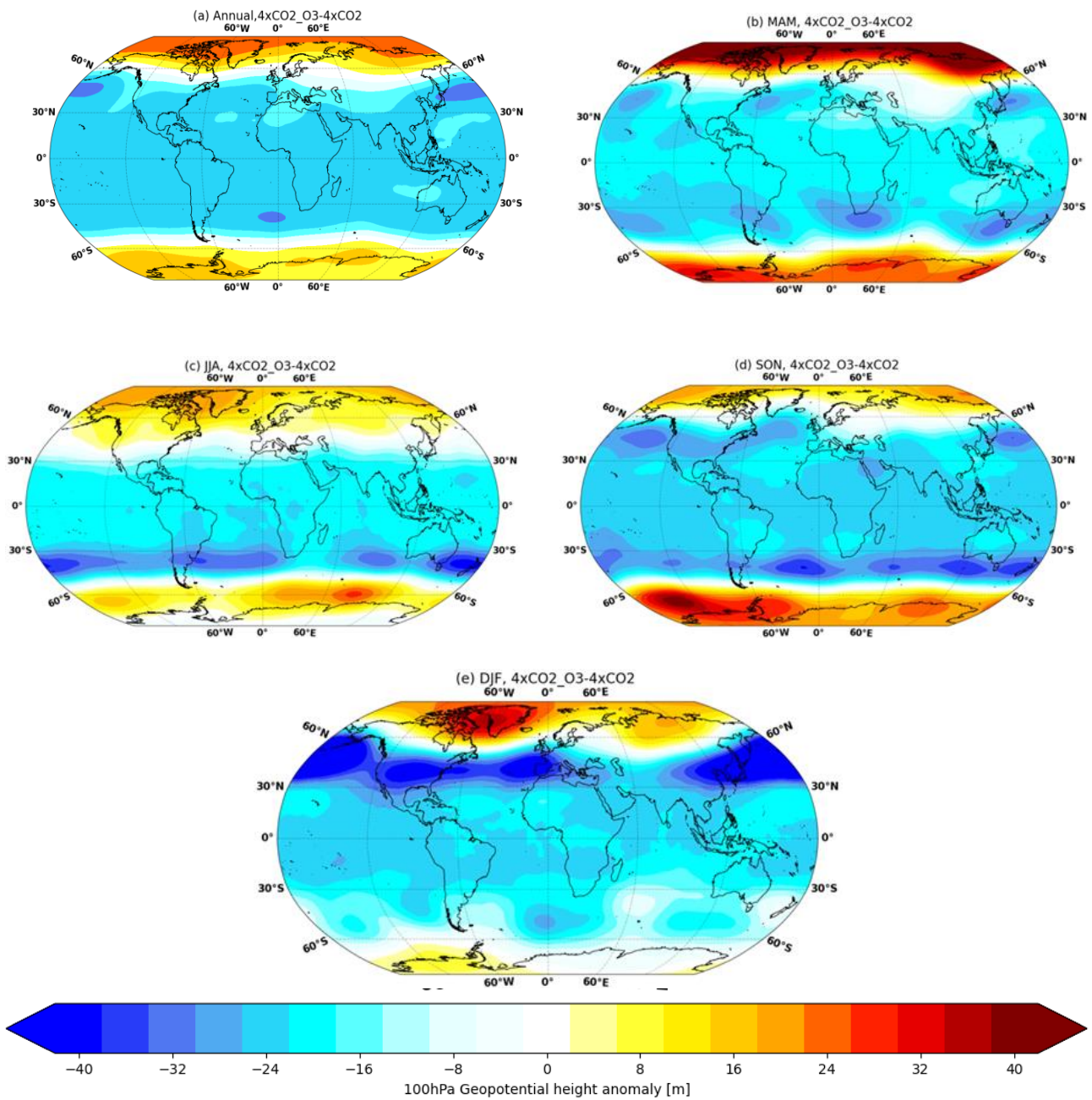


Figure 19: 100 hPa geopotential height anomalies for 4xCO₂_O₃-4xCO₂ simulation in Annual (a), MAM (b), JJA (c), SON (d), and DJF (e). Units are in metres.

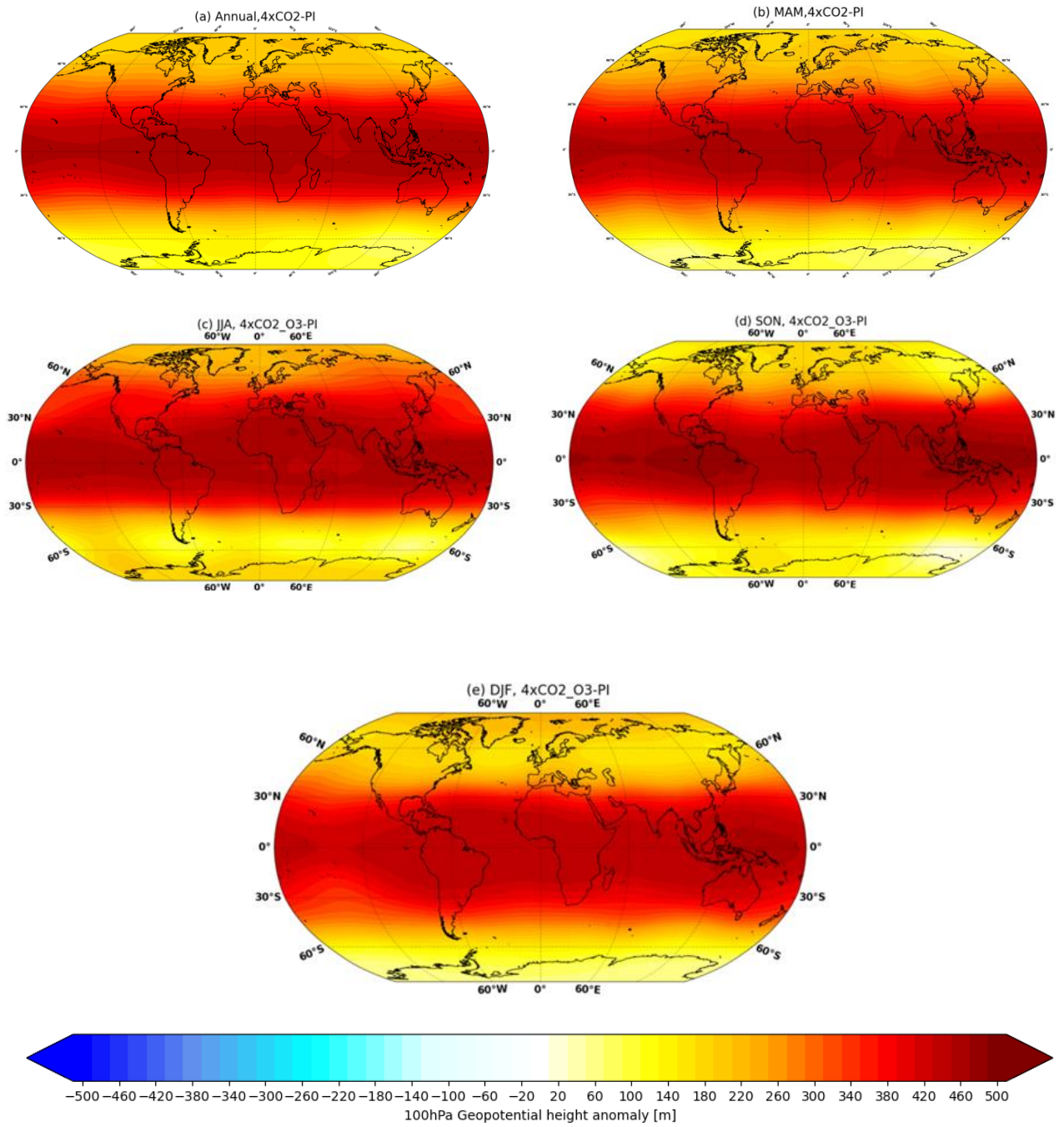


Figure 20: 100 hPa geopotential height anomalies for 4xCO₂-O₃-PI simulation in Annual (a), MAM (b), JJA (c), SON (d), and DJF (e). Units are in metres.

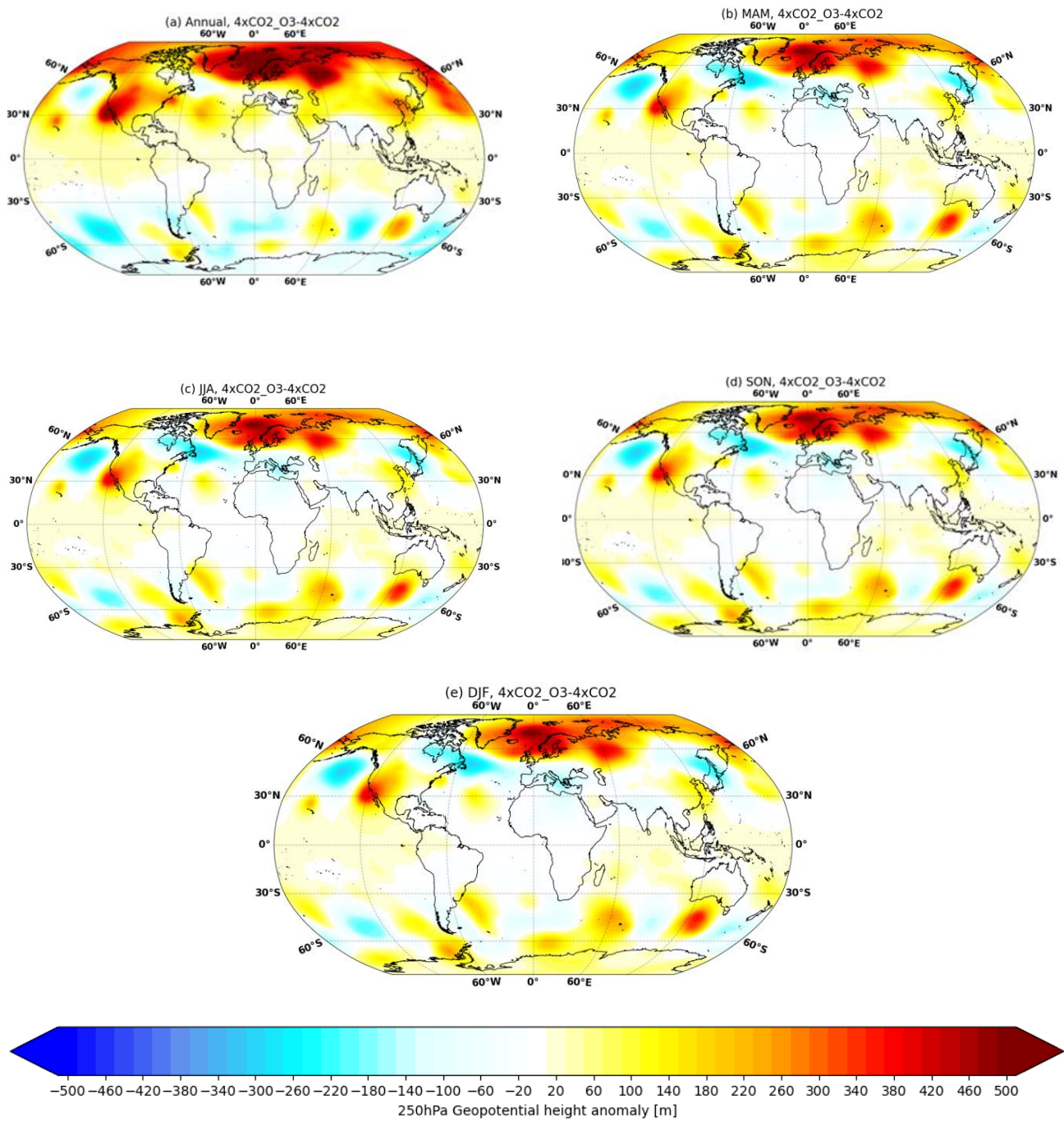


Figure 21: 250 hPa geopotential height anomalies for 4xCO₂_O₃-4xCO₂ simulation in Annual (a), MAM (b), JJA (c), SON (d), and DJF (e). Units are in metres.

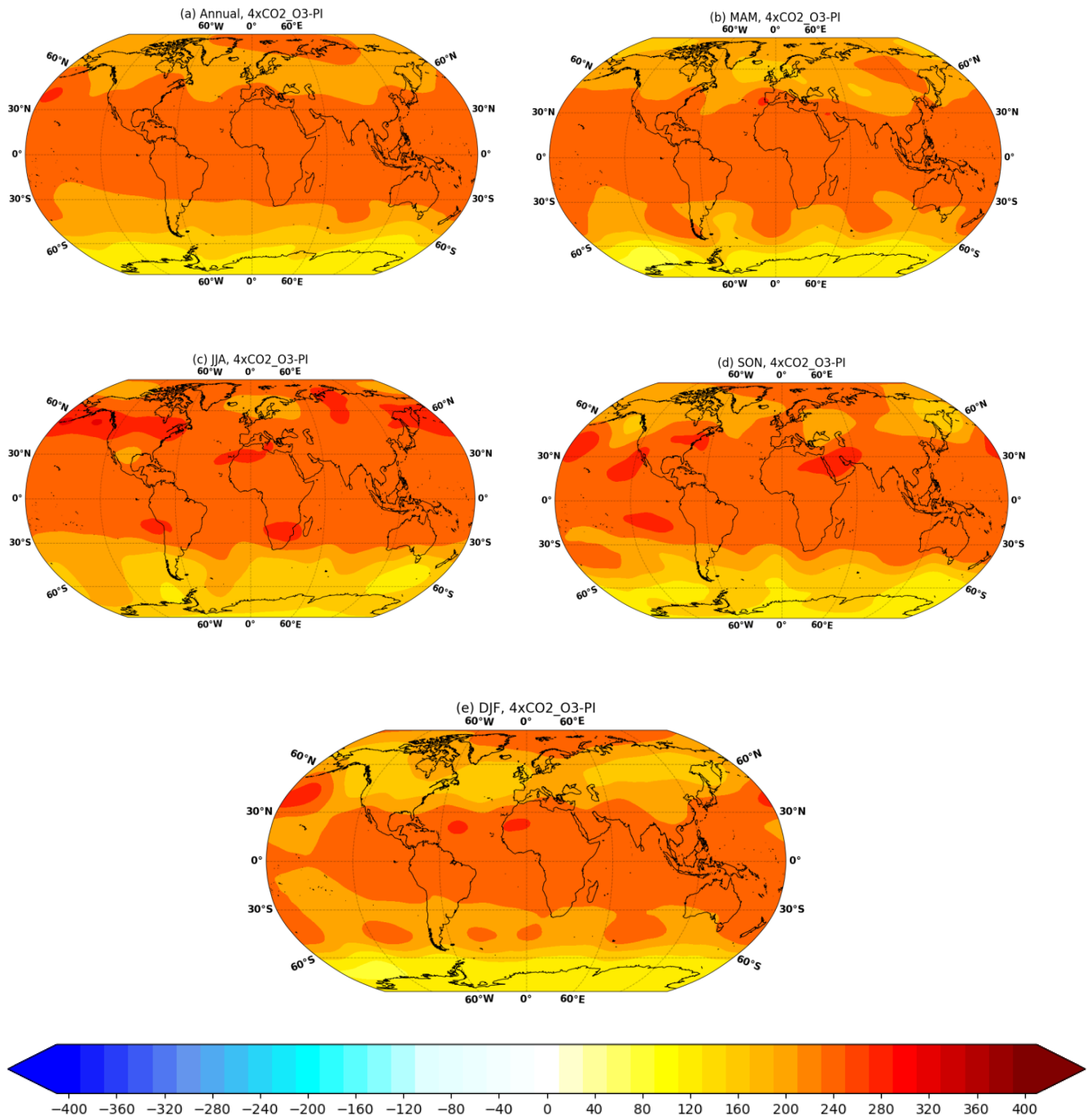


Figure 22: 250 hPa geopotential height anomalies for 4xCO₂-O₃-PI simulation in Annual (a), MAM (b), JJA (c), SON (d), and DJF (e). Units are in metres.

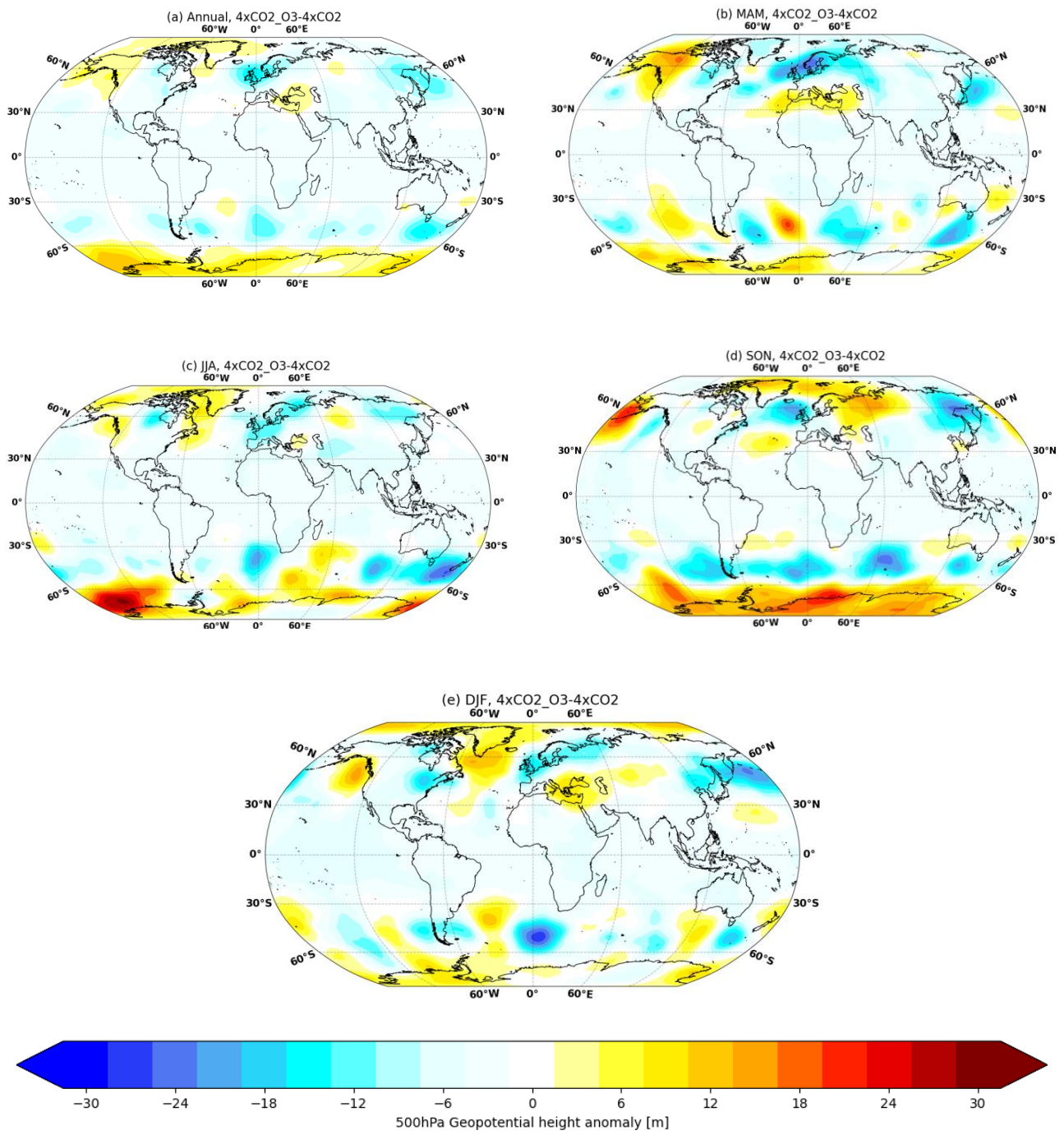


Figure 23: 500 hPa geopotential height anomalies for 4xCO₂_O₃-4xCO₂ simulation in Annual (a), MAM (b), JJA (c), SON (d), and DJF (e). Units are in metres.

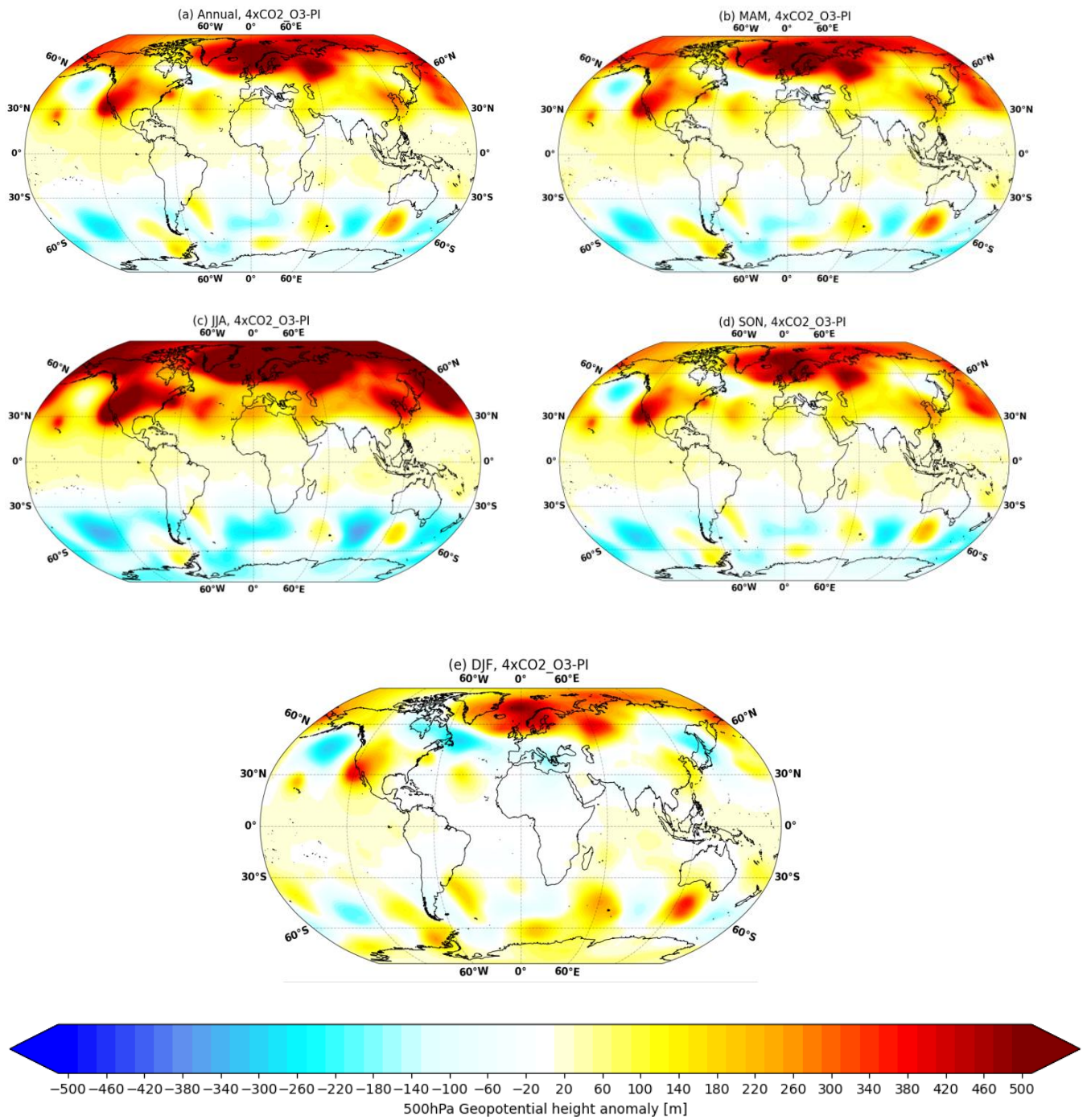


Figure 24: 500 hPa geopotential height anomalies for 4xCO₂_O₃-PI simulation in Annual (a), MAM (b), JJA (c), SON (d), and DJF (e). Units are in metres.

4.10 Zonal mean Geopotential Height

The variability of the troposphere-stratosphere atmospheric circulation describes a firm relationship between the strength of the stratospheric cyclonic vortex and the index of a tropospheric wave-like pattern covering the North Atlantic-Eurasian region (Perlwitz et al., 2000). The zonal mean geopotential height gives a clear visualisation of the climate signal over the whole atmosphere column.

The annual zonal mean geopotential height at 500 hPa, 250 hPa and 100 hPa shows an increase in geopotential height over the polar regions and a decrease over the mid-latitudes and tropics (Fig. 25). There is a large geopotential height decrease observed over the Arctic regions as well as over Antarctica and a corresponding height increase in the mid-latitudes, covering the depth of the troposphere and into the stratosphere (Fig. 26). In Fig. 26, the strongest change of the geopotential height is observed in the upper stratosphere. The strongest impact in the Arctic is observed over region extending from the upper troposphere to the lower stratosphere due to the strong radiative forcing from a quadrupling of CO₂. This initiates the occurrence of severe winter weather conditions. The impact of the changes observed over the Arctic regions can also be visible over the mid-latitudes. For example, one of the driving mechanisms of extreme events (e.g. cold spells, droughts, heatwaves) over the mid-latitudes is the weakening of the polar vortex over the Arctic regions. The weakening of the polar vortex causes the weakening of the jet stream as the temperature over the Arctic increases at the rate of two to three times as compared to the equator (Ionita et al., 2021).

The impact of enhanced atmospheric CO₂ concentration exhibits an increase in the internal variability pattern in the atmosphere (Palmer, 1993) and the polar vortex weakens (Fig. 26).

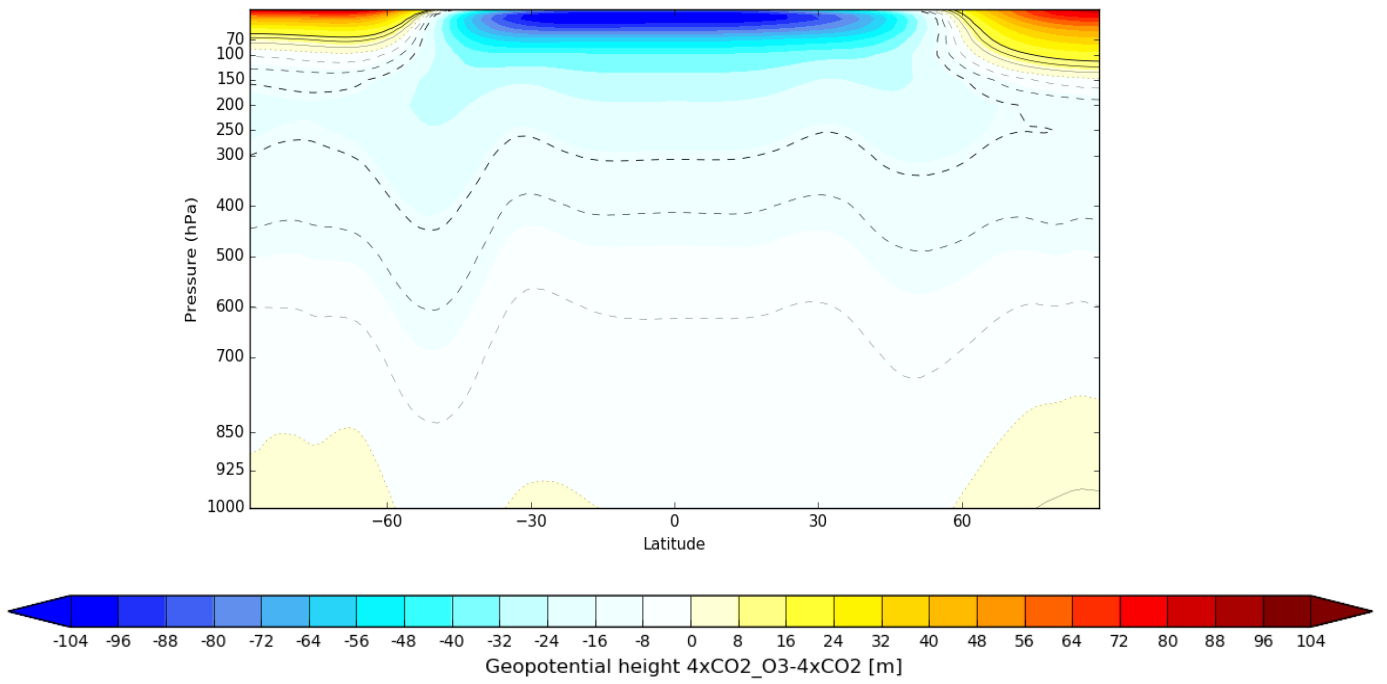


Figure 25: Difference in geopotential height between the 4xCO₂_O₃ and 4xCO₂ simulation. The units of geopotential height are in metre and the units of pressure are in hPa. The dashed contour lines indicate zonal mean isobars.

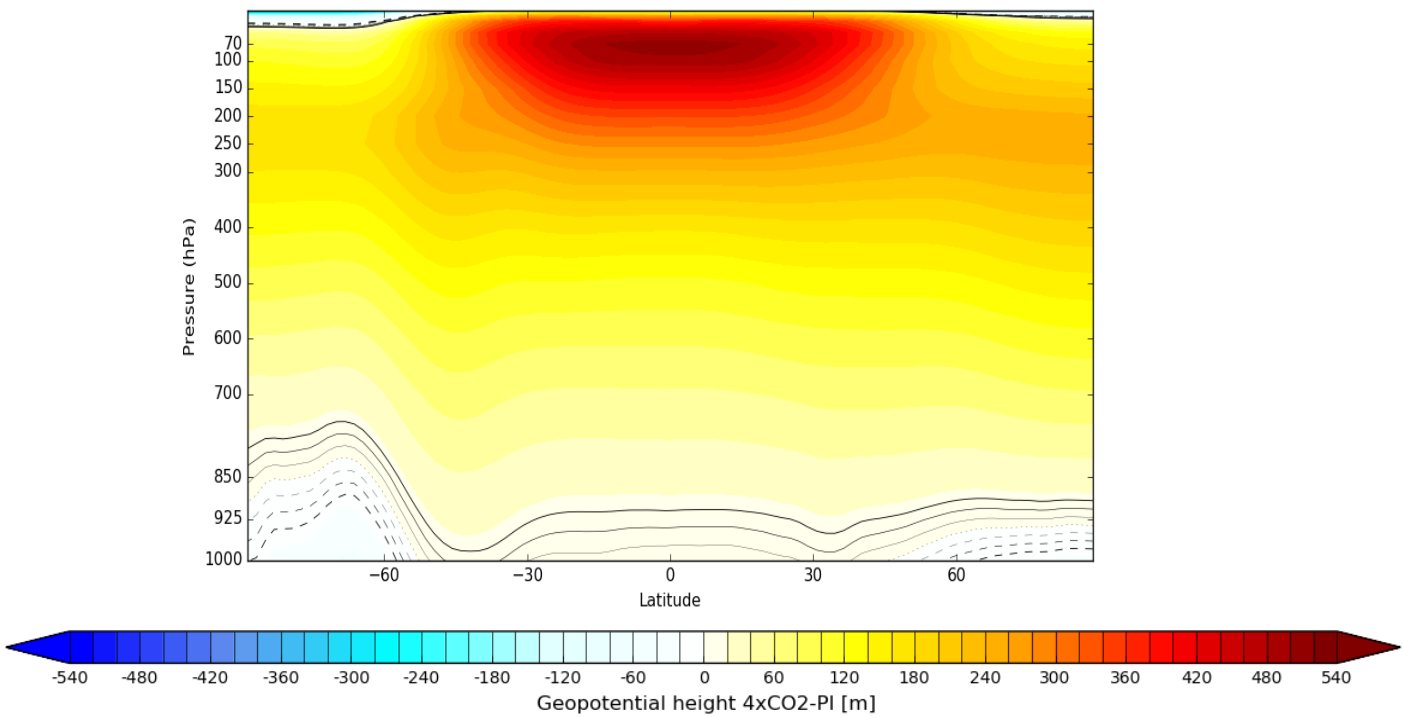


Figure 26: The difference in geopotential height between the 4xCO₂_O₃ and PI simulation. The units of geopotential height are in metre and the units of pressure are in hPa. The dashed contour lines indicate zonal mean isobars.

Discussion

This chapter discusses the major climatic implications due to the modified ozone forcing consistent with a warmer climate state with quadrupled carbon dioxide concentration. This study particularly helped in understanding how the modified ozone forcing with $4\times\text{CO}_2$ affects the climate modelling results and to what extent the large-scale metrics like CS and polar amplification are impacted by the adjustment of ozone. The impact of large-scale metrics such as CS and polar amplification on global geographic patterns of common climate variables like surface temperature, precipitation, vertically integrated water vapour, sea ice concentration are also studied. This chapter also compares some of the important results of this thesis and from other scientific publications which conducted similar research.

5.1 Impact of modified ozone on simulated large-scale global geographic patterns

Ozone is a greenhouse gas and plays an indispensable role in protecting the Earth's surface. Ozone is a key radiative heating agent in the upper troposphere and lower stratosphere (Fueglistaler et al., 2009). Changes in temperatures are vividly observed due to ozone's impact on the climate. Hence one aim was to evaluate the surface temperature patterns obtained from the anomalies in between $4\times\text{CO}_2$ versus PI and then comparing it to the anomalies of the $4\times\text{CO}_2\text{-O}_3$ and $4\times\text{CO}_2$. The $4\times\text{CO}_2$ climate state has been chosen as a suitable time slice for potentially analysing the large-scale climate patterns as a representation of a future warmer-than-present climate state under the circumstance of anthropogenic global warming (Jansen et al., 2007). Analysing the anomaly patterns, it was observed that the surface temperature patterns with respect to $4\times\text{CO}_2$ results in a large-scale warming in the NH high latitudes during boreal winter (up to 29°C ; Fig. 5d). This large-scale warming is related to the increase in the vertically integrated water vapour content in the NH high latitudes indicating a positive contribution of water vapour feedback towards polar amplification (Fig. 13a). Whereas, the ozone-induced change implemented in this study changes the

overall climate signal and resulting in a cooling effect in the NH high latitudes. As seen in Figs. 6(a-e), the presence of the modified ozone forcing causes a cooling of upto -3°C . Hence the adjusted ozone in the high latitudes acts as a counteractive effect of CO_2 . As seen in Figs. 5(a-e), the elevated levels of carbon dioxide in the $4\times\text{CO}_2$ simulation particularly makes it warm there while ozone in comparison makes it colder. The modified ozone forcing does not completely remove the impact of CO_2 , but it mitigates the impact of CO_2 to some extent. Strikingly, the modified ozone also increases the impact due to CO_2 and is the dominant driver behind the relatively intense amplitude of warming in North America (Figs. 6b, 6d) and Western Antarctica (Figs. 6a, 6c, 6d). Discussing the applicability of this result as a future work, if there arises a need to run the model, AWI-ESM-2.1-LR with coupled ice-sheet, then there will probably a need to modify ozone. This entails that, as the ice sheet in Western Antarctica is prone to be unstable for warmer climates, adjusting ozone may be relevant not to underestimate the warming in those regions and hence not to underestimate the effect on ice-sheet stability. It has also been highlighted that modification of ozone in the model contributes in a cooling pattern in the NH high latitudes and there are certain regions both in land and ocean particularly in the mid and low latitudes where ozone does not have any impact at all. Keeping all these climatic effects of the ozone adjustments in mind, it can be further decided if it is relevant to modify ozone, or stick to the pre-industrial ozone from CMIP6 as it is now present in the model.

Consistent with this ozone-induced cooling, a minor reduction in the water vapour content is seen in the $4\times\text{CO}_2\text{-O}_3$ simulation due to the presence of ozone. In the lower latitudes, there is a change in the water vapour although a strong change in temperature is not visible (Fig. 13a). Hence, the water vapour feedback due to ozone is of minor importance in the low latitudes. In the high latitudes, the minor change in water vapour is noticeable because ozone cools the atmosphere and it cannot keep much water vapour as before.

With respect to the vertical temperature structure in Fig. 9, Pithan and Mauritsen (2014) and Feldl et al. (2017) theorise that the upper troposphere experiences a greater warming since the air parcel that rises in the deep convective clouds releases more latent heat that steepens the moist adiabatic lapse rate. On the other hand, the scenario at the Arctic is quite different due to the absence of the deep convection and the strong vertical mixing motion. Hence, the cold dense air at the surface of the Arctic hardly mixes with the lighter air aloft and so most of the warming in the Arctic remains trapped at the surface and is not communicated in the troposphere. This smaller warming in the upper troposphere indicates that outgoing longwave radiation is smaller than it would be in case of vertical uniform warming. Hence, it proves that Arctic can warm more because of the decoupling of the limitation of warming of the surface area before sufficient amount of heat is radiated back to space.

Stratospheric cooling is identified due to the quadrupled carbon dioxide concentration which enhances the infrared cooling to space (Davis et al., 2016) and decreases the upward thermal radiation (Goessling et al., 2016). Consistently, the quadrupled carbon dioxide concentration portrays a canonical temperature response with tropospheric warming and stratospheric cooling.

Figs. 10a and 10b depict that the modified ozone forcing in the 4xCO₂_O₃ simulation induces cooling between -1°C to -3°C in the tropical lower stratosphere (TLS) and warming of about 2.5°C in the stratosphere. In the 4xCO₂_O₃ simulation, due to the induced ozone forcing there is a significant pattern of temperature change observed in the stratosphere (30-80 hPa) in between tropics and high latitudes (Fig. 10b), while there is a monotonic increase in the temperature with respect to height due to 4xCO₂ with little variation across high latitudes.

Similar to my results, are the results of Chiodo and Polvani, (2019) in the SC-WACCM model. They also show that the modified ozone forcing denoted as $\Delta O_3(4xCO_2)$ has a small impact on global surface temperature. The modified ozone in comparison to the 4xCO₂ simulation induces a cooling in the tropical lower stratosphere and a warming in the stratosphere.

Analyses in the framework of the 4xCO₂ simulation, also sheds light on the strongly reduced sea ice concentration in the NH (Fig. 16a) and SH (Fig. 15b). The notable cause behind this sea ice reduction is the amplified warming in the Arctic as seen in Figs. (5a, 5c, 5d, 5e). On the otherhand, ozone has an indirect effect on sea ice concentration via surface temperature. Hence, it is clearly visible in Fig. 16c that the cooling due to the presence of adjusted zone forcing inevitably contributes in the production of more sea ice than a warmer 4xCO₂ climate state as observed in Fig. 16a.

Alongside the surface air temperature patterns with amplified warming as seen in Figs. 5(a-e), the seasonal precipitation anomalies also show diverse and spatial patterns. The warming climate in the 4xCO₂ climate state results in an intensified hydrological cycle, where the global mean precipitation increases by 1% to 3% per degree rise of surface air temperature maintaining a balance in between the atmospheric energy budget (Zhang et al., 2021, Allen et al., 2002, Held et al., 2006). The large-scale precipitation patterns changes with temperatures changing from warm to cold climate states (Li et al., 2013). The ozone adjustments decreases the effect of carbon dioxide mostly in the high and low latitudes and reduces the precipitation upto 14 mm/year. Modified ozone dries off completely Bay of Bengal, Sri Lanka, Indonesia, North-west Australia and amazon (Figs. 12c, 12d, 12a).

5.2 Impact of ozone forcing on climate sensitivity and polar amplification

Another focus of this thesis was to study the impact of the modified ozone forcing in response to $4\times\text{CO}_2$ on the climate sensitivity estimate. The main standpoint was to investigate whether any changes are inflicted on CS that is induced due to the quantification of ozone in agreement with the $4\times\text{CO}_2$ climate state. The primary reason for studying the impact on climate sensitivity with the modified ozone forcing is stated as follows:

- whether it's an advantage or disadvantage from the viewpoint of the usage of the atmosphere-ocean coupled model AWI-ESM-2.1-LR for paleoclimate research in a warmer climate with strongly increased levels of carbon dioxide?
- From a scientific viewpoint, if there is a need to adjust ozone towards correctly implementing CS in our model, AWI-ESM-2.1-LR?

In order to evaluate this, a linear regression methodology suggested by [Gregory et al. \(2004\)](#) was applied. [Gregory et al. \(2004\)](#) analyse CS from quadrupling of CO_2 following the linear regression methodology by extending the trend line to $N=0$ where the TOA net downward heat flux is 0. Fig. 2 of [Gregory et al. \(2004\)](#) shows that the atmosphere-ocean general circulation model HadCM3 slowly reaches equilibrium due to the larger heat capacity of the ocean. The CS sensitivity value estimated from the HadCM3 model is 3.1 K.

In this thesis, a detailed CS analysis by AWI-ESM-2.1-LR is performed following the similar methodology as in [Gregory et al. \(2004\)](#). CS analysis, based on 500 years of simulation data and with the modified ozone forcing is calculated to be 3.34°C (Fig. 14). The linear regression in between TOA radiative imbalance and the global average surface air temperature change (Fig. 14) causes a minor reduction of CS by 2.6% due to the modification of the ozone forcing in compared to the response to quadrupled CO_2 alone. This span of 500 years of model data is relevant to understand the potential robustness of the CS results. This concludes that the slope of the equilibration may change after 500 model years, which implies that the CS estimate has an error as the slope of the regression line is underestimated or overestimated. On a broader conclusion and based on the comparison of the CS analysis with [Gregory et al. \(2004\)](#) it can be stated that adjusting ozone in AWI-ESM-2.1-LR, a fully coupled atmosphere-ocean model has a smaller impact than employing a slab ocean model instead of a full ocean model (albeit in a different model, HadCM3). [Gregory et al. \(2004\)](#) shows that exchanging the ocean in their model has an impact on the CS values which is above the respective impact that I find by adjusting ozone in AWI-ESM-2.1-LR. Hence, adjusting ozone in AWI-ESM-2.1-LR has an effect that is below that of employing reduced ocean physics (as in a slab ocean) in their model, HadCM3.

Hence, drawing inferences from the CS analysis performed in the atmosphere-ocean coupled model, AWI-ESM-2.1-LR, it is well attributed that the impact on CS due to the implementation of the modified ozone forcing in the model is minor than compared to a 4xCO₂ simulation with PI ozone. Therefore, the results broadly confirm and highlight that there is no need to adjust ozone towards the computation of CS in AWI-ESM-2.1-LR.

The findings of the CS analysis is also interpreted in the light of polar amplification. Polar amplification, which defines the amplified warming due to the enormous increase in the CO₂ concentrations in the polar latitudes, is strongly co-related to the CS. Hence it was crucial to observe how much the modified ozone had an impact on the polar amplification. The surface temperature change as seen in Fig. 5e confirms that the amplified warming in the NH high latitudes is sensitive due to the elevated concentration of carbon dioxide and thus resulting in a polar amplification factor of 1.82 (Table 3). As illustrated above, the cooling due to the modified ozone as interpretable from Fig. 6e, significantly reduced the surface temperature and thus resulting in a decreased polar amplification to 1.79 (Table 3).

Conclusion and Outlook

This thesis explores the quantification of the adjusted ozone climatology on the atmosphere-ocean coupled model, AWI-ESM-2.1-LR. Due to the absence of the interactive ozone chemistry in AWI-ESM-2.1-LR, the behaviour of an ozone-simulation-enabled model, HadGEM3 used by [Nowack et al. \(2018\)](#) is replicated. This is successfully done by adding an ozone anomaly that has been computed by the ozone-chemistry-enabled atmosphere-ocean coupled HadGEM3 model for 4xCO₂ to the PI ozone forcing by AWI-ESM-2.1-LR for a 4xCO₂ simulation. Therefore, the model climate is enabled to react to changes of ozone concentrations that are linked to a warmer 4xCO₂ climate state. The constraint in this underlying approach is that the ozone is unable to react to changes in the climate, since the feedback loop from the warmer 4xCO₂ climate state to ozone is missing as ozone is prescribed statically.

The ultimate focus in this thesis is to evaluate how different a warm climate state with quadrupled carbon dioxide concentration would be if it were subject to an ozone concentration that is in agreement with the same warmer climate state, rather than using a current ozone climatology as it is done continually with AWI-ESM-2.1-LR. Hence, it is of significant interest to learn now, before AWI-ESM-2.1-LR becomes a major workhorse, how much of an approximation has to be made regarding principal climate diagnostics in the model, like CS and polar amplification, adhering to AWI-ESM-2.1-LR that cannot simulate ozone interactively.

Henceforth, it is foreseeable that prescribing ozone as an external forcing in AWI-ESM-2.1-LR readily differentiates the various changes in climate in presence or absence of modified ozone. Similar simulation framework is a pretty standard procedure and not novel at all, and thus through this thesis research study the analysis is done for the novel model, AWI-ESM-2.1-LR.

In this thesis, the results are demonstrated based on the PI, 4xCO₂ and 4xCO₂_O₃ simulations. ECHAM6, the state-of-the-art release atmospheric general circulation model, from the Max-Planck-Institute, Hamburg and FESOM 2.0, the hydrostatic ocean circulation model from Alfred Wegener Institute, Helmholtz Centre for Polar and Marine Research (AWI) is efficiently used to generate the monthly mean climate outputs and is successfully implemented to analyse the climate parameters.

Monthly mean values of climate parameters such as surface temperature, precipitation, vertically integrated water vapour, sea ice concentration and geopotential height at 500 hPa, 250 hPa and 100 hPa levels are compared amongst the PI, 4xCO₂ and 4xCO₂_O₃ simulations in order to obtain an illustration on the imposed effects due to the modified ozone forcing in response to abrupt quadrupling of carbon dioxide concentrations.

Surface temperature as a key climate indicator illustrates stronger warming across landmasses with the weaker response over oceans except the Arctic Ocean. Amplified Arctic warming is evidently visible in the NH high latitude (Fig. 5d) as the vertically integrated water vapour almost doubles itself in response to quadrupled carbon dioxide compared to the PI simulation (Fig. 13a). The findings from the 4xCO₂ simulation confirms a strong polar amplification and a ice-free Arctic region due to the enormous carbon dioxide concentration (Fig. 16a). Nevertheless, a robust land-sea contrast is observed all over the year due to the reduced heat capacity of the land in comparison to the ocean, which also results in large shifts of rainfall patterns. However, modification of ozone causes predominant drying patterns in northern and southern hemispheres and in the mid-latitudes covering areas of southern parts of Indian Ocean, scattered parts of Scandinavia (Fig. 12b).

Furthermore, CS is a globally integrated climate signal and it has been shown in Fig. 14 that the modification of the ozone forcing inflict a minor reduction of CS compared to the response of 4xCO₂ alone. The fundamental objective of this thesis was to analyse the impact of modified ozone forcing in the light of climate sensitivity. It can be concluded that, the modified ozone forcing does not make the global CS metric more robust in comparison to the CS with 4xCO₂ and modern CMIP6 ozone concentration.

Despite the promising results presented in this thesis there is still a scope that can motivate further detailed research work in this direction. For general applications, where the climate is controlled by other forcings than just the standard 4xCO₂ for which adjusted ozone fields are available, there is then the need to extend the model with interactive ozone, which will be a major development. Until that is achieved, my thesis can give an idea on how much climate in AWI-ESM-2.1-LR is impacted by ozone, informing on the amplitude of the approximation that is not made by adjusting ozone at all.



Acronyms

AWI-ESM-2.1-LR Alfred-Wegener-Institute Earth System Model-2.1 (Low Resolution).

AAI Arctic Amplification Index.

CDO Climate Data Operators.

CMIP Coupled Model Inter-comparison Project Phase.

CESM1-WACCM The Community Earth System Model-Whole Atmosphere Community Climate Model.

CS Climate Sensitivity.

DJF December-January-February.

ECHAM6 European Center-Hamburg Model, Version 6.

ECMWF European Center for Medium-range Weather Forecasts.

ECS Equilibrium Climate Sensitivity.

FESOM2.0 Finite Volume Sea ice-Ocean Model.

GHG Green-House Gases.

HadGEM2-ES Hadley Centre Global Environment Model version 2.

ITCZ Intertropical Convergence Zone.

JJA June-July-August.

JSBACH Jena Scheme for Biosphere-Atmosphere Coupling in Hamburg.

MPI-M Max Planck-Institute for Meteorology.

MAM March-April-May.

NetCDF Network Common Data Form.

NH Northern Hemisphere.

OASIS3-MCT OASIS3 Model Coupling Toolkit.

PI Pre-Industrial.

SH Southern Hemisphere.

SON September-October-November.

SAT Surface Air Temperature.

TOA Top of Atmosphere.

TLS Tropical Lower stratosphere.



Bibliography

- Adam, O., Schneider, T., and Harnik, N. (2014). Role of changes in mean temperatures versus temperature gradients in the recent widening of the Hadley circulation. *Journal of Climate*, 27: 7450–7461. doi: 10.1175/JCLI-D-14-00140.1
- Allen, M., Ingram, W. (2002). Constraints on future changes in climate and the hydrologic cycle. *Nature*, 419: 228–232. doi: doi.org/10.1038/nature01092
- Arrhenius, S. (1896). On the influence of carbonic acid in the air upon the temperature of the ground. *The London, Edinburgh, and Dublin Philosophical Magazine and Journal of Science*, 41: 237-276. doi: doi.org/10.1080/14786449608620846
- Baldwin, P. M., and Dunkerton, J. T. (2001). Stratospheric Harbingers of Anomalous Weather Regimes. *Science*, 5542: 581-584. doi: 10.1126/science.1063315
- Bellenger, H., Guilyardi, E., Leloup, J., Lengaigne, M., and Vialard, J. (2013). ENSO representation in climate models: from CMIP3 to CMIP5. *Climate Dynamics*, 42: 1999–2018. doi: doi.org/10.1007/s00382-013-1783-z
- Brovkin, V., Raddatz, T., Reick, H. C., Claussen, M., Gayler, V. (2009). Global biogeophysical interactions between forest and climate. doi: doi.org/10.1029/2009GL037543
- Ceppi, P., and Gregory, M. J. (2017). Relationship of tropospheric stability to climate sensitivity and Earth's observed radiation budget. *Proceedings of the National Academy of Sciences of the United States of America*, 114: 13126-13131. doi: doi.org/10.1073/pnas.1714308114
- Chiodo, G., and Polvani, M. L. (2017). Reduced Southern Hemispheric circulation response to quadrupled CO₂ due to stratospheric ozone feedback. *Geophysical Research Letters*, 44: 465-474. doi: 10.1002/2016GL071011
- Chiodo, G., and Polvani, M. L. (2019). The Response of the Ozone Layer to Quadrupled CO₂ Concentrations: Implications for Climate. *Journal of Climate*, 32: 7629-7642. doi: 10.1175/JCLI-D-19-0086.1
- Coumou, D., Rahmstorf, S. (2012). A decade of weather extremes. *Nature Climate Change*, 2:491–496. doi: https://doi.org/10.1038/nclimate1452
- Collins, W. J., Bellouin, N., Doutriaux-Boucher, M., Gedney, N., Halloran, P., Hinton, T., Hughes, J., Jones, D. C., Joshi, M., Liddicoat, S., Martin, G., Connor, O. F., Rae, J., Senior, C., Sitch, S., Totterdell, I., Wiltshire, A., and Woodward, S. (2011). Development and evaluation of an Earth-system model—HadGEM2. *Geoscientific Model Development*, 4:1051-1075.

doi: doi.org/10.5194/gmd-4-1051-2011

Danek, C., Gierz, P., Stepanek, C. and Lohmann, G. (2020). Equilibrium Climate Sensitivity in AWI-ESM: Mechanisms and Effects. Abstract No: EGU2020-17981.
doi: doi.org/10.5194/egusphere-egu2020-17981

Danilov, S., Sidorenko, D., Wang, Q., and Jung, T. (2017). The Finite-volume Sea ice–Ocean Model (FESOM2). *Geoscientific Model Development*, 10: 765–789.
doi: 10.5194/gmd-10-765-2017

Davis, N. A., Seidel, D. J., Birner, T, Davis, S. M., and Tilmes, S. (2016). Changes in the width of the tropical belt due to simple radiative forcing changes in the GeoMIP simulations. *Atmospheric Chemistry and Physics*, 16: 10083–10095. doi: 10.5194/acp-16-10083-2016

Dietmüller, S., Ponater, M., and Sausen, R. (2014). Interactive ozone induces a negative feedback in CO₂-driven climate change simulations. *Journal of Geophysical Research, Atmospheres*, 119: 1796–1805. doi: doi.org/10.1002/2013JD020575

Eyring, V., Bony, S., Meehl, G. A., Senior, A. C., Stevens, B., Stouffer, J. R., and Taylor, E. K. (2016). Overview of the Coupled Model Intercomparison Project Phase 6 (CMIP6) experimental design and organization. *Geoscientific Model Development*, 9: 1937–1958.
doi: doi.org/10.5194/gmd-9-1937-2016

Feldl, N, Anderson, T. B., Bordoni, S. (2017). Atmospheric Eddies Mediate Lapse Rate Feedback and Arctic Amplification. *Journal of Climate*, 30: 9213–9224.
doi: doi.org/10.1175/JCLI-D-16-0706.1

Fernandez, J. (2020). The statistical analysis t-test explained for beginners and experts. Towards data science. Website URL: <https://towardsdatascience.com/the-statistical-analysis-t-test-explained-for-beginners-and-experts-fd0e358bbb62>, Accessed on, 28.12.2021.

Folkens, I., Loewenstein, M., Podolske, J., Oltmans, S. J and Proffitt, M. (1999). A barrier to vertical mixing at 14 km in the tropics: Evidence from ozonesondes and aircraft measurements. *Journal of Geophysical Research*, 104(D18): 22095–22102. doi: 10.1029/1999JD900404

Frierson, D. M. W., Lu, J., and Chen, G. (2007). Width of the Hadley cell in simple and comprehensive general circulation models. *Geophysical Research Letters*, 34, L18804.
doi: doi.org/10.1029/2007GL031115

Fueglistaler, S., Dessler, A. E., Dunkerton, T. J., Folkens, I., Fu, Q., Mote, P. W. (2009). Tropical tropopause layer. *Reviews of Geophysics*, 47. doi: doi.org/10.1029/2008RG000267

Gaudel, A., Cooper, O. R., Ancellet, G., Barret, B., Boynard, A., Burrows, J. P., Clerbaux, C., Coheur, P.- F., Cuesta, J., Cuevas, E., Doniki, S., Dufour, G., Ebojje, F., Foret, G., Garcia, O., Granados Muñoz, M.J., Hannigan, J.W., Hase, F., Huang, G., Hassler, B., Hurtmans, D., Jaffe, D., Jones, N., Kalabokas, P., Kerridge, B., Kulawik, S.S., Latter, B., Leblanc, T., Le Flochmoën, E., Lin, W., Liu, J., Liu, X., Mahieu, E., McClure- Begley, A., Neu J. L., Osman, M., Palm, M., Petetin, H., Petropavlovskikh, I., Querel, R., Rappoe, N., Rozanov, A., Schultz, M. G., Schwab, J., Siddans, R., Smale, D., Steinbacher, M., Tanimoto, H., Tarasick, D.W., Thouret, V., Thompson, A. M., Trickl, T., Weatherhead, E., Wespes, C., Worden, H.M., Vigouroux, C., Xu, X., Zeng, G. and Ziemke, J. (2018). Tropospheric Ozone Assessment Report: Present-day distribution and trends of

- tropospheric ozone relevant to climate and global atmospheric chemistry model evaluation. *Elementa: Science of the Anthropocene*. doi: doi.org/10.1525/elementa.291
- Goessling, H. F., and Bathiany, S. (2016). Why CO₂ cools the middle atmosphere – a consolidating model perspective. *Earth System Dynamics*, 7: 697–715. doi: doi.org/10.5194/esd-7-697-2016
- Gregory, J. M., Ingram, J. W., Palmer, A. M., Jones, S. G., Stott, A. P., Thorpe, B. R., Lowe, A. J., Johns, C. T., and Williams, D. K. (2004). A new method for diagnosing radiative forcing and climate sensitivity. *Geophysical Research Letters*, 31: L03205. doi: doi.org/10.1029/2003GL018747
- Haigh, J., and Pyle, J. (1982). Ozone perturbation experiments in a two-dimensional circulation model. *Quarterly Journal of the Royal Meteorological Society*, 108: 551–574. doi: doi.org/10.1002/qj.49710845705
- Hall, A. (2004). The role of surface albedo feedback in climate. *Journal of Climate*, 17: 1550–1568. doi: doi.org/10.1175/1520-0442(2004)017<1550:TROSAF>2.0.CO;2
- Held, I. M., Hemler, R. S., and Ramaswamy, V. (1993). Radiative Convective Equilibrium with Explicit Two-Dimensional Moist Convection. *Journal of the Atmospheric Sciences*, 50: 3909–3927. doi: doi.org/10.1175/1520-0469(1993)050<3909:RCE>2.0.CO;2
- Held, I. M., & Soden, B. J. (2006). Robust Responses of the Hydrological Cycle to Global Warming, *Journal of Climate*, 19(21): 5686-5699. doi: doi.org/10.1175/JCLI3990.1
- Huang, Y., Xia, Y., and Tan, X. (2017). On the pattern of CO₂ radiative forcing and poleward energy transport, *Journal of Geophysical Research, Atmospheres*, 122: 10578–10593. doi: doi.org/10.1002/2017JD027221
- Ionita, M., Scholz, P., and Grosfeld, K. (2021). July heavy rains and floods in western part of Germany: Evolution of a tragedy! REKLIM, 22 July 2021. Website URL: [eklim.de/en/archive-news/news-2021/july-heavy-rains-and-floods-in-western-germany/](https://www.ecklin.de/en/archive-news/news-2021/july-heavy-rains-and-floods-in-western-germany/). Accessed on, 28.12.2021.
- Jansen, E., Overpeck, J., Briffa, K. R., Duplessy, J.-C., Joos, F., Masson-Delmotte, V., Olago, D., Otto-Bliesner, B., Peltier, W. R., Rahmstorf, S., Ramesh, R., Raynaud, D., Rind, D., Solomina, O., Villalba, R., and Zhang, D. (2007). Palaeoclimate. In *Climate Change 2007: The Physical Science Basis, Contribution of Working Group I to the Fourth Assessment Report of the Intergovernmental Panel on Climate Change*, edited by: Solomon, S., Qin, D., Manning, M., Chen, Z., Marquis, M., Averyt, K. B., Tignor, M., and Miller, H. L., Cambridge University Press, Cambridge, United Kingdom, and New York, NY, 433–497. Website URL: <https://pubs.giss.nasa.gov/abs/ja05100g.html>. Accessed on, 28.12.2021.
- Jonsson, A., Grandpre, De. J., Fomichev, V., McConnell, J., and Beagley, S. (2004). Doubled CO₂-induced cooling in the middle atmosphere: Photochemical analysis of the ozone radiative feedback. *Journal of Geophysical Research Letters*, 109: D24103. doi: doi.org/10.1029/2004JD005093
- Keeble, J., Hassler, B., Banerjee, A., Garcia, C. R., Chiodo, G., Davis, S., Eyring, V., Griffiths, T. P., Morgenstern, O., Nowack, P., Zeng, G., Zhang, J., Bodeker, G., Burrows, S., Smith, C. P., Cugnet, P., Danek, C., Deushi, M., Horowitz, W. L., Kubin, A., Li, L., Lohmann, G., Michou, M., Mills, J. M., Nabat, P., Olivé, D., Park, S., Seland, Ø., Stoll, J., Wieners, H. K., and Wu, T. (2021). Evaluating stratospheric ozone and water vapour changes in CMIP6 models from 1850 to 2100. *Atmospheric Chemistry and Physics*, 21, 5015–5061. doi: doi.org/10.5194/acp-21-5015-2021

- Kim, K. T. (2015). T test as a parametric statistic. *Korean J Anesthesiol*, 68(6): 540–546. doi: doi.org/10.4097/kjae.2015.68.6.540
- Kinne, S., Donnel, O. D., Stier, P., Kloster, S., Zhang, K., Schmidt, H., Rast, S., Giorgetta, M., Eck, F. T., Stevens, B. (2013). MAC-v1: A new global aerosol climatology for climate studies. *Journal of Advances in Modeling Earth Systems*, 5:704-740. doi: doi.org/10.1002/jame.20035
- Knutti, R., Rugenstein, A. A. M., and Hegerl, C. G. (2017). Beyond equilibrium climate sensitivity. *Nature Geoscience*, 10: 727–736. doi: doi.org/10.1038/ngeo3017
- Koldunov, N. V., Aizinger, V., Rakowsky, N., Scholz, P., Sidorenko, D., Danilov, S., and Jung, T. (2019). Scalability and some optimization of the Finite-volume Sea ice–Ocean Model, Version 2.0 (FESOM2), *Geoscientific Model Development*, 12: 3991–4012. doi: doi.org/10.5194/gmd-12-3991-2019
- Kravitz, B., Robock, A., Forster, P. M., Haywood, J. M., Lawrence, M. G., and Schmidt, H. (2013). An overview of the Geoengineering Model Intercoparison Project (GeoMIP). *Journal of Geophysical Research:Atmospheres*, 118:8320-8332. doi: doi.org/10.1002/2013JD020569
- Lacis, A. A., Wuebbles, D. J., and Logan, J. A. (1990). Radiative forcing of climate by changes in the vertical distribution of ozone. *Journal of Geophysical Research: Atmospheres*, 95(D7). doi: doi.org/10.1029/JD095iD07p09971
- Li, G., Harrison, P. S., Bartlein, J. P., Izumi, K., and Prentice, C. I. (2013). Precipitation scaling with temperature in warm and cold climates: An analysis of CMIP5 simulations. *Geophysical Research Letters*, 40: 4018–4024. doi: doi.org/10.1002/grl.50730
- Luo, D., Yao, Y., Dai, A., Simmonds, I., Zhong, L. (201). Increased quasistationarity and persistence of winter Ural blocking and Eurasian extreme cold events in response to Arctic warming. Part II: a theoretical explanation. *Journal of Climate*, 30: 3549–3568. doi: doi.org/10.1175/JCLI-D-16-0261.1
- Meinshausen, M., Vogel, E., Nauels, A., A., Lorbacher, K., Meinshausen, N., Etheridge, M. D., Fraser, J. P., Montzka, A. S., Rayner, J. P., Trudinger, M. C., Krummel, P. B., Beyerle, U., Canadell, G., J., Daniel, S. J. Enting, G. I., Law, M. R., Lunder, R. C., Doherty, O. S., Prinn, G. R., Reimann, S., Rubino, Velders, M. GuusJ., Vollmer, K. M., Wang, J. Ray H., and Weiss, R. (2017). Historical greenhouse gas concentrations for climate modelling (CMIP6). *Geoscientific Model Development*, 10: 2057–2116. doi: doi.org/10.5194/gmd-10-2057-2017
- Manabe, S. and Stouffer, R. (1994). Multiple-century response of a coupled ocean-atmosphere model to an increase of atmospheric carbon-dioxide, *Journal of Climate*, 7: 5–23, doi: doi.org/10.1175/1520-0442(1994)007<0005:MCROAC>2.0.CO;2
- Manabe, S., and Wetherald, R. T. (1967). Thermal Equilibrium of the Atmosphere with a Given Distribution of Relative Humidity. *Journal of Geophysical Research: Atmospheres*, 24: 241–259. doi: doi.org/10.1175/1520- 0469(1967)0242.0.CO;2
- Marsh, D. R., Lamarque, F. J., Conley, J. A., and Polvani, M. L. (2016). Stratospheric ozone chemistry feedbacks are not critical for the determination of climate sensitivity in CESM1(WACCM). *Geophysical Research Letters*, 43: 3928–3934. doi: doi.org/10.1002/2016GL068344

- Maycock, C. A., Randel, J. W., Steiner, K. A. (2018). Revisiting the Mystery of Recent Stratospheric Temperature Trends. *Geophysical Research Letters*, 45: 9919-9933. doi: doi.org/10.1029/2018GL078035
- Muthers, S. (2014). The coupled atmosphere–chemistry–ocean model SOCOL-MPIOM. *Geoscientific Model Development*, 7: 2157–2179. doi: doi.org/10.5194/gmd-7-2157-2014
- Nowack, P. J., Abraham, L., N., Maycock, A. C., Braesicke, P., Gregory, J. M., Joshi, M. M., Osprey, A., and Pyle, A. J. (2015). A large ozone-circulation feedback and its implications for global warming assessments. *Nature Climate Change*, 5(1):41-45. doi: doi.org/10.1038/nclimate2451
- Nowack, P. N., Abraham, L., Braesicke, P., Pyle, J. A. (2018). The Impact of Stratospheric Ozone Feedbacks on Climate Sensitivity Estimates. *Journal of Geophysical Research: Atmospheres*, 123: 4630-4641. doi: doi.org/10.1002/2017JD027943
- Nowack, P., Braesicke, P., Haigh, J., Abraham, L. N., Pyle, J., and Voulgarakis, A. (2018). Using machine learning to build temperature-based ozone parameterizations for climate sensitivity simulations. *Environmental Research Letters*, 13: 104016. doi: doi.org/10.1088/1748-9326/aae2be
- Overland, J., Hall, R., Hanna, E., Karpechko, A., Vihma, T., Wang, M., and Zhang, X. (2020). The Polar Vortex and Extreme Weather: The Beast from the East in Winter 2018. *Atmosphere*, 11(6): 664. doi: doi.org/10.3390/atmos11060664
- Palmer, T. N. (1993). A nonlinear dynamical perspective on climate change. *Weather*, 48: 314-326. doi: doi.org/10.1175/1520-0442(1999)012<0575:AN
- Perlwitz, J., Graf, H., and Voss, R. (2000). The leading variability mode of the coupled troposphere-stratosphere winter circulation in different climate regimes. *Journal of Geophysical Research*, 105: 6915-6926. doi: doi.org/10.1029/1999JD901107
- Pithan, F. and Mauritsen, T. (2014). Arctic amplification dominated by temperature feedbacks in contemporary climate models, *Nature Geoscience*, 7: 181–184, doi: doi.org/10.1038/ngeo2071
- Raddatz, J. T., Reick, H. C., Knorr, W., Kattge, J., Roeckner, E., Schnur, R., Schnitzler, -G. K., Wetzel, P., Jungclaus, J. (2007). Will the tropical land biosphere dominate the climate–carbon cycle feedback during the twenty-first century? *Climate Dynamics*, 29: 565–574. doi: doi.org/10.1007/s00382-007-0247-8
- Rae, D. C., Keeble, J., Hitchcock, P., Pyle, A. J. (2019). Prescribing Zonally Asymmetric Ozone Climatologies in Climate Models: Performance Compared to a Chemistry-Climate Model. *Journal of Advances in Modelling Earth Systems*, 11: 918–933. doi: doi.org/10.1029/2018MS001478
- Rast, S., Brokopf, R., Esch, M., Cheedela, K. S., Gayler, V., Kirchner, I., Kornblüh, L., Rhodin, A., Schmidt, H., Schulzweida, U., Wieners, H. K. (2012). User manual for ECHAM6 version echam–6.1.00–guide–1.3. Website URL: https://icdc.cen.uni-hamburg.de/fileadmin/user_upload/icdc_Dokumente/ECHAM/echam6_userguide.pdf, Accessed on, 28.12.2021.

- Reick, C. H., Raddatz, T., Brovkin, V., Gayler, V. (2013). Representation of natural and anthropogenic land cover change in MPI-ESM, doi: doi.org/10.1002/jame.20022
- Roeckner, E., Dümenil, L., Kirk, E., Lunkeit, F., Ponater, M., Rockel, B., Sausen, R., and Schlese, U. (1989). The Hamburg version of the ECMWF model (ECHAM). In: Boer GJ (ed) Research activities in atmospheric and oceanic modelling. *CAS/JSC Working Group on Numerical Experimentation*, No. 13, 7.1-7.4.
- Scholz, P., Danek, C., and Lohmann, G. (2019). Effects of high resolution and spinup time on modeled North Atlantic circulation. *Journal of Physical Oceanography*, 49: 1159-1181. doi: doi.org/10.1175/JPO-D-18-0141.1
- Scholz, P., Sidorenko, D., Gurses, O., Danilov, S., Koldunov, N., Wang, Q., Sein, D., Smolentseva, M., Rakowsky, N., and Jung, T. (2019). Assessment of the Finite-volume Sea ice-Ocean Model (FESOM2.0) – Part 1: Description of selected key model elements and comparison to its predecessor version, *Geoscientific Model Development*, 12: 4875–4899. doi: doi.org/10.5194/gmd-12-4875-2019
- Schultz, G. M., Stadtler, S., Schröder, S. (2018). The chemistry–climate model ECHAM6.3 HAM2.3-MOZ1.0. *Geoscientific Model Development*, 11: 1695–1723. doi: doi.org/10.5194/gmd-11-1695-2018
- Schulzweida, U., Kornbluh, L., and Quast, R. (2006). Cdo user's guide. Climate data operators, Version, 1(6):205–209.
- Shepherd, T. G. (2008). Dynamics, stratospheric ozone, and climate change. *Atmosphere–Ocean*, 46: 117–138. doi: https://doi.org/10.3137/ao.460106.
- Sidorenko, D., Rackow, T., Jung, T., Semmler, T., Barbi, D., Danilov, S., Dethloff, K., Dorn, W., Fieg, K., Goessling, H. F., Handorf, D., Harig, S., Hiller, W., Juricke, S., Losch, M., Schröter, J., Sein, D. V., and Wang, Q. (2015). Towards multi-resolution global climate modelling with ECHAM6–FESOM. Part I: Model formulation and mean climate. *Climate Dynamics*, 44: 757–780. doi: doi.org/10.1007/s00382-014-2290-6
- Sidorenko, D., Rackow, T., Jung, T., Semmler, T., Barbi, D., Danilov, S., Dethloff, K., Dorn, W., Fieg, K., Goessling, F. H., Handorf, D., Harig, S., Hiller, W., Juricke, W., Losch, M., Schröter, J., Sein, V. D., and Wang, Q. (2015). Towards multi-resolution global climate modeling with ECHAM6–FESOM. Part I: model formulation and mean climate. *Climate Dynamics*, 44: 757–780. doi: doi.org/10.1007/s00382-014-2290-6
- Sidorenko, D., Goessling, F. H., Koldunov, V. N., Scholz, P., Danilov, S., Barbi, D., Cabos, W., Gurses, O., Harigs S., Hinrichs, C., Juricke, S., Lohmann, G., Losch, M., Mu, L., Rackow, T., Rakowsky, N., Sein, D., Semmler, T., Shi, X., Stepanek, C., Streffing, J., Wang, Q., Wekerle, C., Yang H., Jung, T. (2019). Evaluation of FESOM2.0 Coupled to ECHAM6.3: Preindustrial and High Resolution MIP Simulations. *Journal of Advances in Modeling Earth Systems*, 11: 3794 –3815. doi: doi.org/10.1029/2019MS001696
- Son, S. W., Polvani, L. M., Waugh, D. W., Akiyoshi, H., Garcia, R., Kinnison, D. (2008). The impact of stratospheric ozone recovery on the Southern Hemisphere westerly jet. *Science*, 320(5882): 1486–1489. doi: doi.org/10.1126/science.1155939
- Stepanek, C., Samakinwa, E., Knorr, G., Lohmann, G. (2020).

- Contribution of the coupled atmosphere–ocean–seaice–vegetation model COSMOS to the PlioMIP2. *Climate of the past*, 16: 2275–2323.
doi: doi.org/10.5194/cp-16-2275-2020
- Stevens, B., Giorgetta, M., Esch, M., Mauritsen, T., Crueger, T., Rast, S., Salzmann, M., Schmidt, H., Bader, J., Block, K. (2013). Atmospheric component of the MPI-M earth system model: Echem 6. *Journal of Advances in Modeling Earth Systems*, 5(2): 146–172.
doi: doi.org/10.1002/jame.20015
- Taylor, K. E., Stouffer, R. J., and Meehl, G. A. (2012). An overview of CMIP5 and the experiment design. *Bulletin of the American Meteorological Society*, 93(4): 485–498.
doi: doi.org/10.1175/BAMS-D-11-00094.1
- Taylor P. C., Cai, M., Hu, A., Meehl, J., Washington, W., and Zhang, G. J. (2013). A decomposition of feedback contributions to polar warming amplification, *Journal of Climate*, 26: 7023–7043. doi: doi.org/10.1175/JCLI-D-12-00696.1
- Thompson, D. W.J., and Solomon, S. (2002). Interpretation of recent Southern Hemisphere climate change. *Science*, 296: 895–899. doi: doi.org/10.1126/science.1069270
- Valcke, S. (2013). The OASIS3 coupler: A European climate modelling community software. *Geoscientific Model Development*, 6(2), 373–388. doi: doi.org/10.5194/gmd-6-373-2013
- Wang, Q., Danilov, S., Sidorenko, D., Timmermann, R., Wekerle, C., Wang, X., Jung, T., and Schröter, J. (2014). The Finite Element Sea Ice-Ocean Model (FESOM) v.1.4: formulation of an ocean general circulation model. *Geoscientific Model Development*, 7: 663–693.
doi: doi.org/10.5194/gmd-7-663-2014
- Wild, M. (2020). The global energy balance as represented in CMIP6 climate models. *Climate Dynamics*, 55: 553–577. doi: doi.org/10.1007/s00382-020-05282-7
- Williamson, E. C., Zepp, G. R., Lucas, M. R., Madronich, S., Austin, T. A., Ballaré, L. C., Norval, M., Sulzberger, B., Bais, F. A., McKenzie, M. R., Robinson, A. S., Häder, P. D., Paul, D. N., and Bornman, F. J. (2014). Solar ultraviolet radiation in a changing climate. *Nature Climate Change*, 4: 434–441. doi: doi.org/10.1038/nclimate2225
- Xie, F., Li, J., Tian, W., Fu, Q., Jin, F. F., Hu, Y., Yang, Y. (2016). A connection from Arctic stratospheric ozone to ElNiño-Southern oscillation. *Environmental Research Letters*, 11(12): 124026. doi: doi.org/10.1088/1748-9326/11/12/124026
- Yang-chun, F., Yan-chun, H., Xiu-min, M. (2017). The application of Student's t-test in internal quality control of clinical laboratory. *Frontiers in Laboratory Medicine*, 1(3): 125–128.
doi: doi.org/10.1016/j.flm.2017.09.002
- Zhang, K., Wang, T., Xu, M., and Zhang, J. (2019). Influence of Wintertime Polar Vortex Variation on the Climate over the North Pacific during Late Winter and Spring. *Atmosphere*, 10(11), 670. doi: doi.org/10.3390/atmos10110670
- Zhang, W., Furtado, K., Wu, P., Zhou, T., Chadwick, R., Marzin, C., Rostron, J., Sexton, D. (2021). Increasing precipitation variability on daily-to-multiyear time scales in a warmer world. *Atmospheric Science*, 7. doi: doi.org/10.1126/sciadv.abf8021

Appendix A

A.1 PI Geopotential Height at 100 hPa level

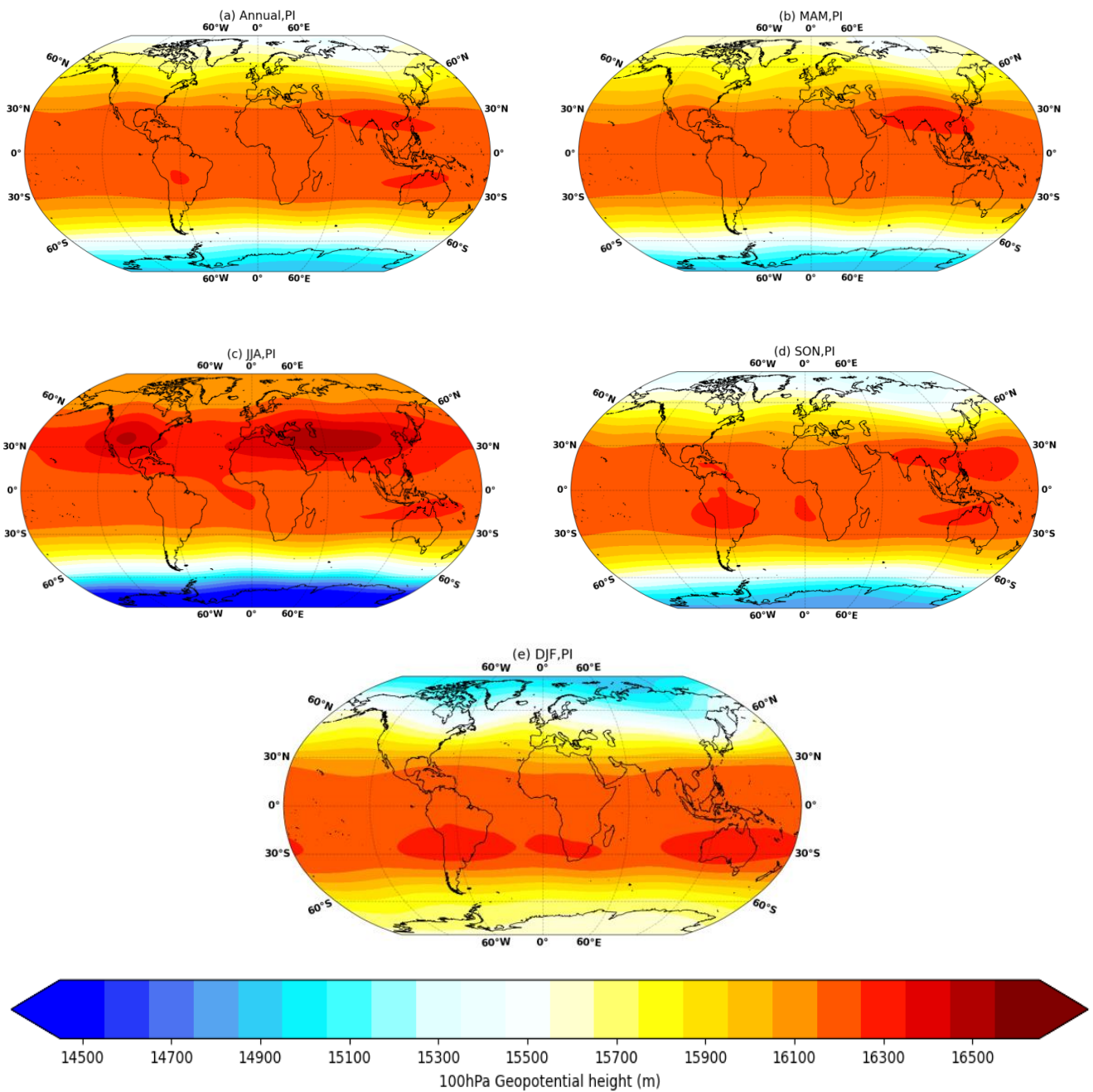


Figure A.1: 100 hPa geopotential height for PI simulation in Annual (a), MAM (b), JJA (c), SON (d), and DJF (e). Units are in metre.

A.2 4xCO₂ Geopotential Height at 100 hPa level

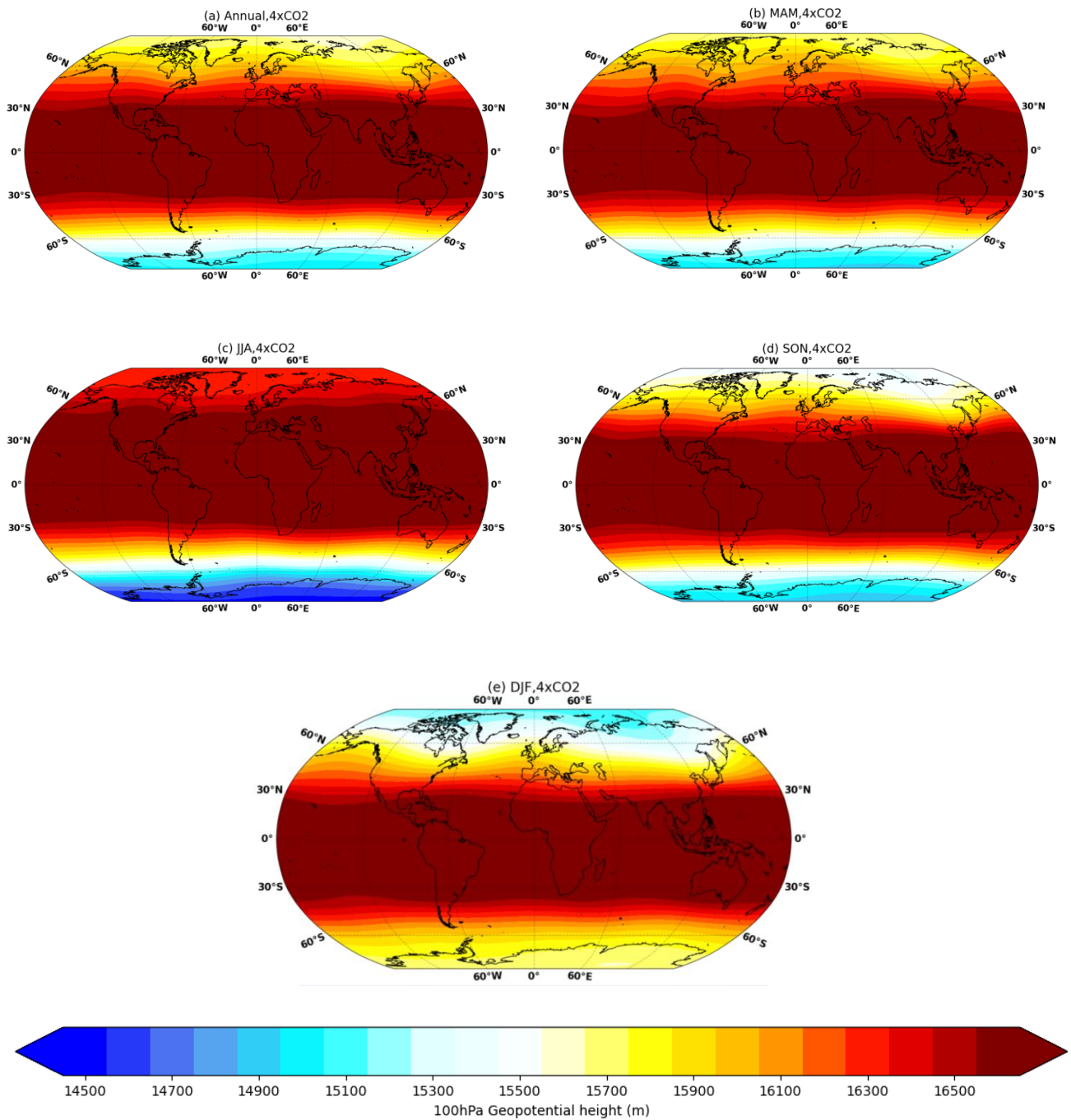


Figure A.2: 100 hPa geopotential height for 4xCO₂ simulation in Annual (a), MAM (b), JJA (c), SON (d), and DJF (e). Units are in metre.

A.3 4xCO₂_O₃ Geopotential Height at 100 hPa level

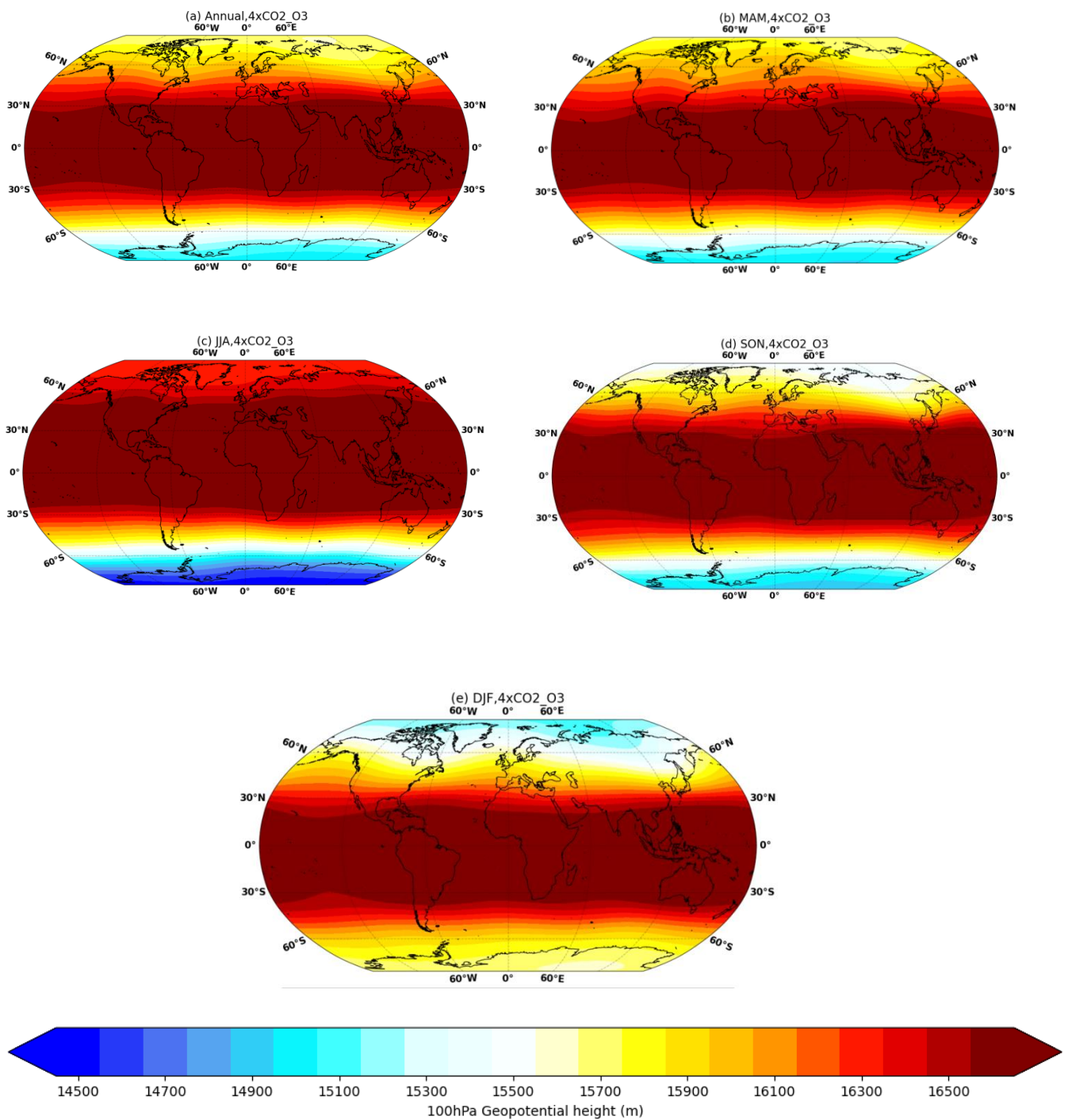


Figure A.3: 100 hPa geopotential height for 4xCO₂-O₃ simulation in Annual (a), MAM (b), JJA (c), SON (d), and DJF (e). Units are in metre.

A.4 PI Geopotential Height at 250 hPa level

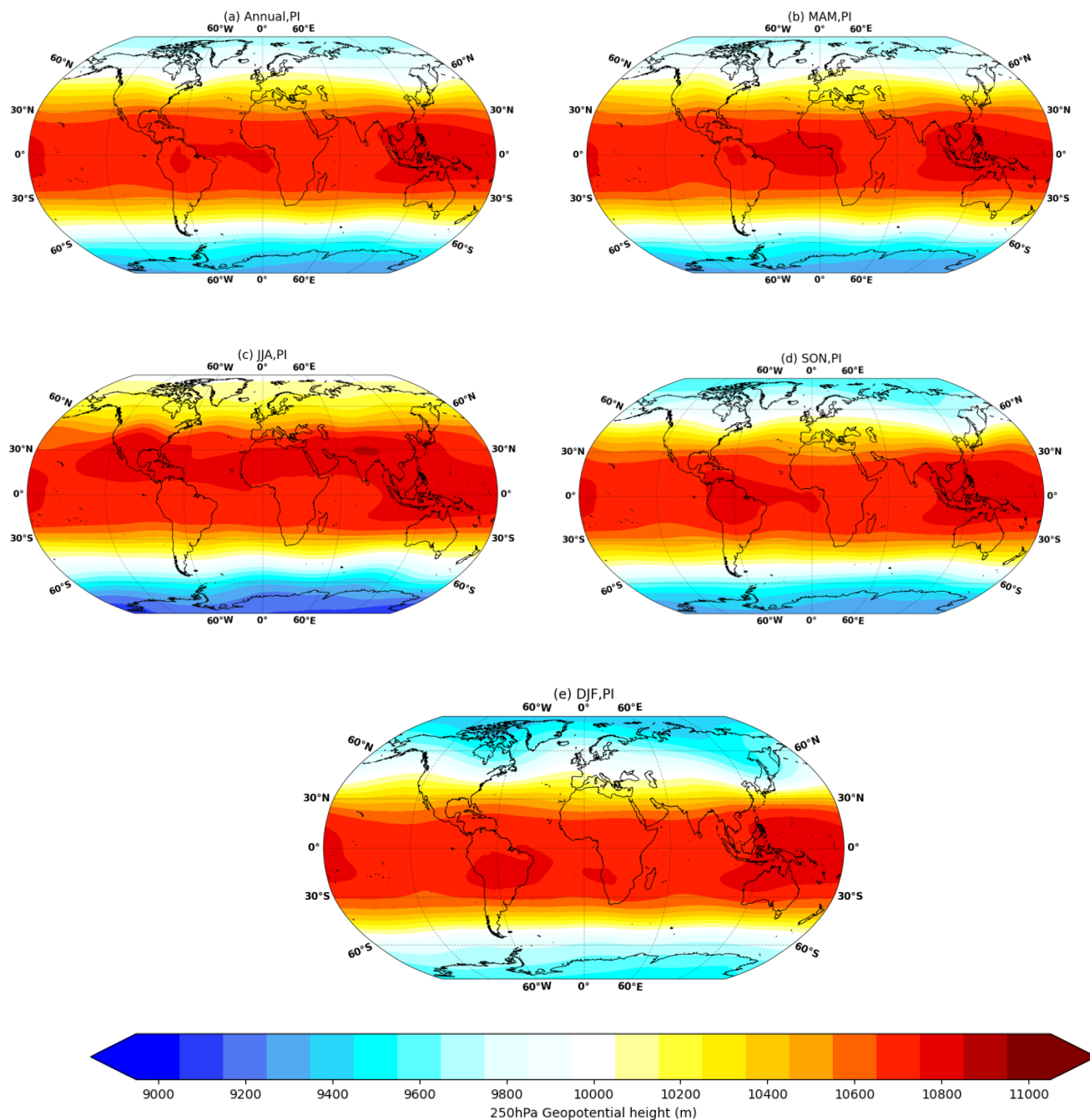


Figure A.4: 250 hPa geopotential height for PI simulation in Annual (a), MAM (b), JJA (c), SON (d), and DJF (e). Units are in metre.

A.5 4xCO₂ Geopotential Height at 250 hPa level

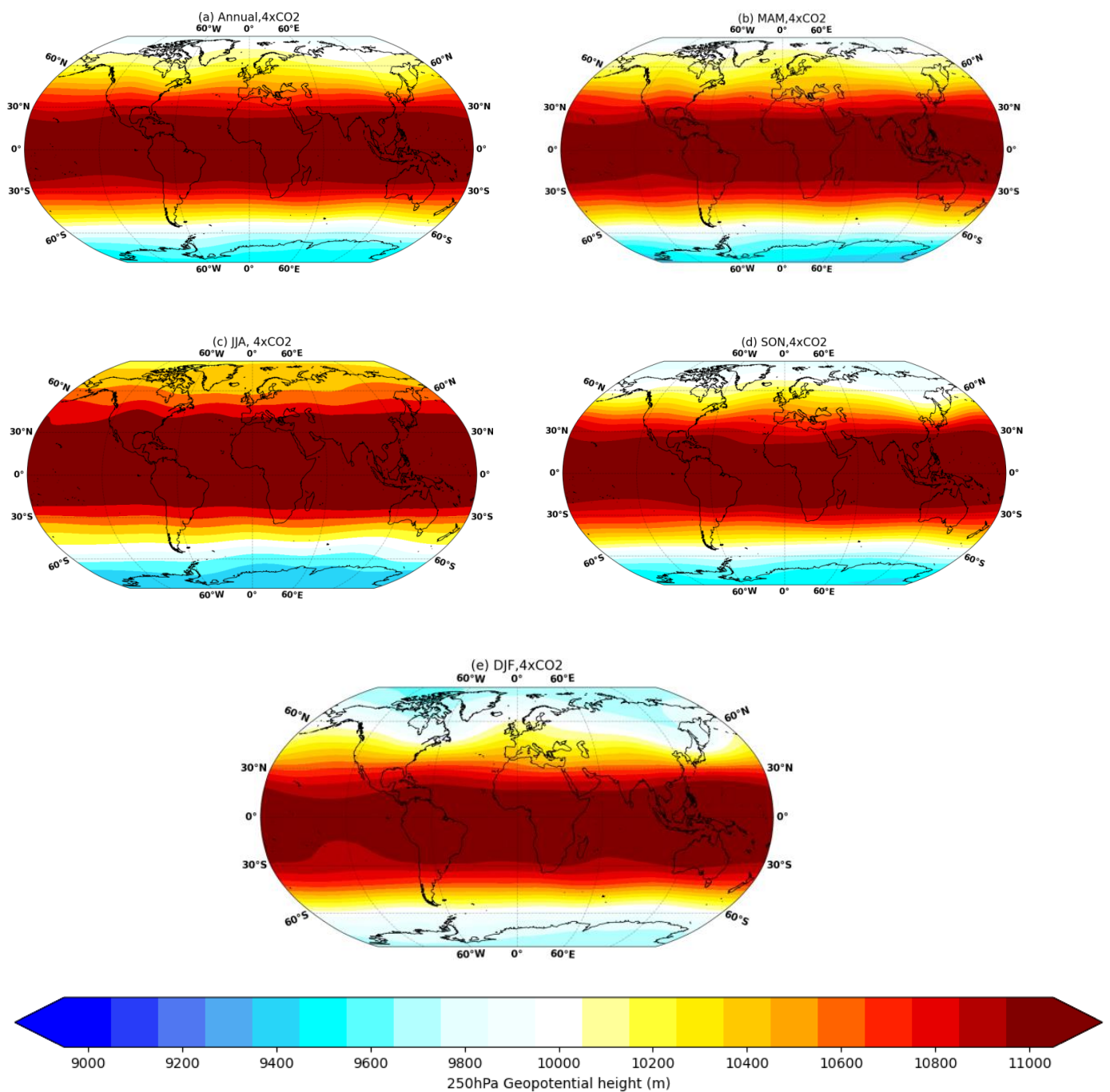


Figure A.5: 250 hPa geopotential height for 4xCO₂ simulation in Annual (a), MAM (b), JJA (c), SON (d), and DJF (e). Units are in metre.

A.6 4xCO₂_O₃ Geopotential Height at 250 hPa level

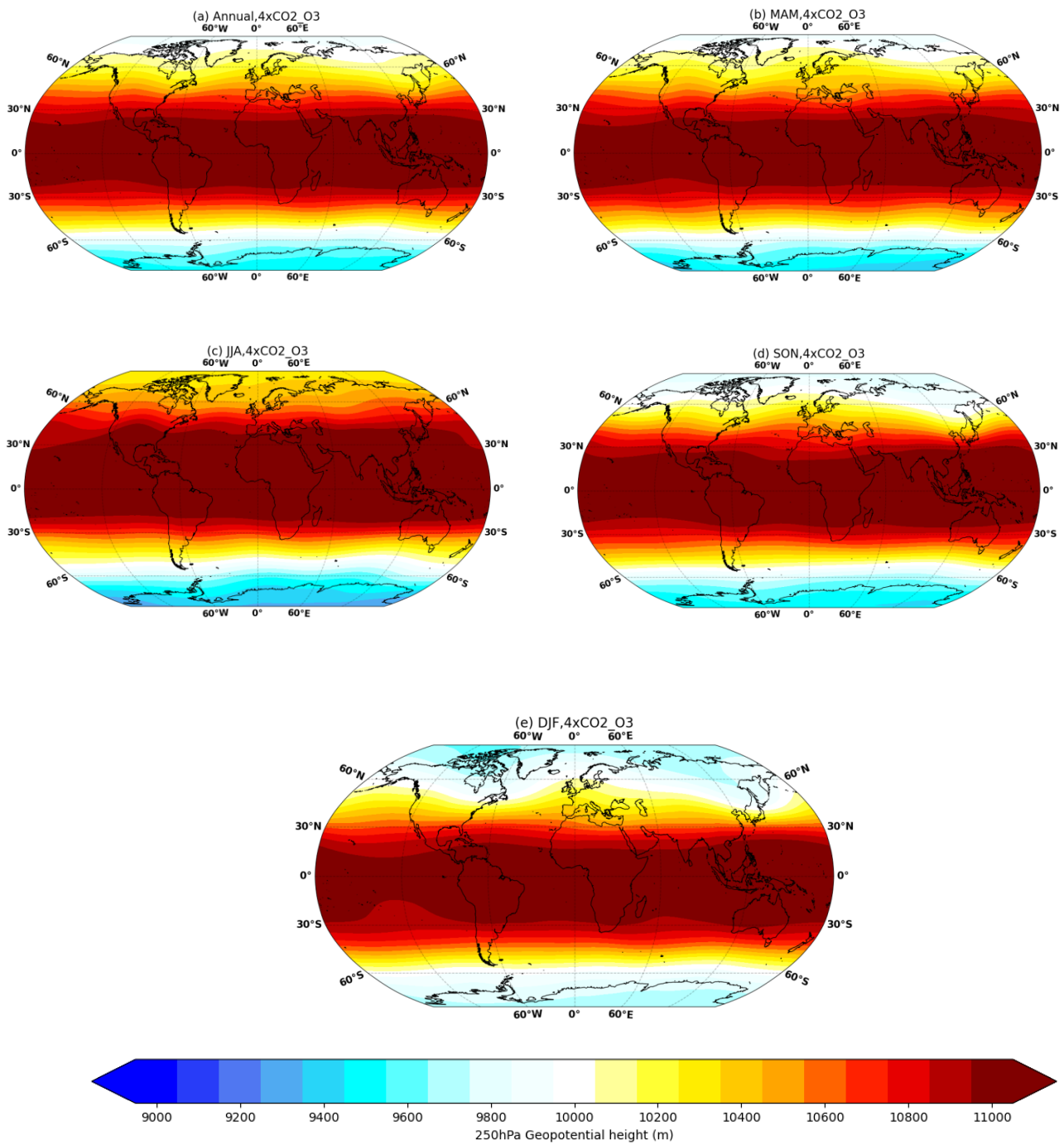


Figure A.6: 250 hPa geopotential height for 4xCO₂-O₃ simulation in Annual (a), MAM (b), JJA (c), SON (d), and DJF (e). Units are in metre.

A.7 PI Geopotential Height at 500 hPa level

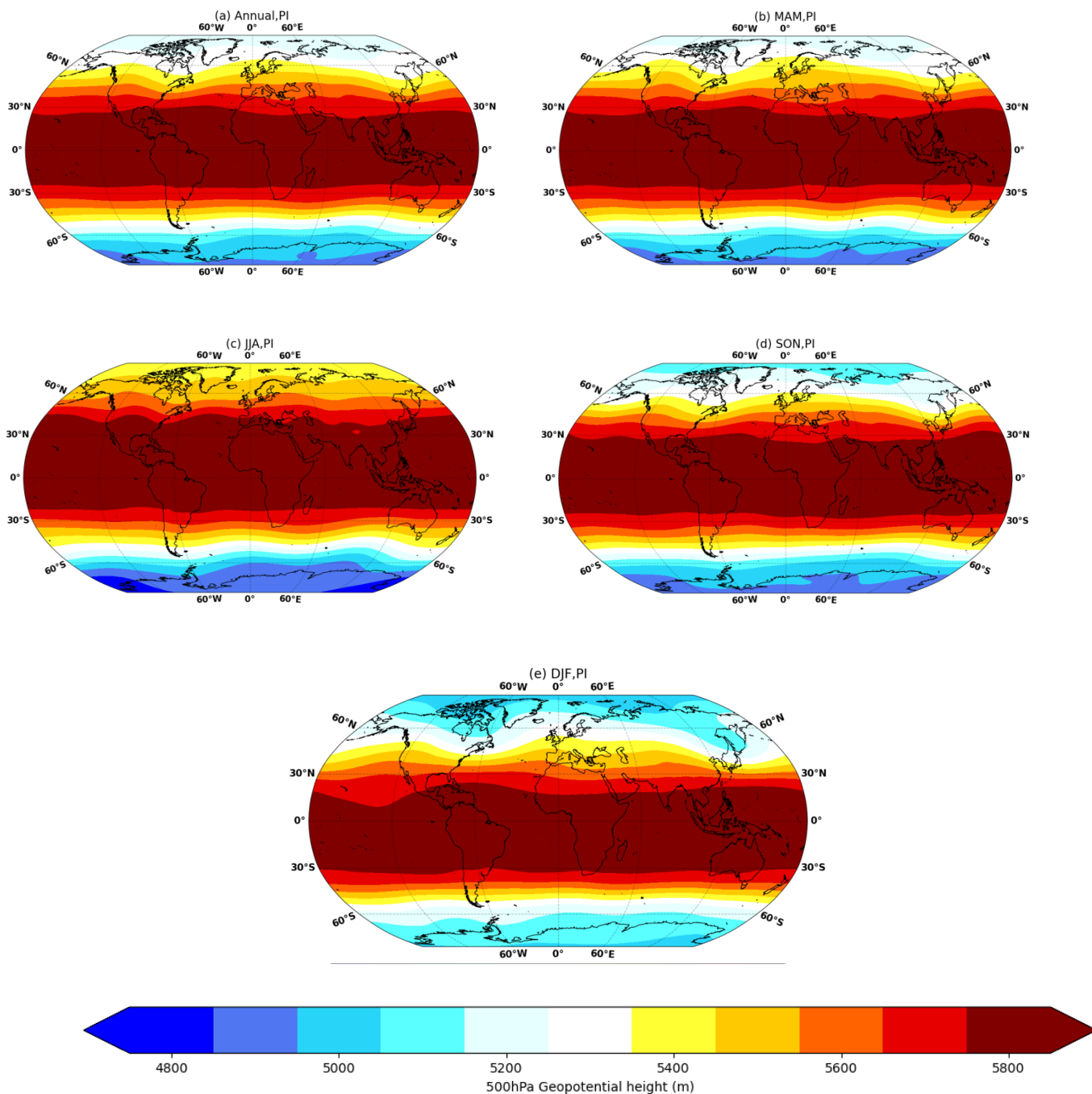


Figure A.7: 500 hPa geopotential height for PI simulation in Annual (a), MAM (b), JJA (c), SON (d), and DJF (e). Units are in metre.

A.8 4xCO₂ Geopotential Height at 500 hPa level

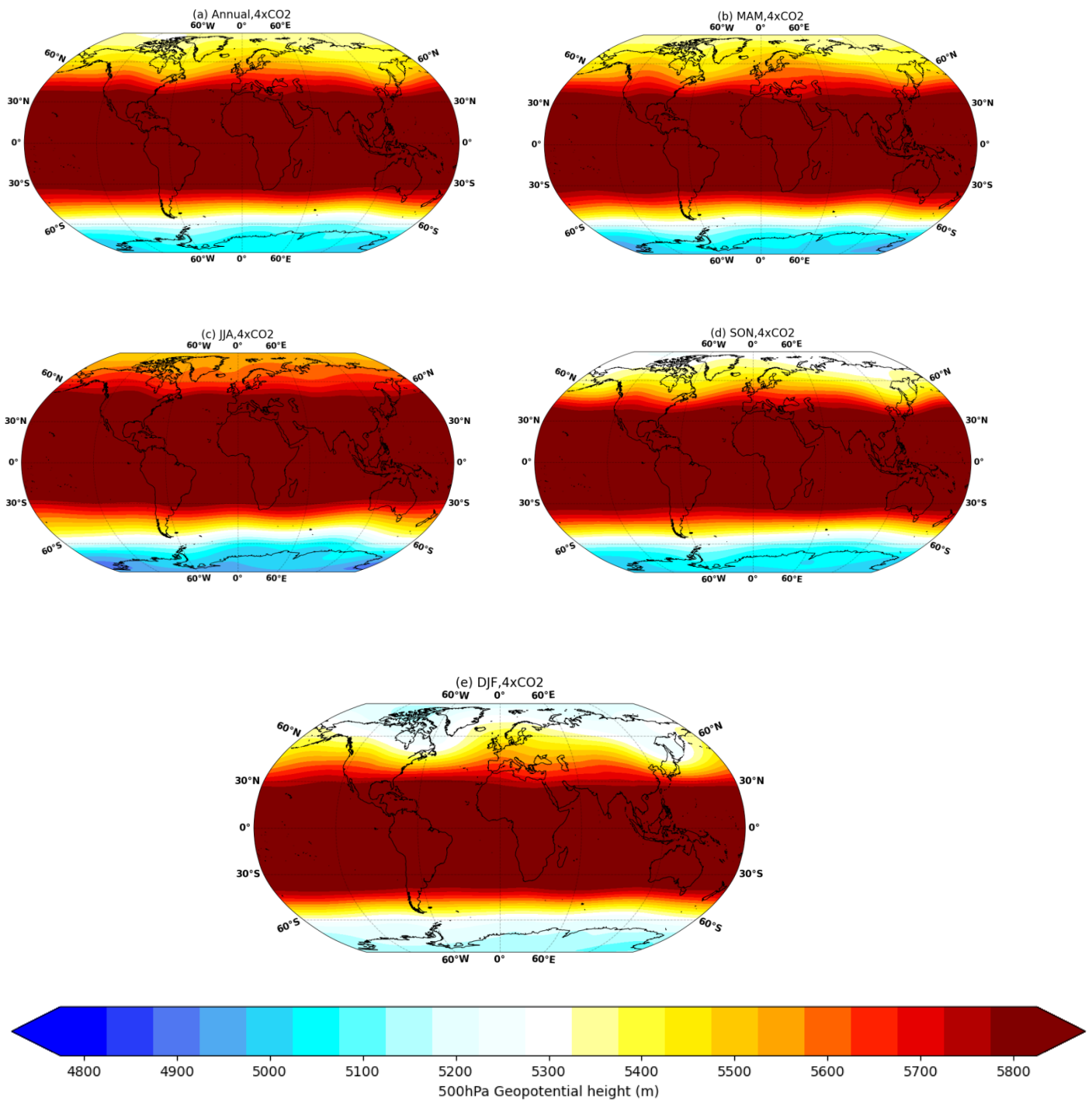


Figure A.2: 500 hPa geopotential height for 4xCO₂ simulation in Annual (a), MAM (b), JJA (c), SON (d), and DJF (e). Units are in metre.

A.9 4xCO₂_O₃ Geopotential height at 500 hPa level

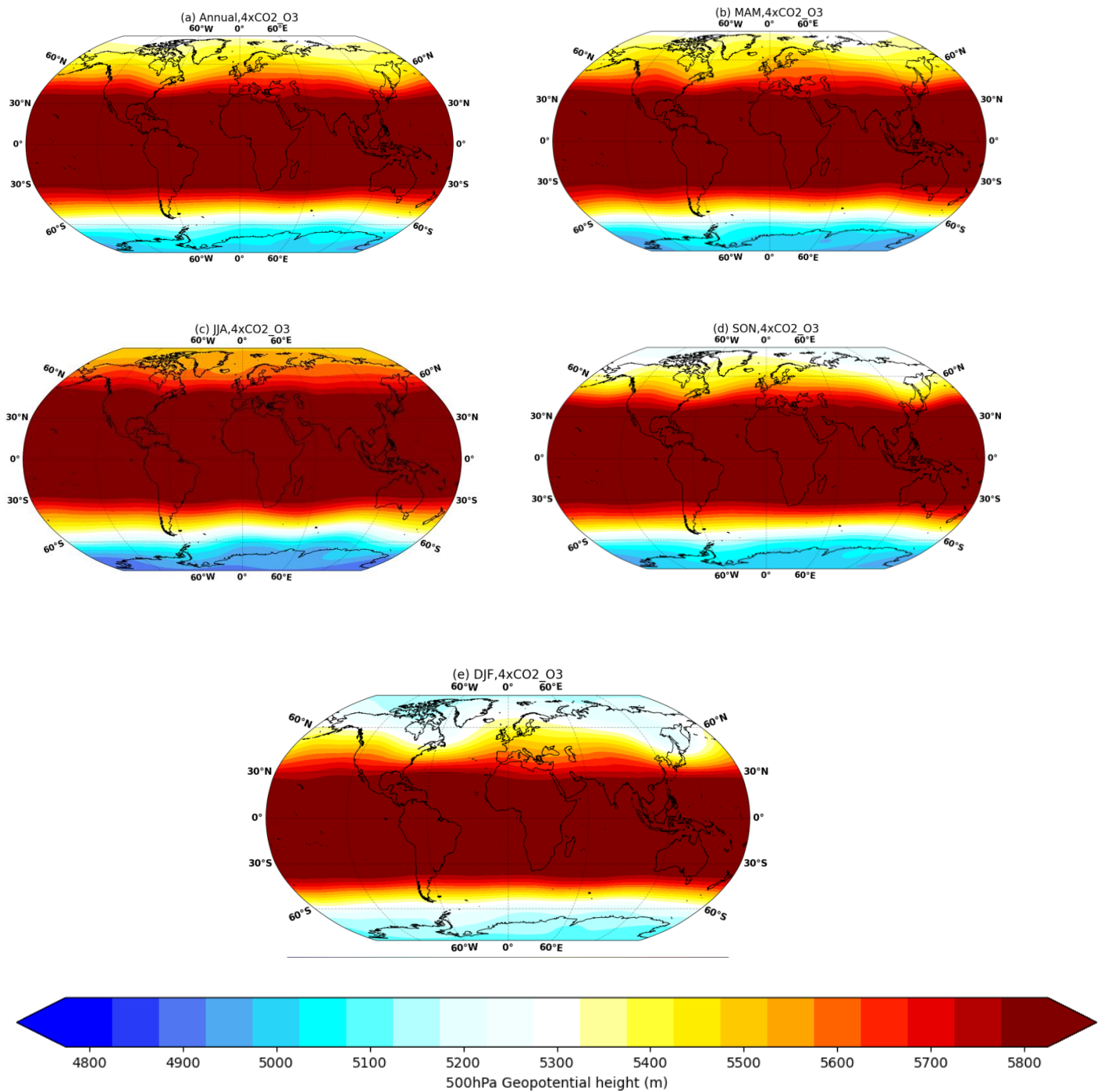


Figure A.9: 100 hPa geopotential height for 4xCO₂-O₃ simulation in Annual (a), MAM (b), JJA (c), SON (d), and DJF (e). Units are in metre.